International Commission on Illumination
Commission Internationale de l'Eclairage
Internationale Beleuchtungskommission

Collection of papers
accepted for the
5th CIE Symposium on Colour and Visual Appearance

CIE x047:2020

The papers of this collection were selected by the International Scientific Committee (ISC) for presentation at the 5th CIE Symposium on Colour and Visual Appearance, Hong Kong, CN, April 21-22, 2020, which, due to the corona pandemic, could not take place.
The papers have not been peer-reviewed by CIE.

CIE Central Bureau
Babenbergerstrasse 9
A-1010 Vienna
Austria
Tel.: +43 1 714 3187
e-mail: ciecb@cie.co.at
www.cie.co.at

Table of Contents

International Commission on Illumination
Commission Internationale de l'Eclairage
Internationale Beleuchtungskommission

OP01

CHANGE OF PERCEIVED CHROMA AND HUE OF OBJECT COLOURS AT DIFFERENT LIGHTING LEVELS DUE TO HUNT EFFECT

Yuki Kawashima & Yoshi Ohno

DOI 10.25039/x47.2020.OP01

Paper accepted for the 5th CIE Symposium on Colour and Visual Appearance

The paper was selected by the International Scientific Committee (ISC) for presentation at the 5th CIE Symposium on Colour and Visual Appearance, Hong Kong, CN, April 21–22, 2020, which, due to the corona pandemic, could not take place. The paper has not been peer-reviewed by CIE.

CIE Central Bureau
Babenbergerstrasse 9
A-1010 Vienna
Austria
Tel.: +43 1 714 3187
e-mail: ciecb@cie.co.at
www.cie.co.at

OP01

CHANGE OF PERCEIVED CHROMA AND HUE OF OBJECT COLOURS AT DIFFERENT LIGHTING LEVELS DUE TO HUNT EFFECT

Kawashima, Y., Ohno, Y.
National Institute of Standards and Technology, Gaithersburg, MD USA
yuki.kawashima@nist.gov

Abstract

Our previous study made an attempt to quantify the perceived chroma changes due to Hunt Effect in lighting for red and green colour samples. For further understanding of Hunt Effect, another vision experiment was conducted using a number of red, green, yellow and blue colour samples to quantify perceived chroma changes as well as hue angle changes at different lighting levels. A reference patch was placed on one side of booth at 100 lx, and 20 to 25 test patches with varied chroma and hue levels were placed on the other side of the booth at 1 000 lx. Subjects viewed each booth with each eye separately (haploscopic view) and chose a test patch that appeared to be closest to the reference patch. Results showed that the chroma at 100 lx was perceived 8 % to 15 % lower compared to the chroma at 1 000 lx, and the hue angles also shifted slightly in different directions for different colours.

Keywords: Hunt Effect, colour fidelity, chroma, lighting, haploscopic view

1 Introduction

It is known that light level can affect perceived chroma of objects, and this effect is called Hunt Effect (Hunt, 1950). According to the Hunt Effect, objects at indoor lighting would appear less saturated than at outside daylight, which is generally at much higher light level than the indoor lighting. Our previous experiment using lighting levels at 100 lx and 1 000 lx verified that the Hunt Effect is effective at light levels for the normal indoor lighting (Kawashima and Ohno, 2019a).

In order to make the colour appearance of objects at the indoor lighting close to that at the daylight, chroma of the object colours need to be increased by the lighting. The perceived chroma of the objects has been related to colour preference and memory. Previous studies suggest that preferred colours of the objects are more saturated than the actual colours (Judd, 1967; Thornton, 1974). For example, Caucasian skin is preferred to be redder than it really is (Sanders, 1959). Furthermore, it was showed that the object colour is memorized to have more saturated colour than the actual colour (Bartleson, 1961; Newhall et al., 1957). However, if Hunt Effect is considered, and if the outside daylight is considered as the reference for the colour appearance of objects, increasing the object chroma by lighting would bring higher colour fidelity, and it would become a matter of colour fidelity. In current colour fidelity metrics, CRI (CIE, 1995) or CIE Colour Fidelity Index (CIE, 2017; IES, 2015), any changes of chroma (increase or decrease) from the reference illuminant is equally penalized, thus a new fidelity metric taking this effect into account will be needed.

Therefore, it is important to quantify the degree in which the Hunt Effect affects the perception of colour saturation and evaluate impact on colour fidelity. Our previous experiment quantified the chroma change for red and green samples due to the Hunt Effect (Kawashima and Ohno, 2019b). However, it is still not clear how much perceived chroma shifts occur on other colours by Hunt Effect, e.g. blue and yellow. In addition to the Hunt Effect, it is known that the light level can affect the perceived hue (Bezold-Brucke effect, von Bezold, 1873). Thus, the magnitude of perceived hue shifts as well as chroma change needs to be quantified when Hunt Effect is to be considered in colour rendering metrics.

Therefore, the purpose of this study is to quantify the changes of perceived chroma and hue for four fundamental colours – red, green, yellow, and blue.

2 Methods

A colour-matching experiment was conducted using a double-booth with 16 channel spectrally tuneable light sources. One side of the double-booth was set at 100 lx and the other side at 1 000 lx. A reference patch was placed on the booth at 100 lx, and a number of test patches with varied chroma and hue levels were placed on the other side of the booth at 1 000 lx. The subject was adapted in haploscopic view condition, so his/her left eye was adapted to the left-side booth and the right eye to the right-side booth. The subject was asked to choose a matching test patch that appeared closest to the reference patch.

Since each eye will not be perfectly adapted to very different light levels with the haploscopic view, it was first tested for how completely the subject was adapted to each light using grey patches before starting the colour matching experiment. After the subject was fully adapted to each light in haploscopic condition, a reference grey patch was placed on one side of the booth at 1 000 lx and five test grey patches having several different lightness levels were placed on the other side of booth at 100 lx. The reference grey patch was the same as the darkest one among the test grey patches. The subject chose a test grey patch that matched the brightness of the reference grey patch. If adaptation of each eye to each light level is perfect, the test grey patch with the same grey level as that of reference grey patch would be chosen. If adaptation is not complete, a lighter grey test patch will be chosen. The difference between the grey level of the matching test patch and the reference grey patch represents incompleteness of the adaptation, which was used to correct the experiment results.

2.1 Apparatus

A double-booth with spectrally tuneable light sources shown in Figure 1 was used for the experiment. The double-booth has a viewing compartment and a light source compartment (see the right figure), and is divided into left and right by a partition wall at its centre (left figure). The light source compartment was hidden by a top cover during the experiment and the subject did not see the light source directly. A view divider is attached to the centre partition wall for the haploscopic view. The inside of the viewing compartment and the centre partition wall are painted in grey. The size of viewing area on each side is 50 cm wide, 65 cm deep, and 37 cm high (in front window). Each side of the light source compartment is equipped with a spectrally tuneable light source which has 16 channels of LED spectra (ranged from 495 nm to 730 nm peak). The spectrum of the light source is controlled with a computer program that can change intensity for each channel. The light-emitting surface of the light source is a diffuser of 10 cm diameter, and there is a large light-transmitting diffuser between the light source compartment and the viewing compartment in the booth, with which good spatial colour uniformity is provided in the viewing area.

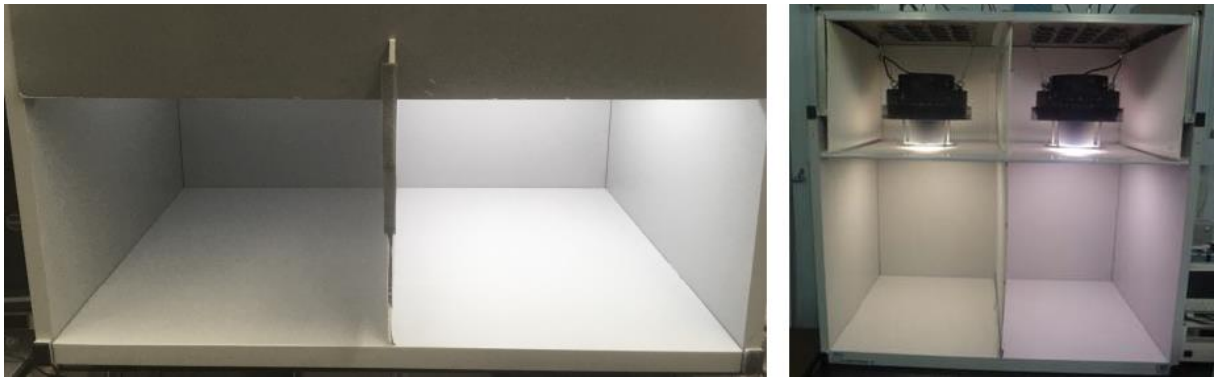

Figure 1 – Photograph of the double-booth.

The light sources need a long time (several hours) to stabilize completely. Therefore, the light sources were kept turned on all the time during the experiment period, and was set to initial condition of the experiment (3 000 K or 6 500 K, 1 000 lx and 100 lx for each side) at least one hour prior to starting the experiment. All the spectral distributions used in the experiment were measured before and after the experiment every day, at the bottom surface of the booth at ≈ 10 cm from the partition wall, and ≈ 25 cm from the front edge of the booth. The measured

chromaticity differences between the booth at 1 000 lx and 100 lx of same CCT settings were set and kept within 0.0035 in $\Delta u'v'$ (in most cases within 0.002 with maximum 0.0035) during experiments.

The expanded uncertainties (k = 2) of the measurements were estimated to be 0.0012 in u', 0.0011 in v', 0.0009 in Duv, 17 K in CCT at 3 000 K and 52 K at 6 500 K for the light spectra used in this experiment. The expanded uncertainty in the relative chromaticity measurement between each pair of light was 0.0002 in u' and v', which is the typical repeatability of the instrument. The expanded uncertainty of illuminance of the spectroradiometer is estimated 3 % (k = 2) for directional incident light, and its uncertainty for relative measurement was 0.2 %, which is the typical reproducibility of the instrument.

2.2 Colour patches and light sources

All patches used in this experiment were produced with a thick matte paper printed with a special professional printer. The colours of patches were adjusted by repeated measurements and re-printing.

Six grey patches (5.4 cm × 5.4 cm) were used for grey scale matching. The five grey patches were used as the test grey patches on the booth at 100 lx and have five different lightness (J' ≈ 75 to 80, or reflectance 49 % to 57 %). The reference grey patch, identical to the darkest grey test patch, was placed on the other side of booth at 1 000 lx.

Four sets of colour patches, red green, yellow and blue, were used for the colour matching experiment. Each set consisted of a reference colour patch and 19 to 25 test colour patches with different chroma and hue levels. The size of each patch was 6.4 cm × 6.4 cm. The reference patches were identical to the most saturated test patch in each colour. Figure 3**Error! Reference source not found.** shows the photographs of all the test colour patches, and Figure 3 shows the (a', b') colour coordinates of these colour patches on CIECAM02 colour space under D65 lighting. The range of chroma difference was $\Delta C_{a'b'} \approx 12$ with intervals of $\Delta C_{a'b'} \approx 3$ for each colour. The range of hue angles was ≈ 12° for red, 9° for yellow and blue, with intervals of 3° for these colours, and 15° for blue with intervals 5°. The interval for blue patch was different because 3° was perceived too small. The colour coordinates of the reference patches are indicated by "X" in Figure 3. The reference patch was not necessarily at the edge of the hue range and not always the same side. The ranges of the hue shift of test patches relative to the reference patch were determined by preliminary experiments. As shown in Figure 2**Error! Reference source not found.**, each set of the test patches were placed in four or five rows by five columns, for different chroma levels at each row and different hue angle shifts for each column. One position in yellow and blue is missing because these colour coordinates could not be produced by the printer. The set of test patches for each colour was put on a grey plate so that the set could be easily replaced by other colours.

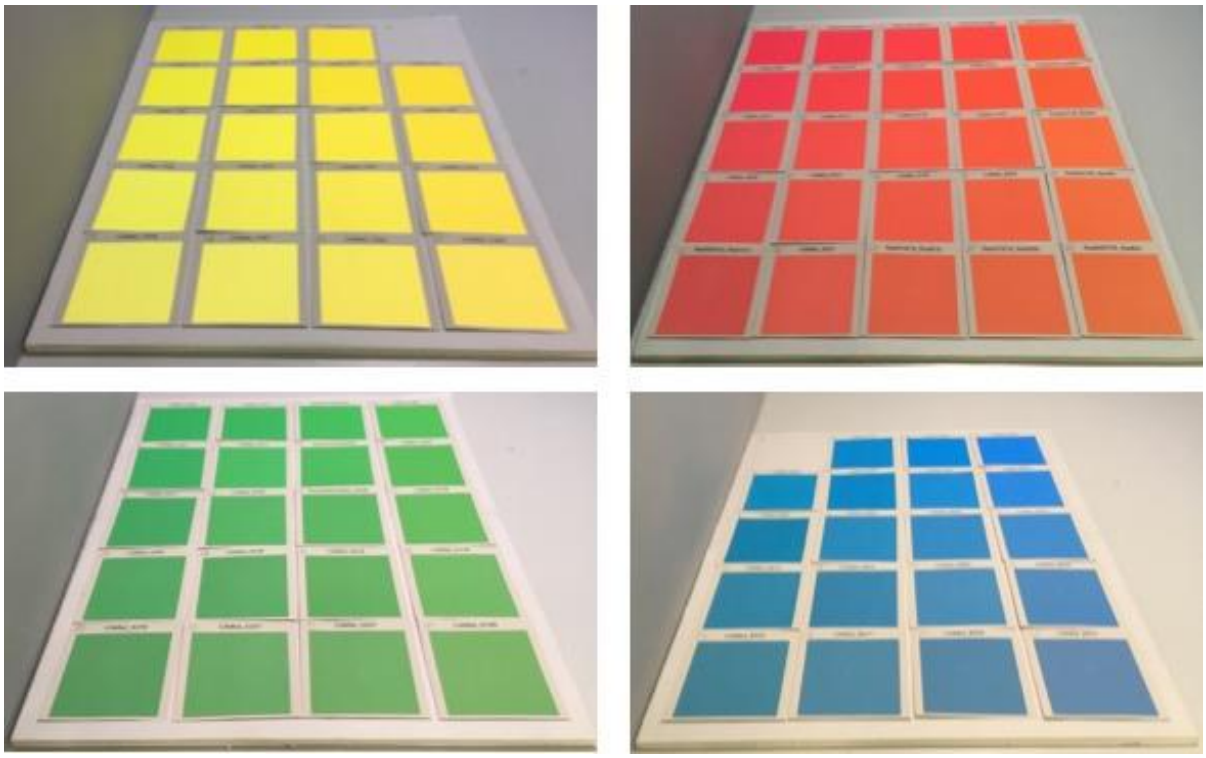

Figure 2 – Photograph of the test colour patches.

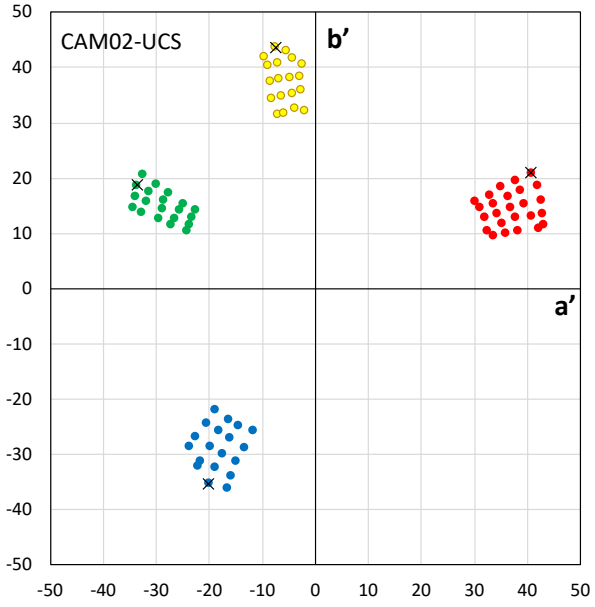

Figure 3 – Colour coordinates of the colour patches on CIECAM02. X marks show the reference patches

Each patch was placed at near the centre partition wall and its centre was ≈ 25 cm from the front edge of the booth. The subject observed the patches at a viewing angle of approximately 45˚ from the normal to the patch surface, and the viewing distance between the targets and subject's eye was ≈ 48 cm. The spectral reflectance of all the patches was measured prior to the experiment, using a telephoto-type spectroradiometer in comparison to a white reference standard.

The lights for both sides were set at the same CCT, 3 000 K or 6 500 K, with Duv = 0 using broadband spectra. The left side of the booth was set at 1 000 lx and the right side was set at 100 lx; and the sides were revered in some conditions. Thus, both illuminance levels were prepared for each side of booth. Figure 4 shows the spectra of the lights used in left and right side of the booths. The spatial nonuniformity in chromaticity u', v' over the area of all test patches on the grey plate under illumination of the 1 000 lx lights, were within 0.001 for both CCTs.

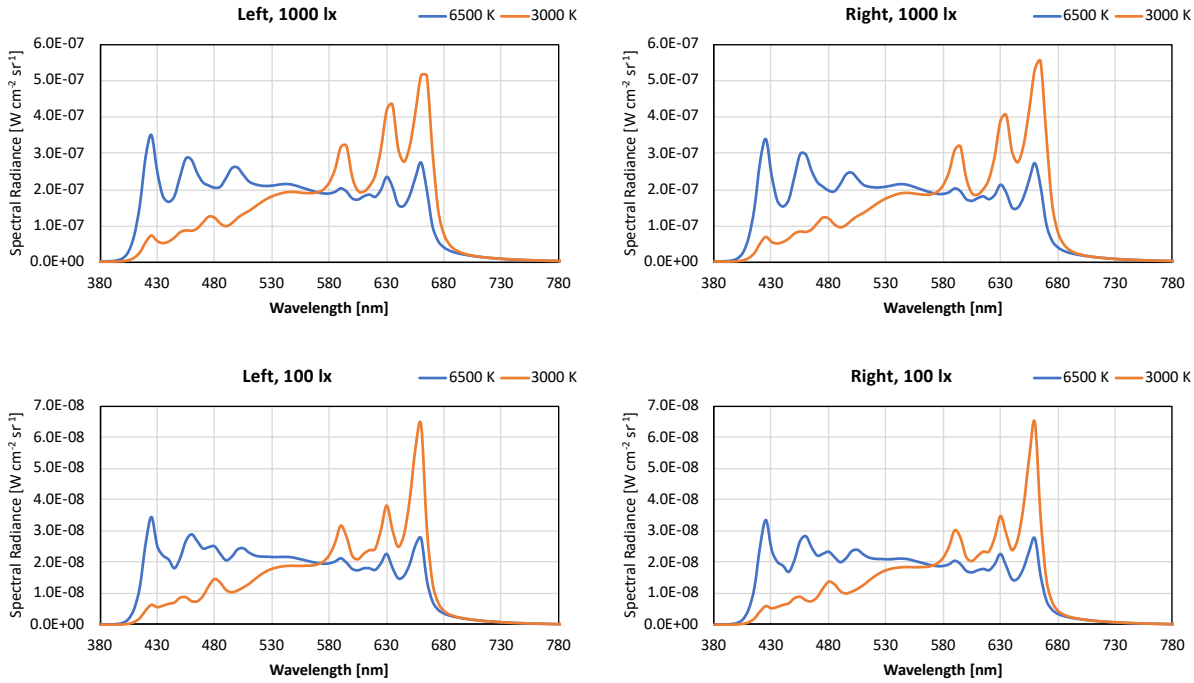

Figure 4 – The spectral distributions of the lights at 1 000 lx and 100 lx for each CCT

2.3 Procedures

Each subject was tested for normal colour vision using Ishihara Test before starting the experiment. The subject was instructed to be seated in front of the booths and viewed the booths with his/her forehead and nose placed against the view divider (haploscopic view) as shown in Figure 5. With the haploscopic view, the left eye viewed only the left side booth, and the right eye viewed only the right side both.

Figure 5 – Experimental scene of the haploscopic view

The colour matching experiment consisted of four sessions according to the CCT condition and the illuminance combination. The illuminance combinations were same in the first two sessions and then switched to the other for next two sessions. The order of the illuminance combination was randomized for each subject. The CCT condition was also used in random order for each of the two sessions with same illuminance combination. In each session, the subject conducted the colour matchings for four colours in random order.

Before starting each session, the subject adapted to each light with each eye. The adaptation time was three minutes for the first and third sessions, or one minutes for the second and fourth sessions. An instruction for the experiment was given to subjects during the adaptation for the first session. After the adaptation, the grey patches were placed in the booths, and the subject conducted the grey scale matching. The results of this grey matching were used to correct the experimental results for imperfect adaptation with the haploscopic view. the subject was asked to select one of grey patches on the booth at 100 lx that matched the brightness of the other side.

After finishing the grey scale matching, grey patches were removed. Then, a set of colour patches, the reference patch and test patches, were placed in the booths, covered by the grey plates. The reference colour patch was placed on the booth at 100 lx, and the test colour patches were placed on the booth at 1 000 lx. One minute later, the experimenter removed the grey plates and the subjects chose a matching test patch closest to the reference patch. When choosing a matching patch, the subjects were allowed to slide the test patches back and forth to compare with the reference patch. After choosing a matching test patch, the colour patches were replaced with the next set of colour patches.

2.4 Observers

A total of 22 subjects participated in this experiment. All subjects have normal colour visions as tested using Ishihara Test. They were 11 males and 11 females with their ages from 18 to 64 years old, consisting of 19 Caucasians, two Blacks and one native American. They were summer-internship students or NIST employees, who were not experts on colour or lighting and completely naïve as to the purpose of the experiment.

3 Results

Figure 6 shows the a', b' coordinates of the patches calculated under the light at each CCT on CIECAM02 colour space. The coloured circles are the patches chosen by at least one subject. In most cases the subjects chose the test patches with lower chroma and slightly different hue angles from the reference patches. The mean coordinate for the matching patches is marked as black-filled circle with error bars. It was found that not only the chroma of the chosen matching patches decreased but also hue angle shifted from the reference patch.

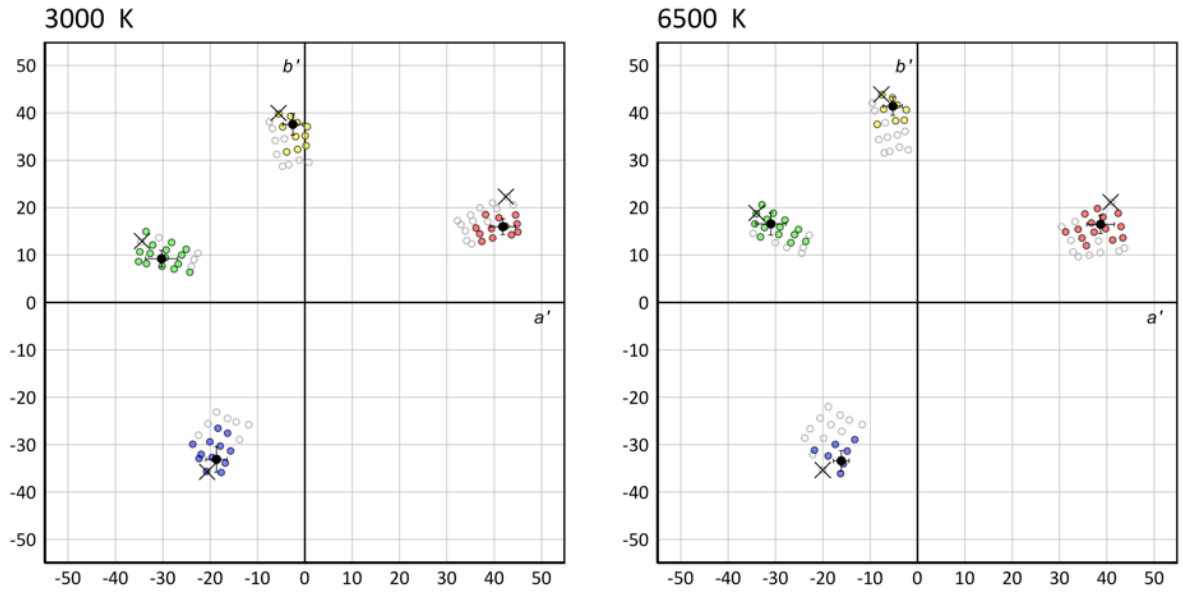

Figure 6 – Colour coordinates for the patches with the light at 3 000 K (left) and 6 500 K (right) on CIECAM02. X marks show the reference patches and circles show the test patches. The coloured circles are the patches chosen by subjects. The black-filled circles with error bar are the mean coordinate for matching patches of each colour. Error bar shows the standard deviation

The results of the grey matching were used to correct the experimental results for imperfect adaptation in the haploscopic condition. Typically, patches of J' ≈ 75 to 77 (where the reference was J' = 75) were chosen by the subjects, indicating some individual variations. In order to correct the chroma of the colour patch based on the grey scale matching, the J' increase from the reference grey patch was used. First, chroma change of the matching patch was calculated as a function of the J' increase by multiplying the spectral reflectance. Then, the chroma change for the J' increase for the chosen matching grey patch was used as a correction value of the chroma change for the matching patch.

Chroma differences between the chosen matching patch and the reference patch in each colour were calculated for each CCT condition. These chroma differences were normalized by chroma of the reference for each colour and CCT, and expressed as relative change in % of chroma, since the chroma of the references were different for each colour and CCT. Figure 7 shows the mean relative chroma differences for each colour and CCT, corrected for the grey matching results. The mean chroma of the chosen matching patch was 8 % to 15 % lower than the reference patch at 3 000 K, and 8 % to 12 % lower at 6 500 K, depending on colour of patches. The difference was largest for green and smallest for yellow. A two-factor Analysis of Variance (ANOVA) was conducted to test the effect of patch colour and CCT. A main effect* of CCT was not found ($F(1, 21) = 1.02$, $p = 0.32$) meaning that there is no statistically significant effect of CCT. However, a main effect* of patch colour was found ($F(3, 63) = 8.13$, $p < 0.01$), which means that the patch colour affects the results among the conditions. Further, there was also an interaction* between the patch colour and CCT ($F(3, 63) = 7.38$, $p < 0.01$), which means that the chroma differences occurred depending on combinations of the conditions.

* "Main effect" and "interaction" are terms for ANOVA (Chambers and Hastie, 1992).

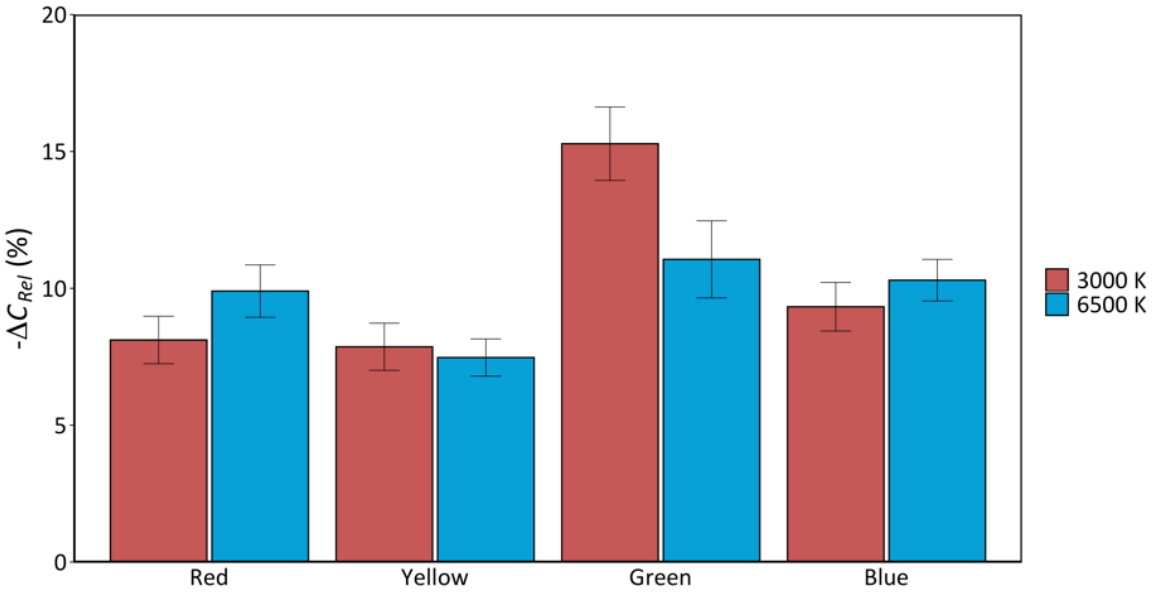

Figure 7 – Relative chroma differences for 3 000 K and 6 500 K. Each bar shows the normalized mean chroma difference between the reference and chosen matching patch. Error bar shows the standard error.

Hue differences were also calculated for each colour and CCT as shown in Figure 8 The changes in hue angle was from -7° to 4° in both CCTs, and the change was most significant in red -7° at 3 000 K. Small changes in the hue angle were seen at 6 500 K and 3 000 K for green and blue, respectively. Furthermore, red and yellow, and green and blue, respectively changed in the same direction.

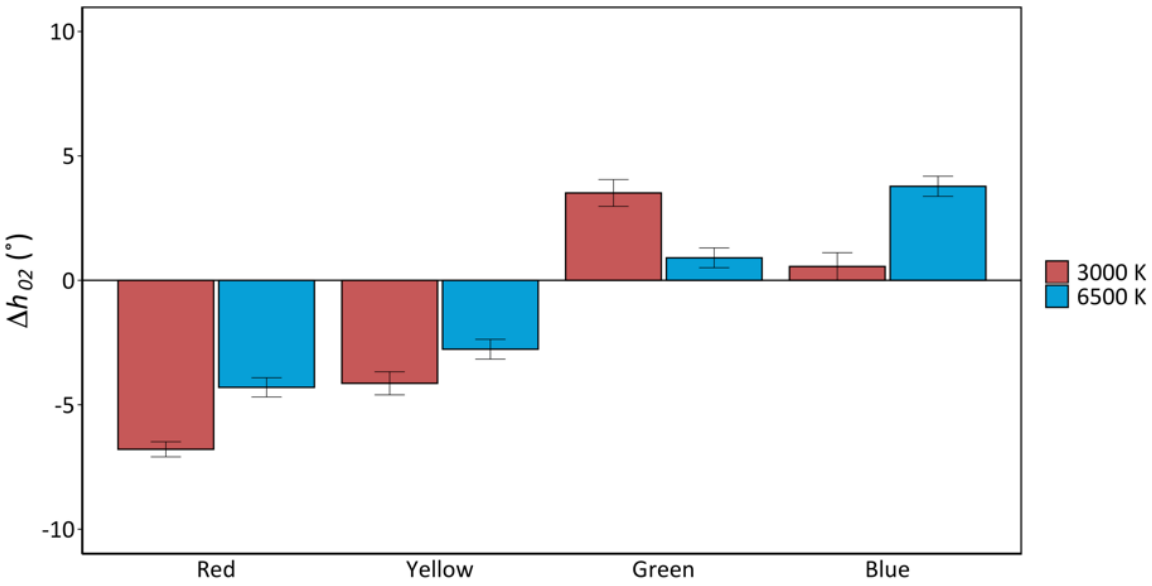

Figure 8 – Hue differences for 3 000 K and 6 500 K. Error bar shows the standard error.

4 Conclusions

The changes in perceived chroma and hue angle between 100 lx and 1 000 lx, by Hunt Effect have been quantified for four different colours. It has been verified that perceived chroma decreases significantly for all four colours in these conditions. As in previous experiments, the green patch showed a greater change in chroma than the red patch. It was also found that yellow and blue had similar chroma change as red. Furthermore, the direction and magnitude

of perceived hue shifts at a lower illuminance level have been quantified. These results may be useful to develop a new colour fidelity model incorporating the Hunt Effect. Further experiments at more different lighting levels are desired.

5 Acknowledgement

The authors thank Semin Oh at Ulsan National Institute of Science and Technology, South Korea, for his valuable contributions in preparing and assisting the vision experiment at NIST. The experiment using human subjects in this study was conducted under NIST Institutional Review Board approval PML-16-0001.

References

BARTLESON, C.J. 1961. Color in Memory in Relation to Photographic Reproduction. *Photogr. Sci. Eng.*, 5(6), 327–331.

CHAMBERS, J.M., HASTIE, T.J. (Eds.) 1992. Statistical Models in S. New York: Chapman and Hall/CRC. DOI: 10.1201/9780203738535

CIE 2017. CIE 224:2017. *CIE 2017 Colour Fidelity Index for Accurate Scientific Use*. Vienna: Commission Internationale de l'Eclairage.

CIE 1995. CIE 013.3-1995. *Method of Measuring and Specifying Colour Rendering Properties of Light Sources*. Vienna: Commission Internationale de l'Eclairage.

HUNT, R.W.G. 1950. The Effects of Daylight and Tungsten Light-Adaptation on Color Perception. *J. Opt. Soc. Am.*, 40(6), 362–371. DOI: 10.1364/JOSA.40.000362

IES 2015. ANSI/IES TM-30-15. *IES Method for Evaluating Light Source Color Renditon*. New York: Illuminating Engineering Society of North America.

JUDD, D.B. 1967. The Flattery Index for Artificial Illuminants. *Illum. Eng.*, 62(10), 593–598.

KAWASHIMA, Y., OHNO, Y. 2019a. VISION EXPERIMENT ON VERIFICATION OF HUNT EFFECT IN LIGHTING, in: PROCEEDINGS OF the 29th Quadrennial Session of the CIE. International Commission on Illumination, CIE, 496–504. DOI: 10.25039/x46.2019.OP68

KAWASHIMA, Y., OHNO, Y. 2019b. QUANTIFYING PERCEIVED CHROMA CHANGES BY HUNT EFFECT IN LIGHTING, in: PROCEEDINGS OF the 29th Quadrennial Session of the CIE. International Commission on Illumination, CIE, 698–705. DOI: 10.25039/x46.2019.PP06

NEWHALL, S.M., BURNHAM, R.W., CLARK, J.R. 1957. Comparison of Successive with Simultaneous Color Matching. *J. Opt. Soc. Am.*, 47(1), 43. DOI: 10.1364/JOSA.47.000043

SANDERS, C.L. 1959. Color Preference for Naural Objects. *Illum. Eng.*, 54(7), 452–456.

THORNTON, W.A. 1974. A Validation of the Color-Preference Index. *J. Illum. Eng. Soc.*, 4(1), 48–52. DOI: 10.1080/00994480.1974.10732288

VON BEZOLD, W. 1873. Ueber Das Gesetz Der Farbenmischung Und Die Physiologischen Grundfarben. *Ann. der Phys. und Chemie*, 226(10), 221–247. DOI: 10.1002/andp.18732261004

International Commission on Illumination
Commission Internationale de l'Eclairage
Internationale Beleuchtungskommission

OP02

VISION EXPERIMENT II ON PERCEPTION OF CORRELATED COLOUR TEMPERATURE

Semin Oh et al.

DOI 10.25039/x47.2020.OP02

Paper accepted for the 5th CIE Symposium on Colour and Visual Appearance

The paper was selected by the International Scientific Committee (ISC) for presentation at the 5th CIE Symposium on Colour and Visual Appearance, Hong Kong, CN, April 21–22, 2020, which, due to the corona pandemic, could not take place. The paper has not been peer-reviewed by CIE.

CIE Central Bureau
Babenbergerstrasse 9
A-1010 Vienna
Austria
Tel.: +43 1 714 3187
e-mail: ciecb@cie.co.at
www.cie.co.at

OP02

VISION EXPERIMENT II ON PERCEPTION OF CORRELATED COLOUR TEMPERATURE

Oh, S.[1], Kwak, Y.[1], Ohno, Y.[2*]
[1] Ulsan National Institute of Science and Technology, Ulsan, SOUTH KOREA
[2] National Institute of Standards and Technology, Gaithersburg, Maryland, USA
ohno@nist.gov

Abstract

This study investigates which chromaticity space, (*u, v*) or (*u', v'*), has a better correlation with human perception when correlated colour temperature is calculated. The vision experiment was conducted using the NIST Spectrally Tuneable Lighting Facility simulating a real-size interior room. A total of 22 subjects evaluated eight different test lighting settings at 2 700 K, 3 500 K, 4 500 K, and 6 500 K with D_{uv} shifts of +0.015 or –0.015. The results showed that the (*u', v'*) chromaticity space was better at a low CCT, 2 700 K, but the results were neutral or (*u, v*) slightly better at high CCTs. The difference depending on CCT can be explained from MacAdam ellipses, i.e., the shape of the ellipses is circular at lower CCTs on the *(u', v')* diagram and deviates from circle as CCT goes higher. There were also differences with subjects' age observed.

Keywords: correlated colour temperature, chromaticity coordinates, visual perception, LED, MacAdam ellipses

1 Introduction

Correlated colour temperature (CCT) is defined by Commission Internationale de l'Eclairage (CIE, 2019), and according to the definition, CCT is calculated as the nearest point to the Planckian locus on the CIE 1960 (*u, v*) chromaticity diagram, which is obsolete. It is questioned in the lighting community why this obsolete chromaticity space is still used and whether the (*u', v'*) chromaticity space would provide better correlation for CCT with human perception. CIE Division 1 established a reportership DR1-67 (Revisiting correlated colour temperature) to investigate this question.

In 2017, our previous study showed that using the *(u', v')* chromaticity space provided overall better correlation with human perception (Kwak et al., 2017), however, futher experimental data were desired to make conclusive recommendations. This previous study used a double-booth with subjects comparing the perceived colours of white sheets. The present study is to provide additional visual data on which chromaticity space, *(u, v)* or *(u', v')*, has better correlation in the perception of CCT. The experiment was conducted using the National Institute of Standards and Technology (NIST) Spectral Tuneable Lighting Facility (STLF) (Miller et al., 2010) simulating an interior room with some furniture and ornaments, for the conditions closer to real lighting applications, at different CCT conditions, 2 700 K, 3 500 K, 4 500 K and 6 500 K.

2 Vision experiment

2.1 Experimental facility

The vision experiment was conducted in a room cubicle (2.4 m × 2.4 m × 2.4 m) of the NIST STLF simulating an interior room with the LED light sources installed at the ceiling of the space. Figure 1 (a) shows a photo of an experiment scene and Figure 1 (b) shows the spectral power distributions (SPDs) of 25 LED channels installed in the NIST STLF. The room cubicle was decorated with some furniture and objects to make the place feel natural. Subjects sat on the couch during the experiment sessions and were asked to look around the entire room space when comparing the lighting colours.

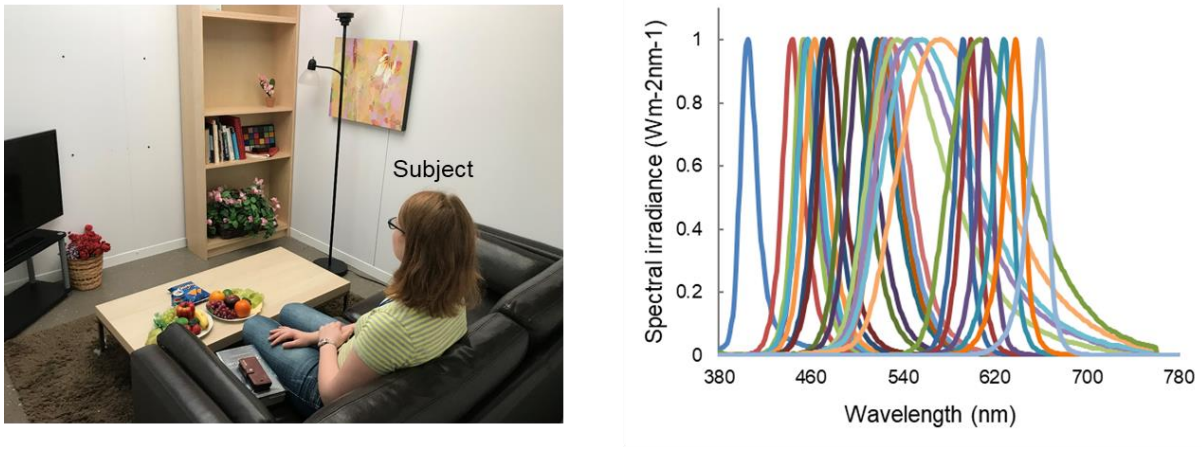

a) Experimental settings

b) The SPDs of 25 LED channels in the NIST STLF

Figure 1 – Experimental settings (left) and the SPDs of 25 LED channels in the NIST STLF (right)

2.2 Reproducibility of STLF

The reproducibility of the chromaticity settings on the NIST STLF at four CCT conditions (the reference spectra described in 2.3) were measured 40 times on different dates over the course of the experiment, thus, a total of 160 measurements were made. The chromaticity and illuminance (set to 300 lx) of the lighting settings were measured on the centre of the table in the room cubicle.

Table 1 summarizes the STLF reproducibility measurement results. Each value shows the average of 40 measurements and its standard deviation. The facility had been very reproducible that its deviation was far less than 1% in all measurement quantities.

Table 1 – The NIST STLF reproducibility test results

Target value		Mean measurement value (±SD)		
CCT (K)	Illuminance (lx)	CCT (K)	Illuminance (lx)	D_{uv}
2 700	300	2704 ± 4	299.5 ± 1.61	-0.0001 ± 0.0001
3 500	300	3487 ± 26	300.9 ± 1.64	0.0001 ± 0.0001
4 500	300	4499 ± 8	299.2 ± 1.53	0.0004 ± 0.0001
6 500	300	6485 ± 16	302.3 ± 1.55	0.0003 ± 0.0001

The colour quantities and illuminance of the lights were measured on the centre of the table in the cubicle. The measurements were made using an array type spectroradiometer with a small integrating sphere input for cosine response, calibrated with a NIST spectral irradiance standard (NIST, 2011). The spectroradiometer measured spectra and illuminance on the table from the 2π solid angle including light from the entire room including reflections from the walls and other objects as well as from the light source itself. The estimated expanded uncertainties (k=2) of measurements varied depending on the spectra, but in all cases, they were within 0.0012 in u', 0.0011 in v', 0.0009 in D_{uv}, 22 K in CCT at 2 700 K, 34 K at 3 500 K, 50 K at 4 500 K, and 92 K at 6 500 K. The expanded uncertainty of illuminance of the spectroradiometer is estimated to be 3 % (k=2) for directional incident light, and its uncertainty for relative measurement was 0.1 %, which is the typical repeatability of the instrument. Also, when the spectrum is changed

on STLF, the spectrum and colour are switched instantly and stable immediately so that sequential comparison of lights was possible.

2.3 Experimental lighting settings

The experiments were conducted for four CCT conditions; 2 700 K, 3 500 K, 4 500 K, and 6 500 K with shifts from the Planckian locus, expressed by D_{uv}. D_{uv} is defined as "the closest distance of the chromaticity coordinates of a light source from the Planckian locus on the (*u'*, 2/3 *v'*) chromaticity diagram and is positive if the chromaticity coordinate of the light source is above the Planckian locus or negative if it is below the Planckian locus" (CIE, 2018).

Figure 2 (a) shows all the lighting settings used in the experiment presented on the *(u', v')* chromaticity diagram, and Figure 2 (b) is a magnified figure for only 6 500 K positive D_{uv} condition. In each CCT condition, two test lights were set for D_{uv} shifts of either +0.015 or –0.015 (black squares in Figure 2). Therefore, the test lights were the off-Planckian points, and each was compared to two reference lights, one being the point on the Planckian locus that had the same CCT calculated under the (*u, v*) diagram (blue circles in Figure 2), and the other being the point on the Planckian locus that had the same CCT calculated under the (*u', v'*) diagram (green circles in Figure 2). Before comparing each pair of lights, subjects were adapted to the midpoint of chromaticities among the test light and two reference lights (so the points at D_{uv}= +0.0075 or -0.0075, yellow diamonds in Figure 2). The illuminance of all lights (test and reference) was set to 300 lx measured at the centre of the table placed at the STLF cubicle.

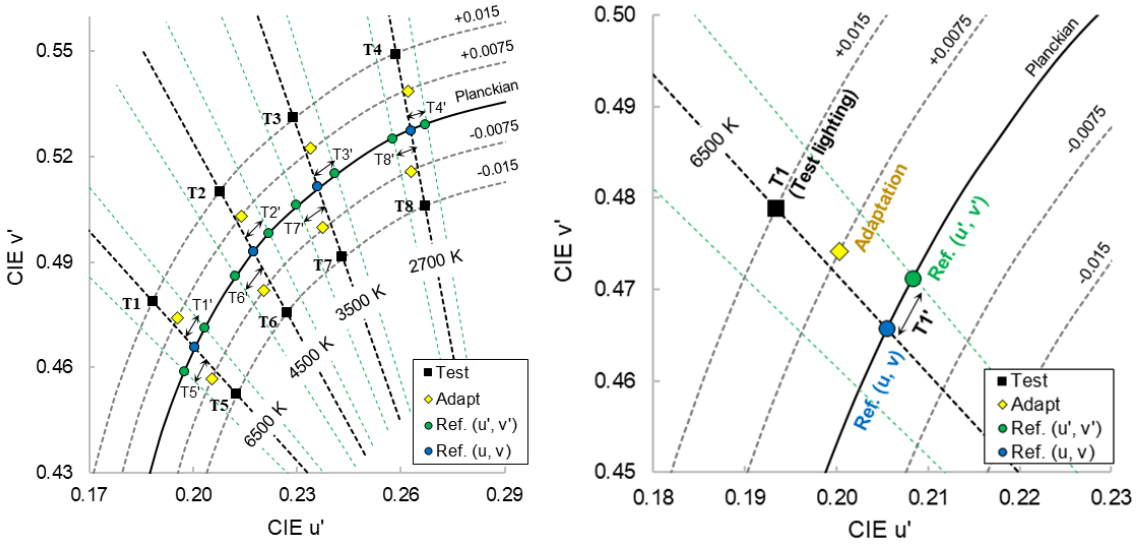

(a) Showing all four CCTs

(b) 6500 K, D_{uv} +0.015 condition magnified

Figure 2 – Test lights, reference lights, and adaptation lights used in the experiment, (a) plotted on the (*u', v'*) chromaticity diagram, and (b) 6 500 K D_{uv} +0.015 condition magnified

As shown in Figure 2 (b), the test light at 6 500 K with D_{uv} shift of +0.015 (T1) is compared to two points on the Planckian locus (T1' pair), one is the point of 6 500 K calculated under the current CCT definition based on (*u, v*) diagram (blue circle), and the other point (green circle) is the point of 6 500 K calculated based on the (*u', v'*) chromaticity diagram. Therefore, it directly compares which chromaticity space, either (*u, v*) or (*u', v'*), resembles the test light better in the perception of CCT.

Figure 3 shows the SPDs of all lighting settings used in this study. To minimize the effects of colour rendition properties in the experiment, broadband spectra were used though there were some peaks in the spectrum due to limitation of the available LED channels of STLF.

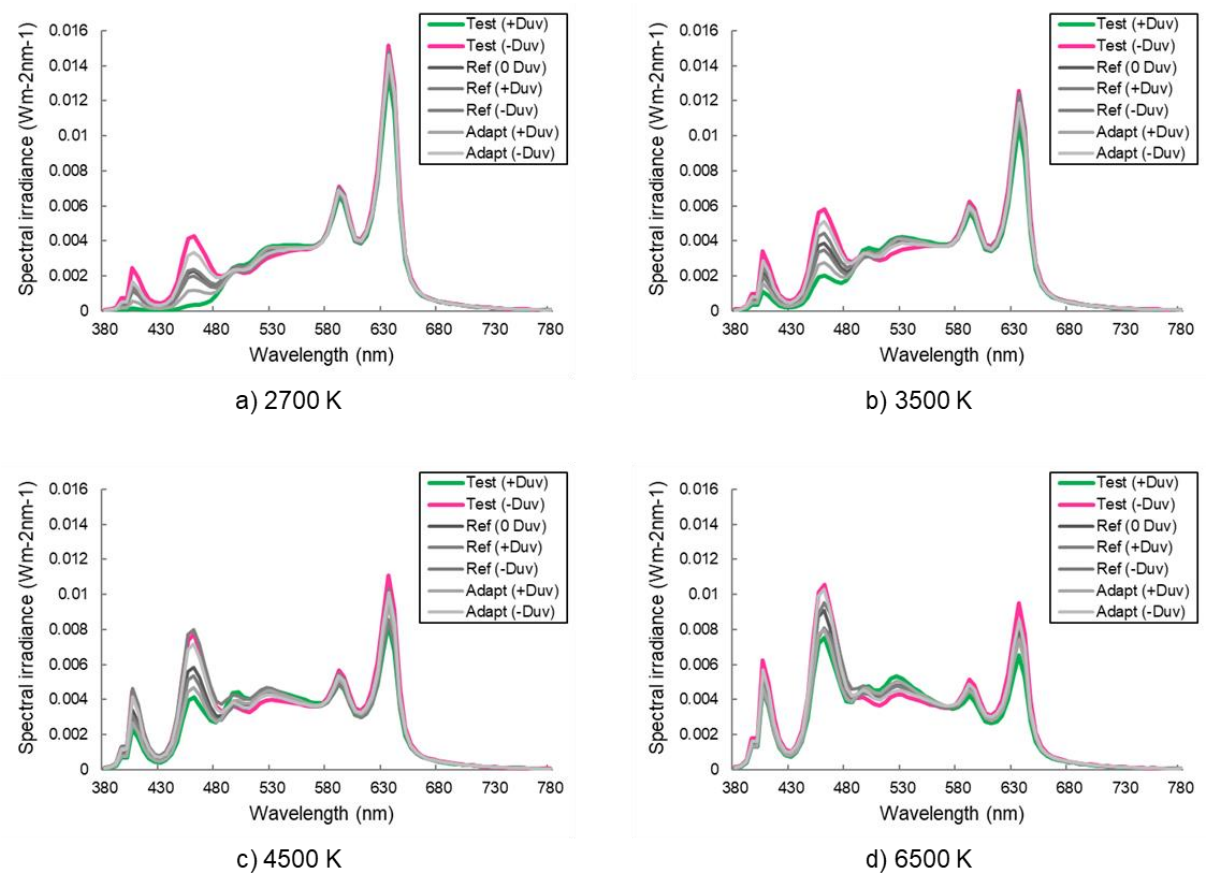

Figure 3 – The SPDs of all lighting settings used in the experiment

2.4 Experimental procedures

Figure 4 summarizes the experimental procedure.

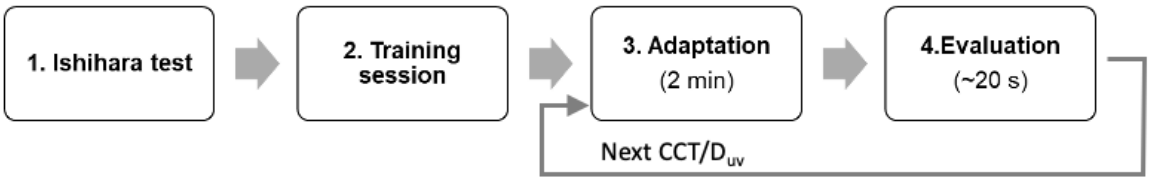

Figure 4 – The flow chart of the experimental procedure

First, all subjects, upon their arrival, had the Ishihara colour vision test under the 4 500 K reference light condition, then introduction was given for the experimental procedures. Prior to the experiment, there was a training session using one or two test light conditions for the subjects to get used to the experimental task. Then, the subject was adapted to the adaptation light for the first test condition for 2 min. After the adaptation, the test light and two reference lights were compared. Test light was called 'Test', the reference light having the same CCT on *(u, v)* was called 'A' and the reference light having the same CCT on *(u', v')* was called 'B'. The lights were presented sequentially in the order, Test-A-B for about 3 seconds each and repeated for Test-B-A. Each subject assessed which of reference light, 'A' or 'B', appeared closer to the test light. It was a forced choice, but subjects were also asked to add 'difficult' if judgement was difficult. The viewing time (3 s each light) was kept short so that the chromatic adaptation condition (to the adaptation point) was maintained during the comparison. Then, the experiment was repeated for other CCT/D_{uv} conditions. The orders of the CCT conditions and D_{uv} (positive or negative) in each CCT were randomly chosen for each subject. An example of the experimental scenes is shown in Figure 1 (a).

2.5 Subjects

For the experiment, a total of 22 subjects were recruited from among NIST employees (having no expert knowledge on lighting) and summer internship students. There were 11 males and 11 females, the age of the group being from 18 to 64 years, and most were Caucasian except three. All subjects had a normal colour vision.

3 Results and discussion

3.1 Data analysis method

To analyse the data, the answer 'A' *(u, v)* was converted to a value of 1 and 'B' *(u', v')* to -1. In case of the 'difficult' answer, it was considered half of the full evaluation. For example, 0.5 point was given when subject chose 'A' but said it was difficult. After the conversion, all subjects' responses were averaged.

3.2 CCT perception experiment results

Figure 5 shows the averaged CCT perception experiment results according to eight different test lighting settings. If the CCT perception score is close to 1, the *(u, v)* chromaticity space works better, otherwise if the value is close to -1, the *(u', v')* is better.

As shown in the figure, it was clear that the *(u', v')* chromaticity space performed better for lower CCT, 2 700 K, especially on the positive D_{uv} test light For the other CCT conditions, there were no significant differences in scores except at 4 500 K positive D_{uv} where *(u, v)* was slightly higher. The result was still not conclusive, except 2 700 K, as the scores were low (absolute values less than 0.3.

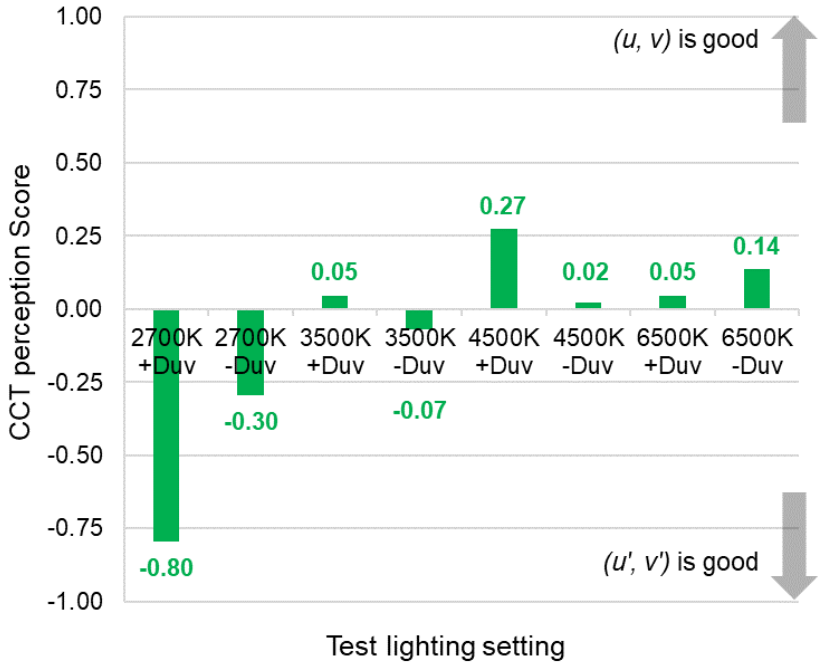

Figure 5 – The averaged CCT perception experiment results

3.3 Results over subject's age

The results were also compared for two different age groups – the older (age 40 or higher, N=7) and the younger (below age 40, N=15). The age 40 was chosen because the aging in the eye is known to begin from the early to mid-40s (American Optometric Association, n.d.).

Figure 6 shows the results of the CCT perception experiment comparing the younger and the older groups.

In 2 700 K, both age groups evaluated the *(u', v')* was better. In the other CCTs, results were different for different age groups. The older group chose *(u', v')* better except the 4 500 K condition, regardless of the D_{uv} direction. However, the younger group evaluated the *(u, v)* better at 3 500 K and 6 500 K, which was the opposite from the older group's result. In case of 4 500 K condition, it was dependent on the D_{uv} direction, i.e., the *(u, v)* was better at +0.015 D_{uv} and the *(u', v')* was better at –0.015 D_{uv}.

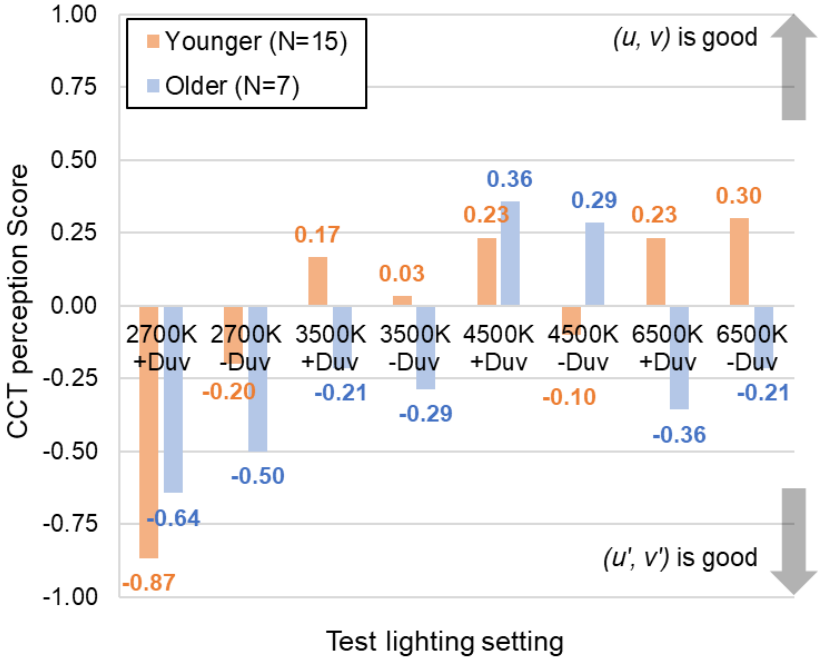

Figure 6 – The experimental results according to subject's age

3.4 Comparison to the results of the previous (2017) experiment

The results of our experiment in 2017 (Kwak et al, 2017) were re-analysed to be compared with the results of the current study in the same format. In the 2017 results, a value of 1 or -1 was given to each subject when his/her response supported (*u, v*) or (*u', v'*), respectively, in the haploscopic and non-haploscopic experiments, and the average values of all subjects for each CCT/D_{uv} condition were calculated. Figure 7 shows the summary results presented in the same format as in Figure 5. Although this experiment was conducted only at two CCTs (3 000 K and 5 500 K) and the number of subjects were limited (12 for haploscopic, 6 for non-haploscopic), the results showed a similar trend that (*u', v'*) was strongly supported at lower CCT (3 000 K) and not consistent or conclusive at higher CCT (5 500 K). The results especially with the non-haploscopic experiment, which was a similar viewing condition to the current study, agreed well with the results of the current study.

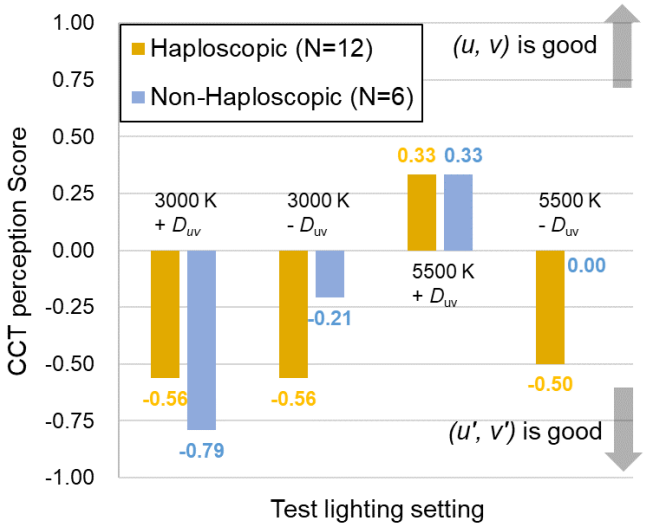

Figure 7 – The results of NIST 2017 experiment analysed in the format of Figure 5.

3.5 Discussion: CCT perception vs. MacAdam ellipses

The experiment results showed that, lower CCT correlates better with the (*u', v'*) chromaticity space, and the results were not conclusive at higher CCTs and (*u, v*) tends to be slightly better at higher CCTs. This trend can be related to MacAdam ellipses (MacAdam, 1942).

Figure 8 shows the 5-step MacAdam ellipses for the range of 2 700 K–6 500 K (IEC 1997) plotted on (*u', v'*) diagram (a) and on (*u, v*) diagram (b). Note that the form of the ellipse (grey circle) is five times the size of just noticeable colour differences from the centre of the ellipse. See also (CIE, 2014) on a similar graphic presentation of MacAdam ellipses.

Figure 8 (a) shows that the shape of the ellipses is almost circular at 2 700 K and 3 000 K on (u', v') diagram, and its shape becomes more oval at higher CCTs. On the other hand, Figure 8 (b) shows the opposite; the shape of the ellipses is near circular at 6 500 K and 5 000 K, and its shape becomes more oval at lower CCTs. This indicates that the *(u', v')* diagram is more uniform at low CCTs with respect to perceived colour differences and the (*u, v*) is more uniform at high CCTs. Although the results of the experiment did not show that (*u, v*) is definitely better at 6 500 K, the overall trend of the results with different CCTs agrees with what MacAdam ellipses indicate.

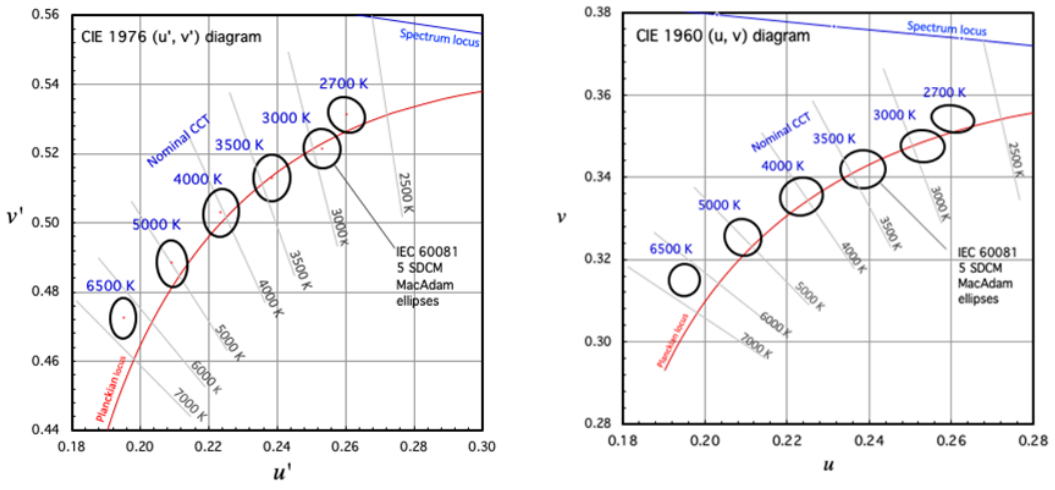

(a) Plotted on *(u', v')* diagram (b) Plotted on *(u, v)* diagram

Figure 8 – The 5-step MacAdam ellipses on (*u', v'*) diagram (a) and on (*u, v*) diagram (b)

4 Conclusion

The vision experiment showed that the (*u', v'*) chromaticity space has better visual correlation with perception of CCT at 2 700 K, while the results at higher CCTs were rather neutral or not conclusive. The results also depended on the age of subjects. Older subjects tend to support *(u', v')* more than younger subjects. The experiment results generally agreed with the results obtained by our previous study (Kwak et al, 2017). With the results for lower CCTs (2 700 K and 3 000 K in the current and previous studies) strongly supporting the *(u', v')* chromaticity space, and also considering the importance of warmer colours of lamps common for indoor lighting, we judge that a CCT definition based on the (*u', v'*) will serve better for the users of lighting. This study performed the experiment in a room-like space, so the situation was more likely to be the scenario of a real-life experience, adding to the more fundamental results obtained from our previous study. Further studies by other institutions are desired to provide more conclusive recommendation. Also, CCT is used not only for lighting but also other applications such as displays. It is hoped that similar studies will be done for such different applications.

References

American Optometric Association (AOA). Adult Vision: 41 to 60 Years of Age. www.aoa.org/patients-and-public/good-vision-throughout-life/adult-vision-19-to-40-years-of-age/adult-vision-41-to-60-years-of-age#1

CIE, 2014. CIE TN 001:2014. Chromaticity Difference Specification for Light Sources

CIE, 2018. CIE 15:2018. Colorimetry, 4th ed.

CIE, 2019. CIE FDIS 017:2019. ILV: International Lighting Vocabulary, 2nd ed.

IEC. 1997. IEC 60081. Double-capped fluorescent lamps – Performance specifications, Annex D.

MacAdam, D. L. 1942. Visual sensitivities to colour differences in daylight. J. Opt. Soc. Am. 32, 32(5), 247-274. DOI:10.1364/JOSA.32.000247.

Kwak, Y., Ha, H., Ohno, Y. 2017. VISION EXPERIMENT ON PERCEPTIN OF CORRELATED COLOUR TEMPERATURE. CIE x044:2017 Proc. of the Conference at the CIE Midterm Meeting 2017, CIE, 512-521. DOI:10.25039 x44.2017. PP06.

Miller, C., Ohno, Y., Davis, W., Zong, Y., and Dowling, K. 2010. NIST spectrally tunable lighting facility for lighting related to vision science experiments, CIE x034 Selected Papers of the Light and Lighting Conference with Special Emphasis on LEDs and Solid State Lighting, May 2009, pp.89-93.

Yoon, H. W. and Gibson, C. E. 2011. NIST Special Publication 250-89 Spectral Irradiance Calibration.

International Commission on Illumination
Commission Internationale de l'Eclairage
Internationale Beleuchtungskommission

OP05

OBSERVER CMF BASED VISUAL APPEARANCE COMPENSATION FOR NOVEL LIGHT SOURCE PROJECTION SYSTEM

Chris Yi-Ho Bai et al.

DOI 10.25039/x47.2020.OP05

Paper accepted for the 5th CIE Symposium on Colour and Visual Appearance

The paper was selected by the International Scientific Committee (ISC) for presentation at the 5th CIE Symposium on Colour and Visual Appearance, Hong Kong, CN, April 21–22, 2020, which, due to the corona pandemic, could not take place. The paper has not been peer-reviewed by CIE.

CIE Central Bureau
Babenbergerstrasse 9
A-1010 Vienna
Austria
Tel.: +43 1 714 3187
e-mail: ciecb@cie.co.at
www.cie.co.at

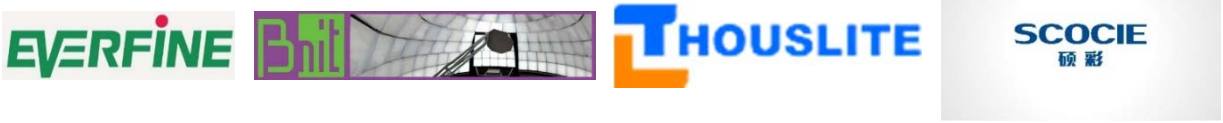

OP05

OBSERVER CMF BASED VISUAL APPEARANCE COMPENSATION FOR NOVEL LIGHT SOURCE PROJECTION SYSTEM

Bai, C.Y.H.[1,2], Tseng, C.F.[1], Lu, T.Y.[1,2], Ou, L.C.[1]
[1] Graduate Institute of Applied Science and Technology, National Taiwan University of Science and Technology, Taipei, CHINESE TAIPEI,
[2] Color Technology Lab, BenQ Corporation, Taipei, CHINESE TAIPEI
D10022503@mail.ntust.edu.tw

Abstract

As display technology expands the color gamut, the potential of experiencing observer metamerism is more likely with narrow bandwidth stimuli displays. Hence, it is desired to investigate whether laser-based projector would introduce observer metamerism compared to halogen-based projector. In addition, it is also desired to develop a quick method to determine an observer's color matching function category.

In this study, a two-part experiment was designed and conducted. Experiment 1 was based on color patches and Experiment 2 was based on test images. The quick method was developed in Experiment 1. Comparison to CIE Standard Observer was also conducted, and the results had suggested the CIE Standard Observer was not suitable for laser-based projection system.

In Experiment 2, a prediction was made to determine the image category. With the quick method, it is much easier to achieve the realization of personalized color management system, hence, reducing the issue of observer metamerism.

Keywords: Observer Metamerism, Observer Category, Projector

1 Motivation and Introduction

As technology evolves, novel light source has been introduced in projection systems to save energy and to expand colour gamut. Novel light source can be LED or Laser based. In order to achieve the two objectives, the light source has to be very efficient in matching human luminous efficiency function V(λ), and also has very narrow bandwidth in R, G, and B primaries. However, an unpredictable drawback is the increased degree of observer metamerism (Asano, 2014). The phenomenon is exhibited when two stimuli with very different spectral power distribution can generate the same cone response (Sarkar, 2010), leading to the same tristimulus values. This is called a metameric match. However, the match is often valid only with one observer and exhibits as a mismatch to another observer under the same condition. Since the second observer has a set a different colour matching functions (CMFs) than the first observer, hence, the metameric match fails, and this is commonly referred as observer metamerism (Chen, 2019).

Observer metamerism may cause an issue in real world applications such as soft proofing and colour grading scenarios. In Alfvin and Fairchild (1997), and Rich and Jalijali's (1995) work, both studies has shown large observer variability which exhibited a serious issue for soft proofing scenario. Asano et al. (2014) utilized colour images in the colour matching experiment on a CCFL backlight LCD monitor and a laser projector for colour grading purpose. The result has also shown that inter-observer variability is larger than intra-observer variability, which indicates observer metamerism can cause a serious issue in colour grading with laser projector.

Since observer metamerism is affecting some real-world applications, it is necessary to look at the solution to this issue. One solution to this issue is to develop a display device which can allow customized CMFs to replace the CIE Standard Observer. The key is how to obtain the personalized CMFs for individual observers. A practical approach to estimate one's CMFs is through predetermined observer CMFs or observer classification since it is not trivial to determine one's CMFs. Sarkar et al. (2010) had developed a method for establishing 8

colorimetric observer categories with two-step algorithm using two spectrally distinctive displays, one CRT monitor and one LED backlight monitor. Colour patches were predicted by different observer categories and displayed on the two displays, and the participants were asked to choose the best matching pair through the experiment procedure. Several base colours were repeated for each participant, and the final observer category was determined by an empirical ranking system to achieve good colour matching among most base colour pairs.

Asano (2015) improved on Sarkar's method, but derived 10 observer categories for his work. A two-step method was utilized in his work, too. A set of 10 000 individual observer CMFs was generated from Monte Carlo simulation, and then a cluster analysis was applied to determine the 10 observer categories (Chen, 2019).

In this study, it is desired to match the colour appearance of the laser-based projection system to the colour appearance of halogen lamp-based projection system. Therefore, it is desired to devise a method to quickly categorize observer's CMFs based on the colours which observer believes they are matched under the two different projection systems. Based on the category, it is desired that the same method can be applied to predict the observer category for images.

2 Experiment

The experiment procedure will be discussed in this section.

2.1 Apparatus Overview

The apparatus used in the experiment is listed and the specification is described in the following:

a. Halogen Lamp Projection System:
   - Model: BenQ LX810STD
b. Blue Laser Projection System:
   - Model: BenQ MX600
c. Projection Screens:
   - Model: Elite Screens
   - 100" 16:9 aspect ratio (Height * Width: 185 cm * 104 cm)
   - Gain: 1:1
   - Viewing Angle: 160°

2.2 Quick Method to Determine Observer Colour Matching Functions

From previous studies, it is desired to determine observer's colour matching function for each person. However, to determine the exact colour matching function often takes enormous amount of time and energy. Hence, it is much more desirable to devise a method to quickly categorize observer's colour matching functions.

The logic behind devising the quick method is described in the following:

The deviation in each individual observer will cause perceived colour difference among different observers even the measured values are the same. The phenomenon is even more sever on modern narrow bandwidth display devices. The idea is to pre-determine a set of colour matching function categories, and using a selection method to determine an observer's category on the novel display. The selection method involves two types of display, one is the narrow bandwidth display, and another is the broad bandwidth display. Observer population simulation, colour patch selection, pre-determined set of colour matching function categories, and method of category determination are also a part of the selection method, and these will be discussed thoroughly in the following sections.

2.2.1 Observer Population Simulation

In order to obtain the variation of observer CMFs, it is necessary to access the CMFs of a large number of populations. For simplicity of this study, the Monte Carlo Simulation of Observer Colour Matching Functions from RIT was utilized. A 10 000 observers were generated using the generator with age between 20 to 30 years old, which fits with the participants age group in both experiment 1 and 2. The field size was set at 10 degrees for colour patch matching. The observer variation in colour matching functions is illustrated in Figure 2, where red lines

represents X bar functions, green lines represents Y bar functions, and blue lines represents Z bar functions.

2.2.2 Colour Patch Selection

Colour patches are selected to determine observer's CMFs. However, it is not possible to randomly select colour patches to fulfil the purpose. Therefore, rules had been established based on the population simulated to obtain the variation of observer CMFs to select colour patches for determine a particular observer's CMFs:

1. Larger variation between observers in CMFs,
2. Wavelengths where r, g, b curves intersect, and
3. Two points near the 380 nm and 780 nm where the devices can reproduce the colours.

The selection process is first based on observer variation in CMFs graph obtained from Monte Carlo Simulation, and then verified on characterization model to determine if the device could reproduce the colour accurately. The final wavelengths selected are: 418 nm, 463 nm, 472 nm, 495 nm, 510 nm, 545 nm, 558 nm, 565 nm, 571 nm, 585 nm, 600 nm, 606 nm, 630 nm, and 660 nm. Total of 14 colour patches are selected. The selection is also plotted on Figure 2.

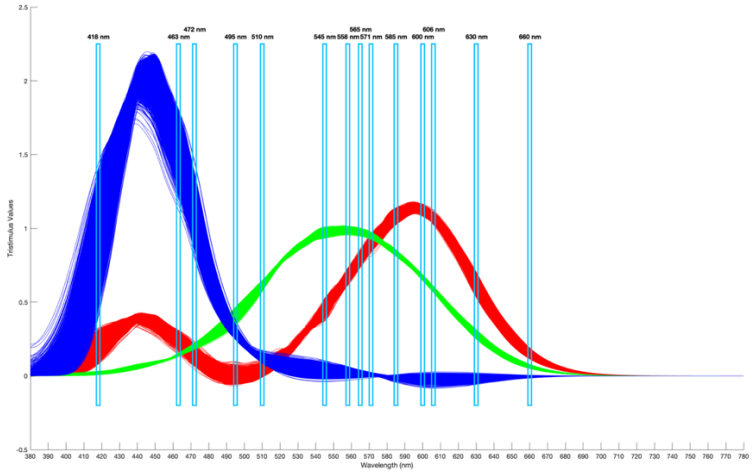

Figure 2 – Final Wavelength Selection based on Monte Carlo Simulation Result

2.2.3 Pre-Determined Colour Matching Function Categories

The pre-determined colour matching function categories are constructed based on the wavelength selected and Monte Carlo Simulation. Seven categories were constructed from the data set with one category consists of the same data as CIE Standard Observer Colour Matching Functions. The other six categories were determined by evenly divided the variation among the observers' colour matching functions from Monte Carlo Simulation, and all seven categories of pre-determined colour matching function categories are illustrated in Figure 3.

2.2.4 Method of Category Determination

The method of category determination used in the experiment is utilizing 'mode' to determine the final category of one observer. The reason behind is it is logical to choose the 'most chosen' category of a particular observer to represent his or her category since the category was chosen when the colour was a match according to the observer. 'Mean' or 'average' category does not represent a meaningful interpretation in this context. For example, if an observer selects the following categories after the experiment: "category 2, category 1, category 2, category 2, category 2, category 3, category 7, category 5, category 2, category 4, category 2, category 2, category 1, category 2", the result would be "category 2" since the most selected category is "category 2".

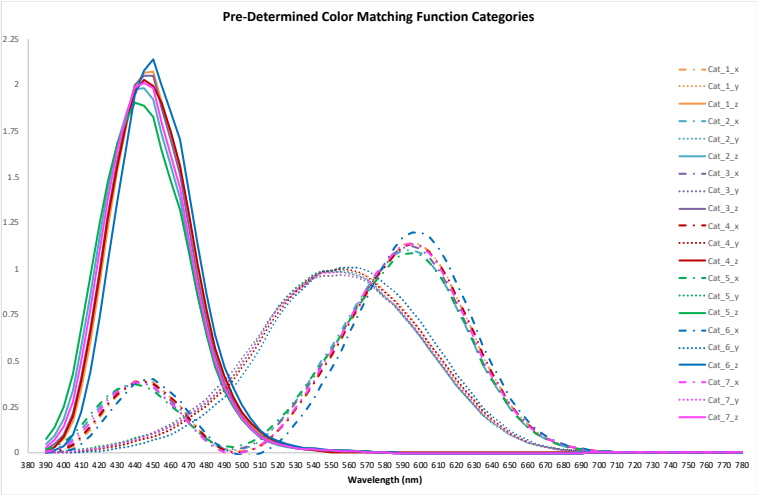

Figure 3 – Pre-Determined Seven Colour Matching Function Categories in xyz Curves

2.3 Experiment 1: Using the Quick Method to Determine Observer Colour Matching Function

A MatLAB program was developed to conduct the experiment using the quick method to determine observer's CMFs. Each session takes about 30 minutes to complete the required task. The experiment setup is illustrated in Figure 4. Please note the distance between the projection screens and the two projection systems are not the same since the focal lengths are not the same for the two projection systems. In order to display the same image size, the distance has to be different. The experiment was conducted in a dark environment, with blue laser projection system projects on the left screen, and halogen lamp projection system projects on the right screen. The halogen lamp projection system servers as the 'reference' display, hence, the colour patches projected are the 'reference patches'. There are 14 reference patches for each observer, and for each reference patch, there are 7 colour patches projected by the blue laser projection system for the observer to choose from. Observer can only choose one colour patch from the 7 colour patches for each reference patch, and has to choose one. All reference patches were shown randomly, and repeated for 3 times. As a result, each observer needs to conduct 42 colour matches. The flow chart of Experiment 1 is illustrated in Figure 5.

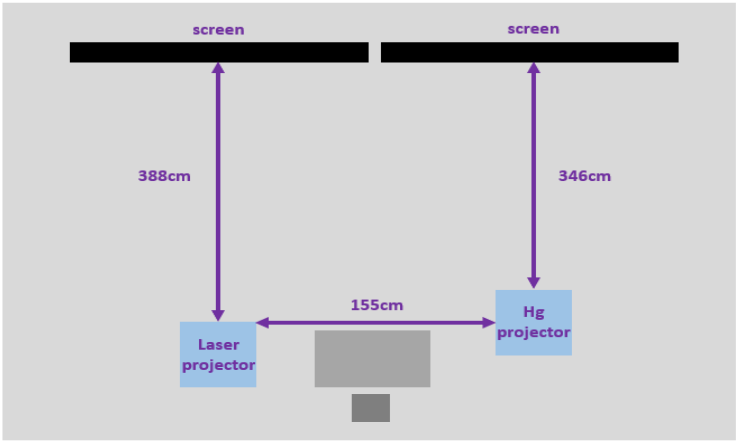

Figure 4 – Illustration of Experiment Setup

On the blue laser projection system screen, there are three buttons to control the flow of the experiment, namely 'Previous', 'Next', and 'Match'. Observer can click on the corresponding button to select the colour patch using 'Previous' or 'Next', or determine if the selected colour patch is a match to the reference patch. If the observer click on 'Match', then the software program will record the colour patch which is a match and display the next reference patch. Between each reference patch, a gray patch will display for 5 second on both projection system

to avoid visual residual effect. The program will continue to display all 42 reference patches and ask for observer's input.

After observer finish all 42 judgement, the program will determine observer's category. However, observer will not know his or her own category since the extra information may interfere with the next experiment.

2.4 Experiment 2: Refining Pre-Determined Categories and Applying Observer Colour Matching Function to Images

There are two goals to be fulfilled in Experiment 2. The first goal is to verify the individual observer colour matching function category can also be applied to images, and it also performs better than the Standard Observer CMFs. The second goal is to utilize the quick method devised in Experiment 1 and to verify the observer category determined by the quick method could correlate to the image category that the observer chosen. The flow chart of Experiment 2 is illustrated in Figure 6. A MatLAB program was developed to conduct the experiment. A set of images was pre-selected and rendered for different observer colour matching function categories. The set of images used in the experiment consists of 8 images and is exhibited in Figure 7.

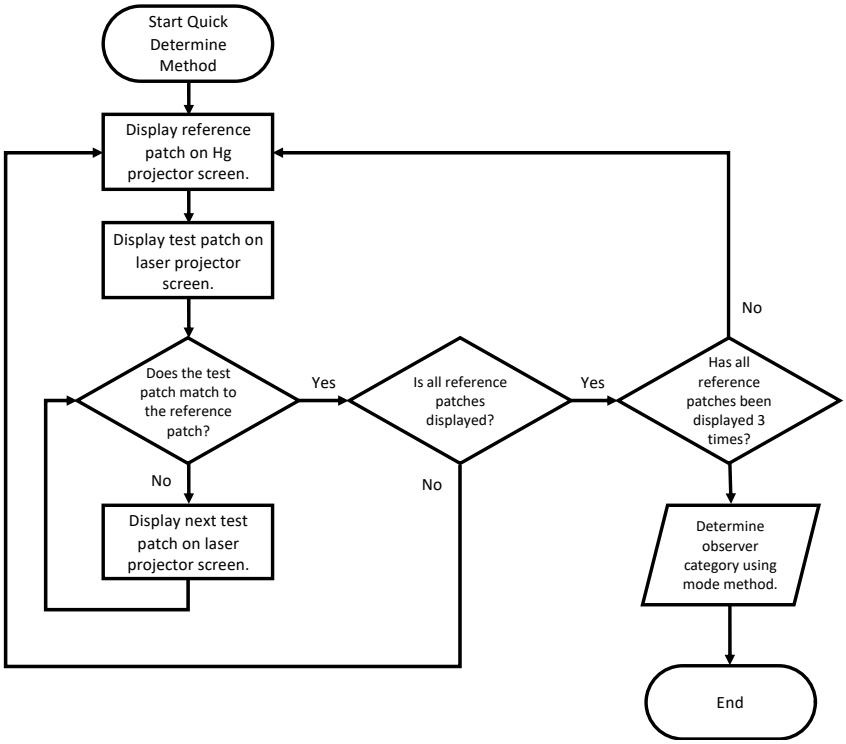

Figure 5 – Flow Chart of the Quick Method to Determine Observer Colour Matching Function

The selection of the 8 images consists of natural colours such as sky, grass, flowers, trees and sunset, skin tone colours, familiar objects, such as cakes, wine bottles, fabrics, music instrument, boats, yarns, crayons, and standard colour patches and neutral colours.

From Experiment 1, it could be concluded that the result could be further grouped into fewer categories. This trend could help further simplifying the experiment. By grouping into fewer number of new categories, observers could be more focused and judging less comparison. Observers were asked to conduct a quick method of colour patch determination first (without repetition), and then followed by the image experiment part. The same experiment setup, environment and procedure as in Experiment 1 were taken in Experiment 2. The only differences were using images and fewer categories in the image experiment part. Each image was repeated for 3 times, hence, a total of 24 judgement was made for each observer. After the observer finish all 24 judgement, the program will also determine the observer's category for

the image judgement. A comparison with the colour patch category will also be conducted in order to validate the usefulness of the quick method devised in Experiment 1.

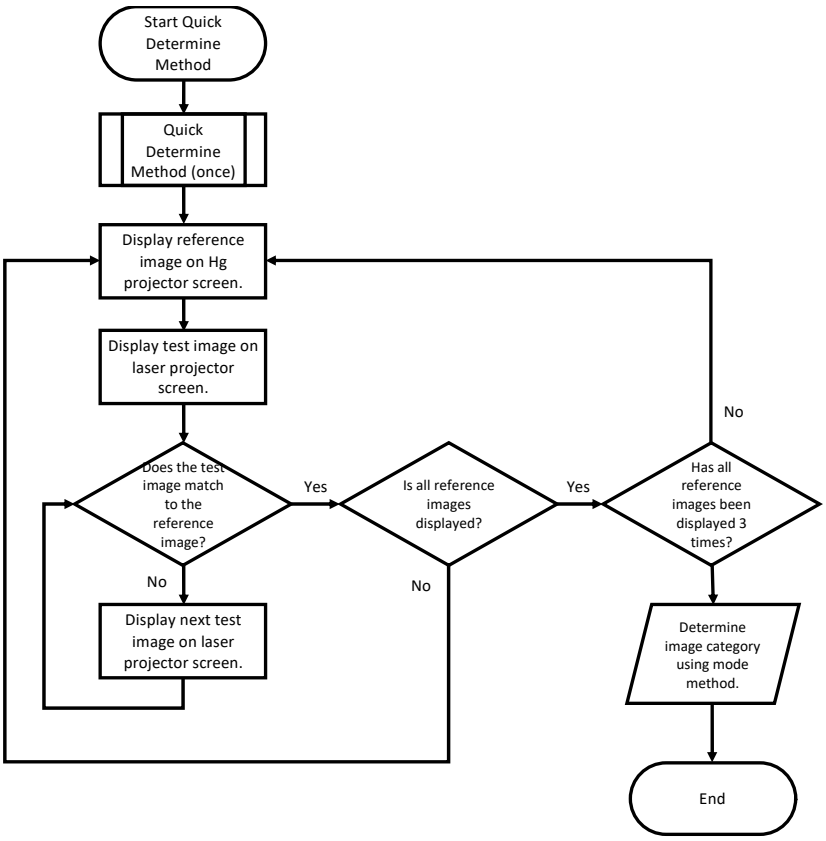

Figure 6 – Flow Chart of Determine Image Category in Experiment 2

Figure 7 – Eight Test Images Used in the Experiment Consisting of Natural Colours, Skin Tones, Familiar Colours and Standard Colour Patches and Neutral Colours

In summary, Experiment 1 investigates the feasibility of the quick method of determining observer colour matching function category using halogen and laser projection systems. In Experiment 2, it will first utilize the quick method to determine the colour matching function category, then conduct the image experiment to determine the image category. It is expected that the quick method could predict the outcome of the image category, and this hypothesis would be verified in Experiment 2. Also, the outcome of both experiments will determine if the CIE Standard Observer is suitable for this group of observer or not.

3 Results and Discussions

In this section, the results and the findings of the experiment will be discussed.

3.1 Results of Experiment 1

Fifty participants were involved in Experiment 1 with 28 male and 22 female university students (age between 20 to 30). When combining all 14 colour patches results together, the response could be plotted in a histogram shown in Figure 8. In Figure 8, the number of categories is plotted against of the responses, and can be concluded that category 5 has the most responses, whereas category 2 has the least responses. Category 4 represents the CIE 1964 10° Standard Observer; however, it does not have the most responses. This leads to the conclusion that the CIE 1964 10° Standard Observer may not be the optimum colour matching function for this group of observers.

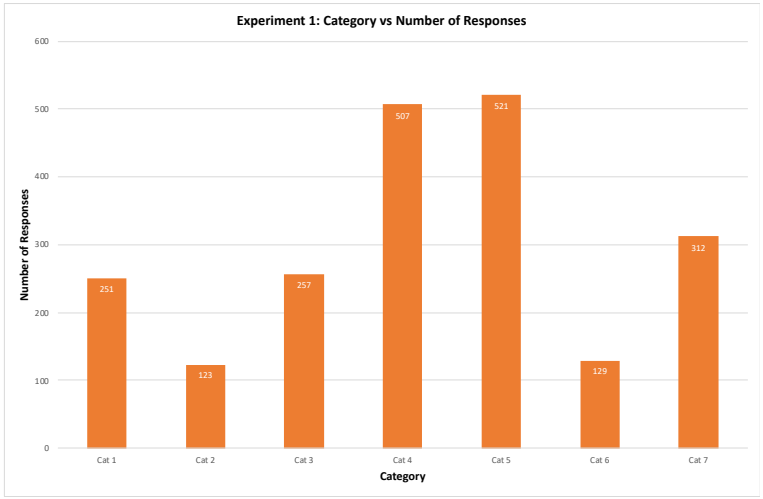

Figure 8 – Category versus Number of Responses for Experiment 1 Result

When all fifty observers' responses are plotted against in terms of X, Y and Z curves, as shown in Figure 9 (a), (b) and (c), respectively, X and Z curves exhibit a clear pattern which can divide all the responses into three groups. Hence, based on the pattern, the X, Y, and Z curves could be divided into three categories and shown in Figure 10 (a), (b) and (c) respectively. The median number was taken to obtain the final X, Y and Z curves.

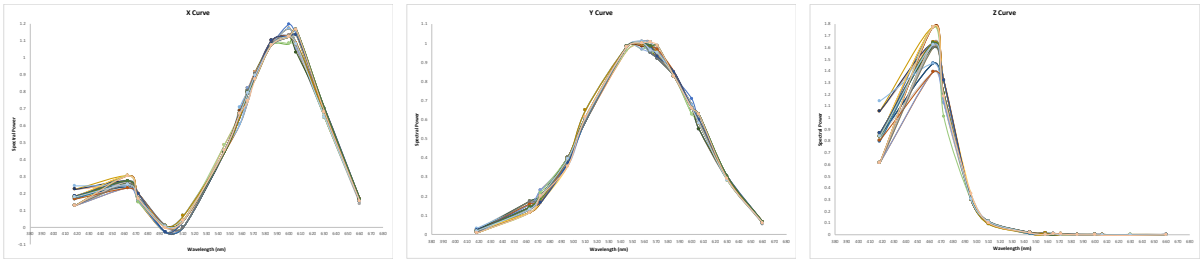

(a) (b) (c)

Figure 9 – (a) All 50 Observers' Responses Plotted in Terms of X Curves. (b) All 50 Observers' Responses Plotted in Terms of Y Curves. (c) All 50 Observers' Responses Plotted in Terms of Z Curves.

3.2 Results of Experiment 2

Thirty participants were involved in Experiment 2 with 18 male and 12 female university students (age between 20 to 30). After the new four observer categories were established (three new observer categories plus the CIE 1931 2° Standard Observer), all the test images were transformed to the new observer categories accordingly. A series of psychophysical experiment were conducted to determine the best matched colour matching function for this group of observers.

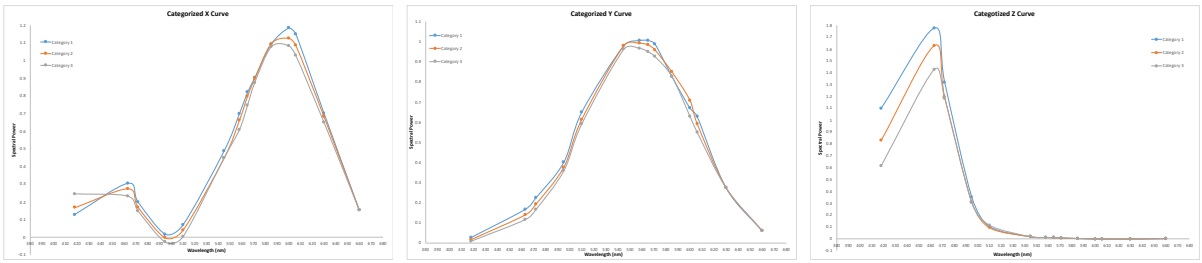

(a) (b) (c)

Figure 10 – (a) Categorized X Curves for All 50 Observers' Responses. (b) Categorized Y Curves for All 50 Observers' Responses. (c) Categorized Z Curves for All 50 Observers' Responses.

3.2.1 Image Preparation

Eight test images were selected for Experiment 2, and the images are exhibited in Figure 7. Test images were carefully selected to enclosed as many hues and scenarios as possible, including grayscale, skin tone, natural scene, familiar and colourful objects. All the test images were transformed by the image pipeline defined in Figure 11.

Figure 11 – Image Pipeline for Transforming Test Images from Standard Observer to New Observer Categories

3.2.2 Data Analysis for Experiment 2 Result

The first goal of Experiment 2 was to verify the individual observer colour matching function category can also be applied to images, and it also performs better than the CIE 1931 2° Standard Observer colour matching function. The result of all thirty observers' responses is shown in Figure 12. From Figure 12, it is obvious to determine that Category 2 was the most representative category for this group of observers. Category 4 represents the CIE 1931 2° Standard Observer; hence, it can be concluded that the new observer category is more preferred than the CIE 1931 2° Standard Observer on the blue laser projection system.

The second goal of Experiment 2 was to utilize the quick method devised in Experiment 1 and to verify the observer category determined by the quick method could correlate to the image category that the observer chosen. The relationship between the new image category used in Experiment 2 and original observer category used in Experiment 1 is described in Table 2. Based on the relationship provided in Table 2, the outcome of the quick method from Experiment 1 had been changed to the new image categories. The results of Experiment 2 are summarized in Table 3. The response from the quick method after converted to the new image categories, the image categories determined from Experiment 2, and whether the predicted category matched to the actual category is indicated in Table 3. There were total of 30 observers participated in Experiment 2, and 18 responses were 'Yes', and 12 responses were 'No'. The prediction successful rate is 60.0 %. The performance of the quick method is not bad given the complex context it needs to handle. But there are certain places can be improved in the future version:

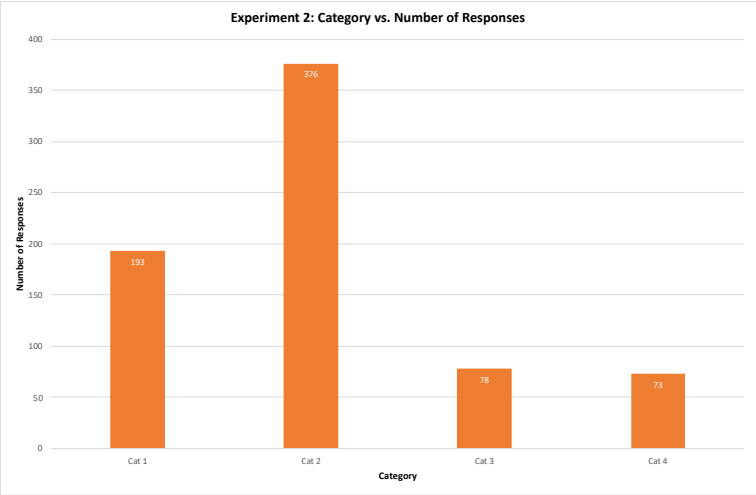

Figure 12 – Category versus Number of Responses for Experiment 2 Result

1) For the quick method to predict the image category, use field size of 2° to conduct the matching rather than 10°.
2) Use a more accurate characterization model for the projection system so that the RGB values interpolated could correspond to the exact wavelength required. A 13x13x13 3D LUT is recommend for this purpose.
3) Eliminate reference colour patches with high 'inconsistent' response rate. Inconsistent response may indicate observers could not find the 'correct' matching test colour patch.

Table 2 – Relationship between the New Image Category and Original Observer Category Used in Experiment 1

New Image Category	Original Category
Category 1	Category 1 & 3
Category 2	Category 2, 5 & 7
Category 3	Category 6
Category 4	CIE 1931 Standard Observer

In summary, two goals set for Experiment 2 were met. The new image category 2 was found to be better suited for the group of observers participated in the experiment than using the CIE 1931 2° Standard Observer. And it was found to be possible to predict the image category from the quick method devised from the colour patch. Although the success rate is 60.0 %, with a few improvements in the future, it could be a viable method to determine observer's individual colour matching category.

Table 3 – Experiment 2 Results Using the Quick Method to Predict Observer's Image Category

Obs	1	2	3	4	5	6	7	8	9	10	11	12	13	14	15
Exp 1	2	1	1	2	2	1	2	1	2	1	2	2	1	1	2
Exp 2	2	1	1	2	2	2	2	2	2	2	2	2	1	2	2
Match	Y	Y	Y	Y	Y	N	Y	N	Y	N	Y	Y	Y	N	Y
Obs	16	17	18	19	20	21	22	23	24	25	26	27	28	29	30
Exp 1	2	2	1	4	2	2	2	4	4	1	2	1	1	1	1
Exp 2	1	2	1	2	1	2	2	2	2	2	2	1	1	2	2
Match	N	Y	Y	N	N	Y	Y	N	N	N	Y	Y	Y	N	N

4 Conclusion

While display technology advances, the enlargement in colour gamut is a particular item needs to be drawn attention to. Large colour gamut could produce to more vivid colours, but also incorporate narrow bandwidth primaries and could lead to higher potential of observer metamerism. Laser projection system is one particular device that suffering from this phenomenon severely. A solution to this is to incorporate individual observer's CMFs in the projection system. Hence, this study focused on whether a quick method could be devised to predict an observer's colour matching function category.

Two experiments were designed and conducted in this study; Experiment 1 was based on 14 reference colour patches, and Experiment 2 was based on 8 test images. After both experiments were conducted, it was found that the current CIE Standard Observer is not suitable for the laser-based projection system. A different observer category was chosen in both experiments for this group of observers. Hence, this concludes that observer metamerism was introduced in laser projection system more severely than halogen-based projection system.

There was a 60.0 % success rate to predict the image category from the quick method using colour patches in Experiment 2. The success rate could be improved if the field size of the colour patches were changed from 10° to 2°, a better characterization model was introduced, and the colour patches with high inconsistency were eliminated. But it is still encouraging that a few simple colour matching trials could determine one's colour matching function category. This is a one missing piece from developing a personalized colour management system in order to have the optimal viewing experience and accuracy.

References

Alfvin R.L., Fairchild M.D., (1997). Observer variability in metameric color matches using color reproduction media. *Color Research and Application.* **22**(3), 174-188.

Asano, Y., Fairchild, M., Blond´e, L., Morvan, P., (2014). Observer variability in color image matching on a LCD monitor and a laser projector. *22nd Color and Imaging Conference and 2nd Congress of the International Academy of Digital Pathology. November 14, 2014. Boston, Massachusetts, USA.* Springfield: Society of Imaging Science and Technology, pp. 1-6.

Asano Y., (2015). *Individual Colorimetric Observers for Personalized Color Imaging*. PhD. thesis, Rochester Institute of Technology.

Chen Q., Feng L., Li Y., Cai S., (2019). Reviews on Observer Metamerism and Individual Color Vision Variability. In: P. Zhao, Y. Ouyang, M. Xu, L. Yang, Y. Ren, eds. *Advances in Graphic Communication, Printing and Packaging, Proceedings of 2018 9th China Academic Conference on Printing and Packaging*. Berlin: Springer. pp. 23-30.

Rich D.C., Jalijali J., (1995). Effects of observer metamerism in the determination of human color-matching functions. *Color Research and Application.* **20**(1), 29-35.

Sarkar A., Blond´e L., Callet P.L., Autrussear F., Morvan P., Stauder J., (2010). A color matching experiment using two displpays: design considerations and pilot test results. *Fifth European Conference on Color in Graphics, Imaging and Vision, CGIV. June 2010, Joensuu, Finland.* Springfield: Society of Imaging Science and Technology, pp. 414-422.

International Commission on Illumination
Commission Internationale de l'Eclairage
Internationale Beleuchtungskommission

PP07

HDR IMAGING FOR LUMINANCE AND MELANOPIC RADIANCE: CAMERAS AND SPECTRAL POWER DISTRIBUTIONSRACT TITLE

Thijs Kruisselbrink et al.

DOI 10.25039/x47.2020.PP07

Paper accepted for the 5th CIE Symposium on Colour and Visual Appearance

The paper was selected by the International Scientific Committee (ISC) for presentation at the 5th CIE Symposium on Colour and Visual Appearance, Hong Kong, CN, April 21–22, 2020, which, due to the corona pandemic, could not take place. The paper has not been peer-reviewed by CIE.

CIE Central Bureau
Babenbergerstrasse 9
A-1010 Vienna
Austria
Tel.: +43 1 714 3187
e-mail: ciecb@cie.co.at
www.cie.co.at

PP07

HDR IMAGING FOR LUMINANCE AND MELANOPIC RADIANCE: CAMERAS AND SPECTRAL POWER DISTRIBUTIONS

Kruisselbrink, T.W., Dangol, R., van Loenen, E.J.
[1] Eindhoven University of Technology, Eindhoven, THE NETHERLANDS
[2] Intelligent Lighting Institute, Eindhoven, THE NETHERLANDS
t.w.kruisselbrink@tue.nl

Abstract

The luminance, measured using HDR imaging, is relevant to achieve quality lighting. However, the accuracy and applicability of such systems are not warranted. In this study, the capabilities of six different cameras to measure the luminance and melanopic radiance were assessed, based on simulations, relative to 205 spectral power distributions. Moreover, the luminance was determined based on the conventional model and an alternative model aiming to limit the spectral mismatch. The spectral responsivity of the cameras as well as the correlated colour temperature and the full spectrum index showed to be affecting the measurement performance. Large gains in performance were achieved if the luminance calculation was optimized by limiting the spectral mismatch (10,3 % to 2,9 %). Moreover, for melanopic radiance measurements, large differences in measurement errors occurred between cameras (20,0 % to 1,9 %). As a result, the camera and luminance calculation model should be chosen carefully.

Keywords: Luminance; Melanopic Radiance; Spectral Mismatch; Camera

1 Introduction

The luminance distribution, relevant for high quality lighting (Gentile et al., 2016; Kruisselbrink et al., 2018; Van Den Wymelenberg, 2012), can be measured using camera-based systems, such as high-end, commercially available, luminance cameras but also using off-the-shelf cameras (Inanici, 2006; Kruisselbrink et al., 2017). These systems generally use High Dynamic Range (HDR) imaging, where sequential exposure bracketing is applied to capture the dynamic range of the real world (Reinhard et al., 2006). Subsequently, the luminance can be determined by combining the Red (R), Green (G) and Blue (B) tristimuli values of each pixel of the HDR image.

Nevertheless, the accuracy and applicability of these camera systems can still be improved. The luminance is generally calculated using fixed weighting factors for the R, G, and B tristimuli originating from the translation of the sRGB to XYZ colour space, irrespective of camera spectral responsivity and scene illuminant. It is believed that this model which uses these fixed weighting factors has an negative impact on the measurement accuracy as they can introduce significant spectral mismatches due to its assumptions (Cauwerts et al., 2019; Kruisselbrink et al., 2019). First, the Spectral Power Distribution (SPD) is generally not identical to the CIE Standard Illuminant D65. Cai performed identical measurements under different types of SPDs and found significant differences in performance (Cai, 2011), indicating that the SPD has an influence on the accuracy. Second, the camera spectral responsivity does not necessarily align with the sRGB responsivity. For instance, Wu et al. indicated that the spectral responsivity of the camera can have severe disparity with the RGB colour space as manufacturers aim to achieve compelling colours (Wu et al., 2019). As a result, different cameras, with different spectral responsivities, might have varying capabilities in terms of luminance distribution measurements.

Moreover, the applicability of luminance cameras can be extended by measuring other spectral sensitivities such as α-opic radiances that are found to be relevant for the Non-Image Forming (NIF) effects of light (CIE, 2018). Especially, the melanopic radiance, impacting the intrinsically photosensitive retinal ganglion cells (ipRGCs) can be considered important as this results in biological and behavioural effects of light (Lucas et al., 2014). However, the integration process

of the different α-opic radiances is not understood completely yet. Therefore, it is recommended to provide all α-opic quantities (n=5). This system is currently also adopted by the CIE (CIE, 2018).

The objective of this study is to simulate the capabilities of six different cameras in relation to luminance measurements using HDR imaging. Moreover, we explore to what extent the accuracy of each camera can be improved by using an alternative model, incorporating the spectral responsivity and the spectral power distribution (SPD), to determine the luminance. Additionally, the alternative model was also applied to explore the feasibility of measuring α-opic radiances using these camera systems, which might make such systems very suited for human centric lighting applications. In this study only the melanopic radiance was simulated using the six different cameras as a proof of principle.

2 Method

Six commercially available cameras were selected, ranging from high-end DSLRs to simple smartphone cameras with, visually, significantly different spectral responsivities. Their spectral responsivities were selected from 400 nm to 720 nm with steps of 10 nm. The green and blue channels of the cameras are illustrated in Figure 1. The spectral responsivities originate from a database by Jiang et al. (2013). The spectral responsivities of HDR images was considered identical to the camera's raw spectral responsivity (Lenseigne et al., 2013). Additionally, 205 SPDs, as illustrated in Figure 2, of light sources that are commercially available were collected, containing LEDs (117), fluorescents (35), incandescent (17), halogens (31), metal halides (4) and sodium pressure lamps (1) from 300 nm to 900 nm with steps of 0,5 nm originating from the LSPDD database by Roby and Aubé (2012).

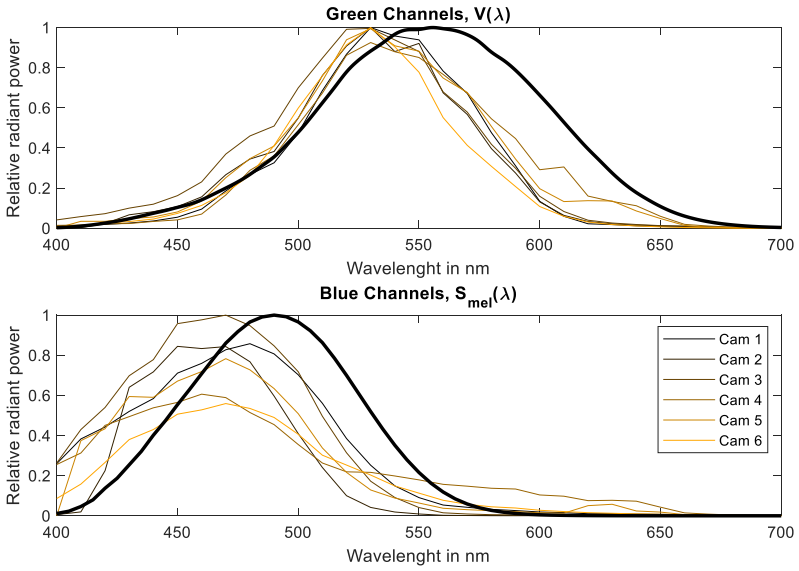

Figure 1 – The spectral responsivities of the green and blue channels of the 6 cameras. Additionally, the luminous efficiency curve $\mathbf{V}(\boldsymbol{\lambda})$ and the melanopic sensitivity $\mathbf{S_{mel}}(\boldsymbol{\lambda})$ are illustrated in black.

The luminance, considering one single pixel, was calculated based on simulations, using MATLAB r2017a, for all 205 SPDs using the spectral responsivities of the six cameras and two distinct luminance models that were proposed by Kruisselbrink et al. (Kruisselbrink et al., 2019). These models determine the weighting factors of the R, G, and B tristimuli according to the conventional and a spectral mismatch indicator (f_1') optimization. The latter method is a camera and SPD dependent optimization incorporating the effect of the camera's spectral responsivity as well as the SPD of the light source.

In the conventional method, the luminance (L) was calculated using a linear combination of the R, G, and B coefficients using fixed weighting factors in order to approximate the luminous

efficiency curve $V(\lambda)$. The linear combination was based on the transformation of the sRGB colour space to the XYZ colour space applying "reference primaries, CIE standard illuminant D65, and standard CIE Colorimetric Observer with 2° field of view" (Inanici, 2006). The luminance, according to the conventional method, was calculated according to Equation (1).

$$\mathrm{L} = k \cdot (0.2125 \cdot R + 0.7154 \cdot G + 0.0721 \cdot B) \quad (1)$$

where

L is the luminance;
k is the photometric calibration factor;
R is the red channel;
G is the green channel;
B is the blue channel.

The alternative luminance model was based on the General $V(\lambda)$ Mismatch Index f_1' (CIE, 2014), generally used to indicate the spectral properties for general light measurements. The metric was applied because a single pixel of a luminance camera can be considered a photometer. The inputs for this metric were the $V(\lambda)$ and the spectral responsivities as illustrated in Figure 1. Moreover, instead of Standard Illuminant D65, the 205 SPDs served as input to determine the most suitable weighting factors for R, G and B for each individual SPD according to Equation (2). The weighting factors that were found were applied in a similar fashion as the conventional method. For an extensive explanation of this model we refer to (Kruisselbrink et al., 2019).

$$arg\ min\ f_1',\ subject\ to\colon \begin{cases} r \in (0,1) \\ g \in (0,1) \\ b \in (0,1) \\ r+g+b=1 \end{cases} \quad (2)$$

where

f_1' is the General $V(\lambda)$ Mismatch Index;
r is the weighting factor for the red channel;
g is the weighting factor for the green channel;
b is the weighting factor for the blue channel.

The simulations resulted in weighting factors for the R, G, and B channel for each individual camera and SPD. The measurement error (δ_L) between the approximated luminance using the simulated cameras and the actual luminance (perfect $V(\lambda)$ match) was assessed based on the correlated colour temperature (CCT) and the full spectrum index (FSI), which are both one-dimensional indicators of the SPD that were expected to have an effect on the luminance calculation performance.

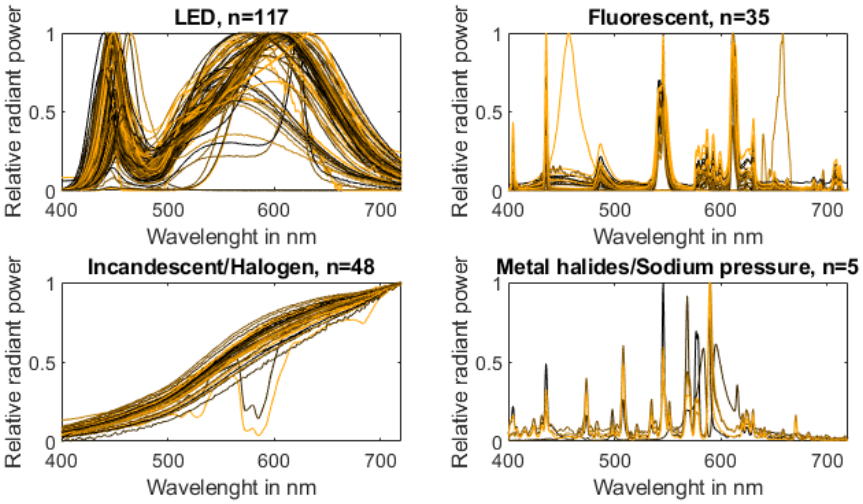

Figure 2 – Implemented spectral power distributions originating from LSPDD database

The CCT, the temperature of a Planckian radiator associated with the chromaticity of the SPD, was calculated according to the method by Hohm and Krochmann (Hohm & Krochman, 1975). For 7 SPDs the CCT could not be calculated because the distance to the Plackian locus was disproportionate, therefore, these SPDs were not considered for the respective analyses. The FSI (Rea et al., 2005) is a metric that indicates how much a SPD differs from an equal energy spectrum, which was deemed relevant to indicate the continuity of the SPD. The FSI was calculated based on the sum of squared deviations between the cumulative SPD and cumulative equal energy spectrum. A FSI of 0 represents an equal energy spectrum, bigger FSI values are associated with non-continuous, or peaky, SPDs.

Additionally to the luminance, the simulations according to the alternative model were also conducted for the melanopic radiance. The melanopic radiance was determined by replacing the $V(\lambda)$ by the $S_{mel}(\lambda)$ as illustrated in Figure 1. The conventional method was disregarded as this was not applicable for the melanopic radiance.

3 Results

In this section the simulation results according to the conventional model and the alternative, spectral mismatch based, model for luminance and for melanopic radiance measurements are displayed.

3.1 Conventional method

The conventional model to calculate the luminance using cameras introduced large deviations as is illustrated in Table 1. Spectral mismatches up to 46 % were found, which can be considered very large as the lowest DIN classification for luminance meters is below 5 % (DIN, 2017). Moreover, large differences were found for the measurement error (δ_L), both the mean as the standard deviation exhibit large differences. High spectral mismatches align with high average (and standard deviation) measurement errors. Based on the results, it is likely that the spectral responsivity of camera 4 has the most similarities with the sRGB responsivity as it performs relatively well.

Table 1 – Average spectral mismatch and average, non-absolute, luminance measurement error for camera 1 to 6 according to the conventional model. The standard deviations are illustrated between brackets.

	Cam 1	Cam 2	Cam 3	Cam 4	Cam 5	Cam 6
f_1'	40,8 % (4,1 %)	39,8 % (2,8 %)	46,5 % (3,2 %)	17,0 % (1,2 %)	26.9 % (1,1 %)	42,2 % (4,8 %)
δ_L	-12,7 % (8,0 %)	-13,0 % (11,1 %)	-16,8 % (14,1 %)	-3,6 % (4,0 %)	-7,5 % (6,6 %)	-13,7 % (8,4 %)

Figure 3 illustrates the absolute measurement error, as indicated in Table 1, relative to the CCT. In general, all cameras show a similar trend where high inaccuracies were introduced for low CCTs. The error decreases towards a CCT of 6500K. This effect was mainly visible for cameras with high spectral mismatches, for cameras with relatively low spectral mismatches the dependency on the CCT, or SPD, was limited. The error decreased towards a CCT of 6500K because this is the CCT of the standard illuminant applied in the conventional method. It is expected that for CCTs higher than 6500K the errors will increase again. This indicates that there is a dependency on the SPD, indicated using the CCT (Figure 3), when the conventional method is applied to calculate the luminance.

A similar analysis was conducted using FSI as an indicator for the SPD (Figure 4), instead of the CCT. Again, a clear trend was found, showing a dependency on the SPD. Figure 4 illustrates that using the conventional method to calculate the luminance was more accurate for SPDs that have a full spectrum, such as an incandescent. On the other hand, it illustrates that it has more difficulties to measure SPDs that contains peaks such as fluorescent light sources. In contrast to

Figure 3, this effect was also clearly visible for the cameras with a relatively low spectral mismatch, in these cases only the magnitude of the errors was lower compared to the others.

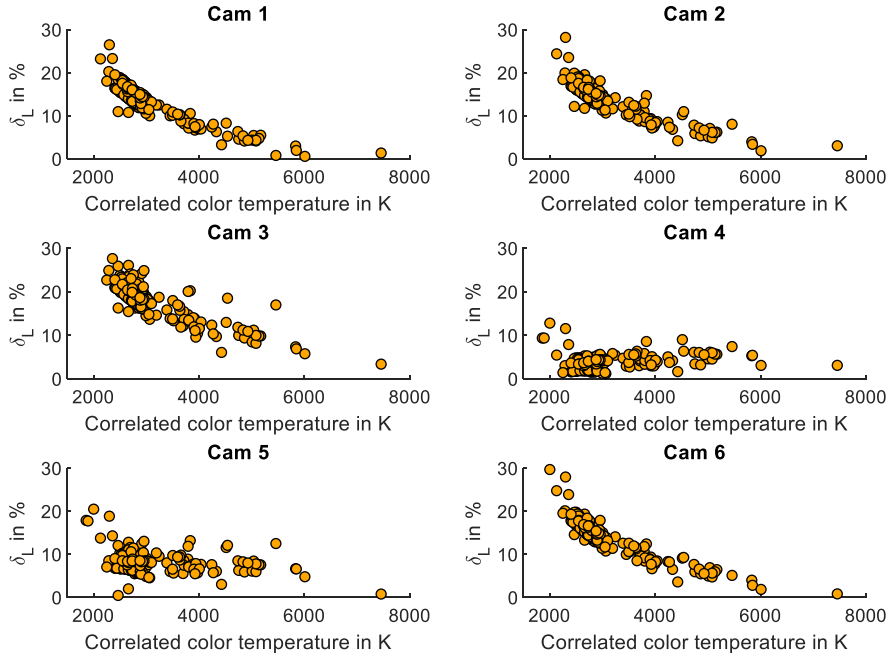

Figure 3 – Relation between the CCT and the absolute measurement error of the luminance cameras according to the conventional method

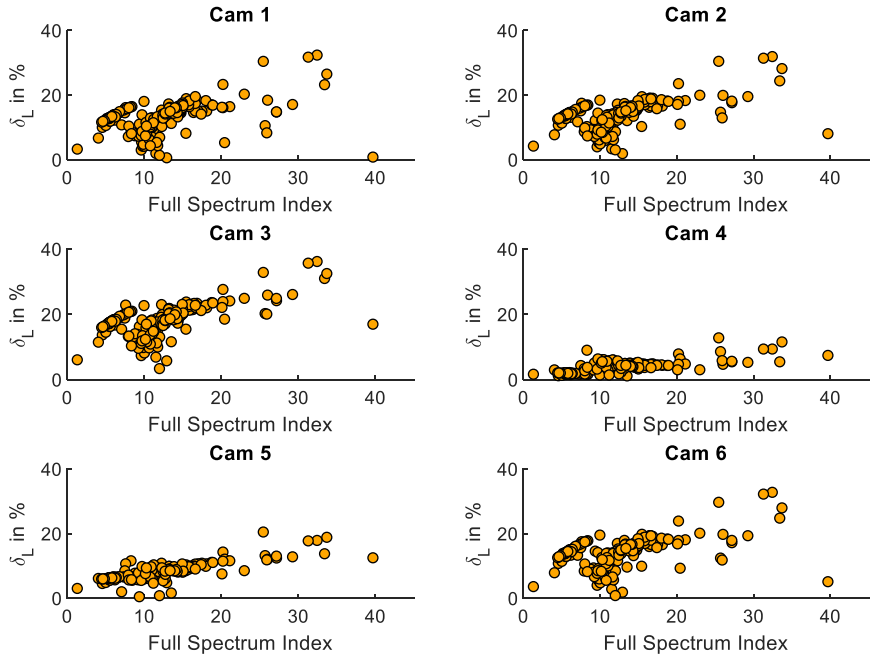

Figure 4 – Relation between the FSI and the absolute measurement error of the luminance cameras according to the conventional method.

3.2 Spectral mismatch optimization

Based on the optimized luminance calculation, according to the alternative model, the spectral mismatches and measurement errors have been reduced drastically, as is shown in Table 2. The maximum spectral mismatch has been reduced to approximately 20 % compared to a spectral mismatch of 46 % for the conventional method. Consequently, the measurement error has been decreased to a maximum of approximately 6 %. Especially, for camera 6 the optimization was fruitful. On the other hand, the performance for camera 4 did not show a significant improvement. Moreover, for this camera, the weighting factors for R, G, and B channels were relatively similar to the conventional method. For the other cameras, the weighting factors were largely different to the conventional method. First, the blue channel was generally not required as the information of the blue part of the spectrum was captured using the green channel. Moreover, a larger part of the red part of the camera was required because the maximum responsivity of the green channel was generally below 550 nm, which requires the red channel to compensate.

Table 2 – Average r,g,b weighting factors, spectral mismatches and, non-absolute, luminance measurement errors for camera 1 to 6 according to alternative model. The standard deviations are illustrated between brackets.

	Cam 1	Cam 2	Cam 3	Cam 4	Cam 5	Cam 6
r	0,52 (0,02)	0,42 (0,02)	0,46 (0,02)	0.21 (0,01)	0,28 (0,01)	0,51 (0,01)
g	0,48 (0,02)	0,58 (0,02)	0,54 (0,02)	0,76 (0,04)	0,72 (0,01)	0,49 (0,01)
b	0,00 (0,00)	0,00 (0,00)	0,00 (0,00)	0,02 (0,00)	0,00 (0,00)	0,00 (0,00)
f_1'	17,7 % (1,0 %)	19,8 % (0,8 %)	20,8 % (1,2 %)	16,0 % (0,3 %)	20,9 % (0,3 %)	11,0 % (0,8 %)
δ_L	-1,8 % (2,9 %)	-4,5 % (3,7 %)	-5,6 % (4,2 %)	-2,3 % (1,8 %)	-2,8 % (1,1 %)	-1,6 % (2,3 %)

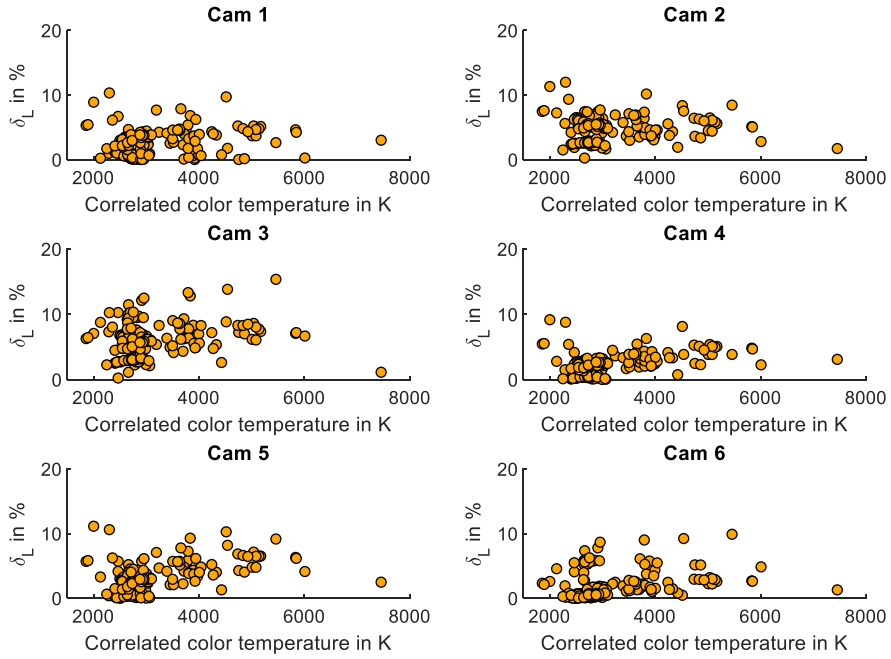

Figure 5 – Relation between the CCT and the absolute measurement error of the luminance cameras according to the alternative model.

Due to the optimization for each individual SPD the dependency on the CCT was almost non-existing. Figure 5 illustrates that no clear pattern was occurring between the CCT and the measurement error. In contrast to the conventional method, the maximum absolute error was generally reduced to approximately 10 % compared to a maximum error of > 30 % for the conventional method.

Figure 6 shows that, in contrast to the CCT, the optimization remained dependent on the FSI. The performance for full spectrum SPDs was still higher than for SPDs with peaks. Apparently, continuous SPDs were easier to match using only three channels of the cameras' responsivity. For peaky SPDs the specific wavelengths might not be present in the cameras' responsivity. Again, for high performing cameras, the dependency on the FSI decreases. A hypothetical camera with a perfect spectral match will show no dependency to the FSI or any performance indicator.

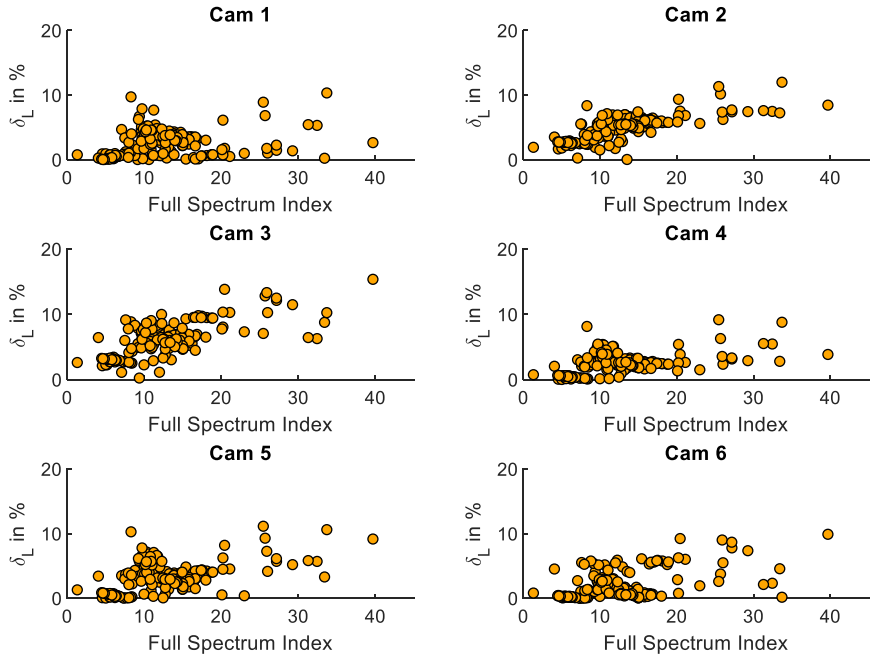

Figure 6 - Relation between the FSI and the absolute measurement error of the luminance cameras according to the alternative model.

3.3 Melanopic Radiance

In the analysis, for the melanopic radiance, one single SPD was discarded as it contained one single peak at 650 nm, which was outside the melanopic sensitivity. As expected, the accuracy of the optimized luminance (Section 3.2) was not achieved. Table 3 gives an indication of the measurement capabilities of the cameras for the melanopic radiance. Cameras are, after all, developed for measurements that match our visual experience. Nevertheless, for some cameras the performance was better than for the conventional luminance measurements, although the variance between cameras was quite high. It shows that the capabilities were largely dependent on the spectral responsivity of the camera, for instance, camera 4 performed well for the conventional luminance measurement, but was not able to accurately measure the melanopic radiance. Similar to the optimized luminance, the melanopic radiance was generally measured with only two channels, in this case the red channel was not required. The blue channel was highly normative as this aligns relatively well with the melanopic sensitivity (Figure 1).

Figure 7 illustrates that for cameras that have large measurement errors (δ_S), there was some dependency to the CCT. Difficulties arise when the melanopic radiance was measured for SPDs with a low CCT. This error was introduced by the misalignment between the high amount of energy for longer wavelengths and the melanopic sensitivity for the lower wavelengths. The resulting measurement errors can be very high (> 100 % for camera 4, cropped out of Figure 7 for readability) but for others it was reasonable.

Again,

Figure 8 illustrates an almost linear dependency on the FSI, which is much clearer for the low performing cameras. So, the melanopic radiance is more accurately measured for full spectrums, similar to the findings in Section 3.2.

Table 3 – Average r,g,b weighting factors, spectral mismatches and, non-absolute, measurement errors for camera 1 to 6 for melanopic radiance measurements (δ_S). The standard deviations are illustrated between brackets.

	Cam 1	Cam 2	Cam 3	Cam 4	Cam 5	Cam 6
r	0,00 (0,00)	0,00 (0,00)	0,00 (0,00)	0,00 (0,00)	0,00 (0,00)	0,00 (0,00)
g	0,12 (0,02)	0,29 (0,03)	0,28 (0,03)	0,06 (0,03)	0,16 (0,03)	0,11 (0,03)
b	0,88 (0,02)	0,71 (0,03)	0,72 (0,03)	0,94 (0,03)	0,84 (0,03)	0,89 (0,03)
f_1'	33,6 % (0,8 %)	39,5 % (1,0 %)	37,1 % (1,0 %)	62,4 % (2,0 %)	44,4 % (1,0 %)	37,0 % (1,7 %)
δ_S	-3,1 % (2,7 %)	11,1 % (5,7 %)	1,9 % (3,7 %)	20,0 % (26,9 %)	4,2 % (4,2 %)	6,4 % (7,1 %)

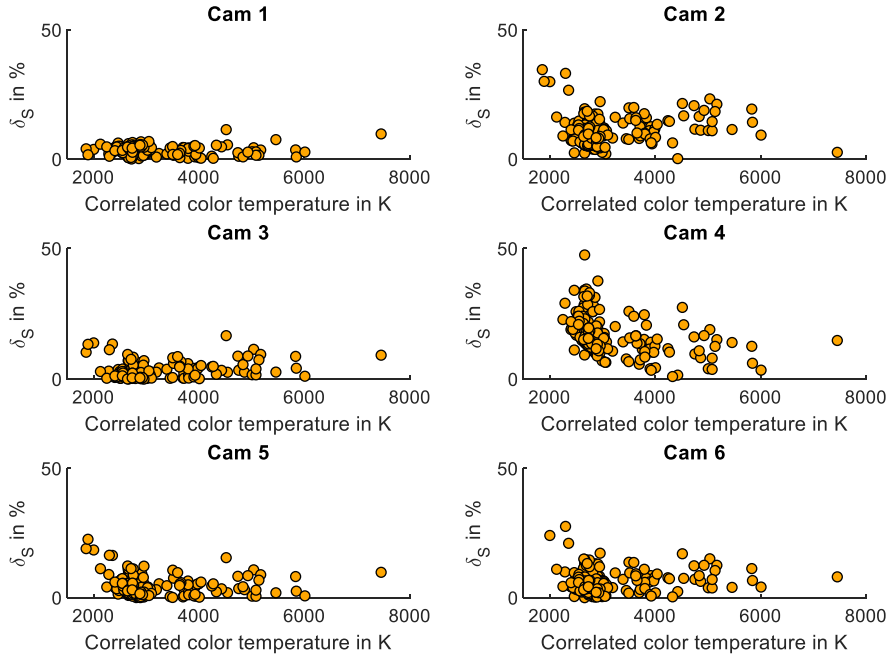

Figure 7 – Relation between the CCT and the absolute measurement error of the melanopic radiance measurement according to the alternative model

4 Discussion and Conclusion

The objective of this study was to assess, based on simulations, the capabilities of six cameras to measure the luminance and melanopic radiance. Besides the conventional model to calculate the luminance, an alternative model, which was based on the General $V(\lambda)$ Mismatch Index, was used to assign the most suitable weighting factors for the R, G and B channels for luminance and melanopic radiance measurements.

The conventional model, to calculate the luminance, introduced significant average luminance measurement errors ranging from approximately 4 % to 17 %. In all cases, the alternative model was able to reduce the average measurement errors, ranging from approximately 2 % to 6 %, to a large extent. Additionally, some cameras were able to measure the melanopic radiance relatively accurate with average measurement errors below 5 %. However, large differences were found between cameras, one camera was not able to provide accurate measurements (> 20 %).

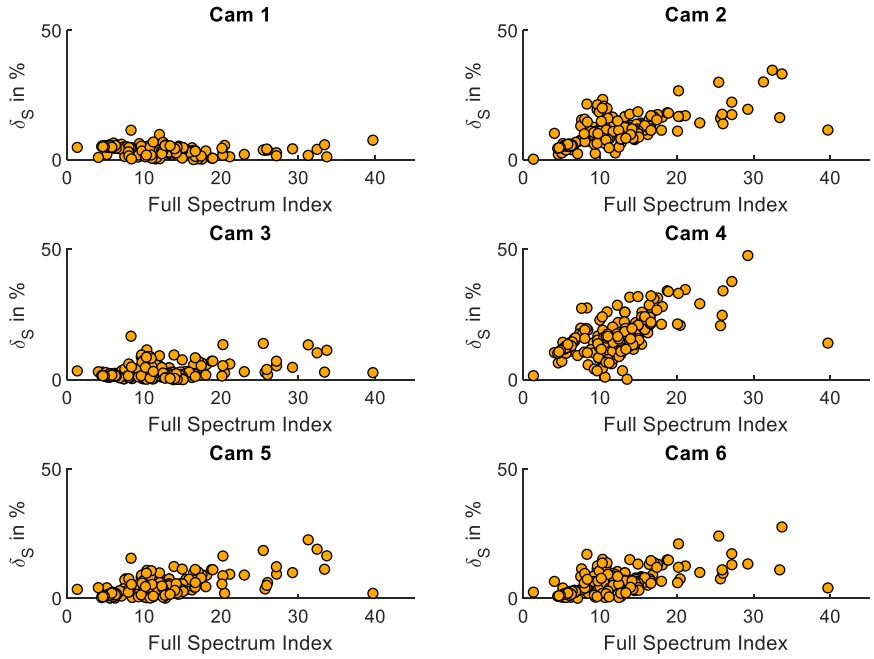

Figure 8 – Relation between the FSI and the absolute measurement error of the melanopic radiance measurement according to the alternative model

This study indicated that luminance and melanopic radiance measurements are sensitive to the SPD of the light source. Both the CCT and the FSI are proven to influence the performance of the camera systems. The CCT, roughly indicating which wavelengths contained the most energy, affected the performance for measurements with the conventional model and the melanopic radiance measurement. For the conventional method, SPDs very different to standard illuminant D65 had a lower performance because the R, G, and B channels of the camera were combined such that a more bluish (6500K) light source was measured accurately. For this reason, the blue channel determined approximately 7 % of the luminance. This effect disappeared for the alternative model because the weighting factors were specifically determined for each individual illuminant, resulting in almost no importance of the blue channel. Nevertheless, the standard deviation for the improved weighting factors was low, indicating that it is fairly safe to use the mean weighting factors instead of SPD dependent weightings (Table 2 and Table 3). For the melanopic radiance, low CCT light sources performed worse as they mainly contained energy in the reddish part of the SPD, while the melanopic sensitivity is sensitive to the blue part. As only three channels, in practice only two, were applied, the blue component could not be extracted exclusively. Consequently, also energy outside the melanopic range was captured, which reduced the performance.

As expected, the FSI showed that continuous SPDs were generally measured more accurately. Especially, very peaky SPDs did not perform well as the sensitivity of the cameras can be very low for these specific wavelengths. For continuous SPDs, the wavelengths with low sensitivity are easily accounted for by the wavelengths with high sensitivity.

Large differences were found between cameras, as their spectral responsivities differ. Hence, their capabilities to capture the luminous or melanopic sensitivities vary. The differences for the optimized luminance measurements were limited as most cameras aim to achieve a visually pleasing image which results in high sensitivity, and overlap between the channels, for the range of the luminous sensitivity ($V(\lambda)$). Using the optimization, the most suitable combination between channels can be found, which differed significantly for the different cameras. The melanopic radiance showed the biggest differences between cameras as their sensitivity was generally low for the relevant wavelengths. Moreover, the blue channels were not aligned as well with the melanopic sensitivity as the green channels were aligned with the luminous sensitivity.

When a low spectral mismatch is achieved, the dependency on the SPD is low. However, when the spectral mismatch is significant, which is often the case for these camera systems, then the SPD is relevant. For instance, the CCT and FSI of a SPD have a larger influence on low performing cameras as wavelengths outside the region of interest are captured as well.

This study showed that the conventional method to calculate the luminance can introduced significant errors. It is therefore, advised to either pick a suitable camera, which spectral responsivity is suitable, and/or optimize the weighting factors for the R, G and B channels. Consequently, the spectral mismatches can be reduced drastically, reducing the sensitivity to the SPD. Moreover, it was shown that the melanopic radiance can be approximated by such camera systems. However, the applied camera has even higher importance, as some cameras are not able to achieve an acceptable spectral match and differences between weighting factors for different SPDs were limited.

It is recommended to perform physical measurements to validate the results found. In this study, only simulations were conducted, which might not always be a correct impression of reality (Kruisselbrink et al., 2019). For instance, the spectral responsivity of the cameras might be different in practice. Moreover, the imaging pipeline is more complex as illustrated in the applied models. Finally, 205 SPDs were applied that are commercially available. However, in practice the light source will have a mixed character containing daylight as well as an artificial light source.

References

Cai, H. (2011). Camera Aided Luminance Measurement of the Luminous Surfaces of Different Light Sources. *AEI 2011*, 272–279. https://doi.org/10.1061/41168(399)33

Cauwerts, C., Jost, S., & Deroisy, B. (2019). Calibration of high dynamic range images for applied color and lighting research. *Journal of the Optical Society of America A*, *36*(11), C130. https://doi.org/10.1364/JOSAA.36.00C130

CIE. (2014). *Characterization of the performance of illuminance meters and luminance meters: Vol. ISO/CIE 19*.

CIE. (2018). *IE System for Metrology of Optical Radiation for ipRGC-Influenced Responses to Light: Vol. CIE S 026*. https://doi.org/10.25039/S026.2018

DIN. (2017). *DIN 5032 Photometry - Part 7: Classification of illuminance meters and luminance meters*.

Gentile, N., Dubois, M. C., Osterhaus, W. K. E., Stoffer, S., Naves David Amorim, C., Geisler-Moroder, D., Jakobiak, R., Amorim, C. N. D., Geisler-Moroder, D., & Jakobiak, R. (2016). A toolbox to evaluate non-residential lighting and daylighting retrofit in practice. *Energy and Buildings*, *123*, 151–161. https://doi.org/10.1016/j.enbuild.2016.04.026

Hohm, W., & Krochman, J. (1975). ERMITTLUNG DER AEHNLICHSTEN FARBTEMPERATUR. *FARBE*, *24*(1–6), 91–96.

Inanici, M. N. (2006). Evaluation of high dynamic range photography as a luminance data acquisition system. *Lighting Research and Technology*, *38*(2), 123–136. https://doi.org/10.1191/1365782806li164oa

Jiang, J., Liu, D., Gu, J., & Susstrunk, S. (2013). What is the space of spectral sensitivity functions for digital color cameras? *Proceedings of IEEE Workshop on Applications of Computer Vision*, 168–179. https://doi.org/10.1109/WACV.2013.6475015

Kruisselbrink, T. W., Aries, M. B. C., & Rosemann, A. L. P. (2017). A Practical Device for Measuring the Luminance Distribution. *International Journal of Sustainable Lighting*, *19*(1), 75–90. https://doi.org/10.26607/ijsl.v19i1.76

Kruisselbrink, T. W., Dangol, R., & Rosemann, A. L. P. (2018). Photometric measurements of lighting quality: An overview. *Building and Environment*, *138*, 42–52. https://doi.org/10.1016/j.buildenv.2018.04.028

Kruisselbrink, T. W., Dangol, R., Rosemann, A. L. P., & van Loenen, E. J. (2019). Spectral tuning of luminance cameras: A theoretical model and validation measurements. *Lighting Research & Technology*. https://doi.org/10.1177/1477153519880231

Lenseigne, B., Jacobs, V. A., Withouck, M., Hanselaer, P., & Jonker, P. P. (2013). Color sensitivity of the multi-exposure HDR imaging process. *Advanced Optical Technologies*, *2*(2), 159–169. https://doi.org/10.1515/aot-2013-0002

Lucas, R. J., Peirson, S. N., Berson, D. M., Brown, T. M., Cooper, H. M., Czeisler, C. A., Figueiro, M. G., Gamlin, P. D., Lockley, S. W., O'Hagan, J. B., Price, L. L. A., Provencio, I., Skene, D. J., & Brainard, G. C. (2014). Measuring and using light in the melanopsin age. *Trends in Neurosciences*, *37*(1), 1–9. https://doi.org/10.1016/j.tins.2013.10.004

Rea, M. S., Deng, L., & Wolsey, R. (2005). Full-Spectrum Light Sources. *Lighting Answers*, *7*(5).

Reinhard, E., Ward, G., Pattanaik, S., & Debevec, P. (2006). *High Dynamic Range Imaging: Acquisition, Display, and Image-Based Lighting (The Morgan Kaufmann Series in Computer Graphics)*. Morgan Kaufmann Publishers Inc.

Roby, J., & Aubé, M. (2012). *LSPDD | Light Spectral Power Distribution Database*. http://galileo.graphycs.cegepsherbrooke.qc.ca/app/en/lamps

Van Den Wymelenberg, K. G. (2012). Evaluating Human Visual Preference and Performance in an Office Environment Using Luminance-based Metrics [University of Washington]. In *University of Washington*. https://doi.org/10.1017/CBO9781107415324.004

Wu, Y., Kämpf, J. H., & Scartezzini, J. L. (2019). Design and validation of a compact embedded photometric device for real-time daylighting computing in office buildings. *Building and Environment*, *148*, 309–322. https://doi.org/10.1016/j.buildenv.2018.11.016

International Commission on Illumination
Commission Internationale de l'Eclairage
Internationale Beleuchtungskommission

PO12

OPTIMAL TEXT-BACKGROUND LIGHTNESS COMBINATIONS OF TABLET DEVICES FOR VISUAL COMFORT UNDER A WIDE RANGE OF ILLUMINANCE LEVELS

Hsin-Pou Huang et al.

DOI 10.25039/x47.2020.PO12

Paper accepted for the 5th CIE Symposium on Colour and Visual Appearance

The paper was selected by the International Scientific Committee (ISC) for presentation at the 5th CIE Symposium on Colour and Visual Appearance, Hong Kong, CN, April 21–22, 2020, which, due to the corona pandemic, could not take place. The paper has not been peer-reviewed by CIE.

CIE Central Bureau
Babenbergerstrasse 9
A-1010 Vienna
Austria
Tel.: +43 1 714 3187
e-mail: ciecb@cie.co.at
www.cie.co.at

PO12

OPTIMAL TEXT-BACKGROUND LIGHTNESS COMBINATIONS OF TABLET DEVICES FOR VISUAL COMFORT UNDER A WIDE RANGE OF ILLUMINANCE LEVELS

Huang, H.P.[1], Wei, M.[2,*], Ou, L.C.[3]
[1] Chihlee University of Technology, New Taipei City, CHINESE TAIPEI; [2] The Hong Kong Polytechnic University, Kowloon, HONG KONG; [3]National Taiwan University of Science and Technology, Taipei, CHINESE TAIPEI
minchen.wei@polyu.edu.hk

Abstract

The psychophysical experiment was carried out to investigate how illuminance level affected the visual comfort for e-reading on a tablet device. 44 Asian observers between 19 and 25 years of age (mean = 21.5, SD = 1.2) participated in the experiment, comprising 20 observers evaluated the visual comfort experiment under dark condition, 300 lx and 3 000 lx and 24 observers evaluated the visual comfort experiment under 150 lx, 1 500 lx and 15 000 lx. The experimental results show that the visual comfort interval scale below 1 500 lx conditions (i.e. Dark, 150 lx, 300 lx and 1 500 lx) were similar to each other, but not to the visual comfort interval scale above the 1 500 lx conditions (i.e. 3 000 lx and 15 000 lx). For the same lightness difference between text and background, the observers' judgements show that they felt more comfortable to read the document using white background than the document using black background under high illuminance level.

Keywords: Visual comfort, Tablet device, Illuminance level, Reading

1 Introduction

With the advances in mobile devices technology, e-reading on mobile devices is becoming more and more necessary in human's daily life. Human rely on e-reading devices to read news, get information, play games, and communicate with family and friends under different ambient lighting conditions, from lower illuminance level at night to higher illuminance level under daylight or from lower correlated colour temperature (CCT) level at warm lighting room to higher CCT level at cooler lighting room. Many mobile device manufacturers and studies consider how ambient lighting condition may affect the mobile interface design to promote user visual comfort and preference [Chen and Lin 2004, Lin and Huang 2006, Na and Suk 2015, Na and Suk 2016]. Our previous study investigated how ambient lighting condition affected the observers visual comfort for e-reading, and found that the visual comfort for e-reading the 20 text-background lightness combinations under different CCT levels were highly correlated. Comparing the results of the Pearson correlation coefficient between different CCT levels, these tendency of high correlation between different CCT levels does not appear to different illuminance levels. Our previous study showed that the Pearson correlation coefficient between the judgments under the dark surround and under the 3 000 lx condition was 0.5. However, the previous experiment was carried out with an ambient illuminance level below 3 000 lx to investigate the visual comfort for e-reading in interior environments [Huang et al 2018]. With the above in mind, this study aimed to investigate how ambient illuminance level (including outdoor illuminance of 15 000 lx) affected the visual comfort for e-reading.

2 Methods

A paired comparison psychophysical experiment was carried out to investigate the visual comfort in a viewing booth, which was uniformly illuminated using either a 14-channel spectrally tunable LED device or a four-channel spectrally tunable LED device (ARRI SkyPanel S60-C) to produce light sources. The LED device was carefully adjusted to produce five light sources, comprising five levels of illuminance (i.e. 150 lx, 300 lx, 1 500 lx, 3 000 lx and 15 000 lx) with a horizontal CCT of 6 500 K, the relative spectral power distributions (SPDs) of these five light

sources are shown in Figure 1 and Table 1 show the colorimetric characteristics of the ambient lighting conditions, measured using a calibrated JETI specbos 1211TM spectroradiometer. Apart from the five levels of illuminance, a dark condition was considered in this study. 44 Asian observers between 19 and 25 years of age (mean = 21.5, SD = 1.2) participated in the experiment, comprising 20 observers evaluated the visual comfort experiment under dark condition, 300 and 3 000 lx and 24 observers evaluated the visual comfort experiment under 150 lx, 1 500 lx and 15 000 lx. All observers had kept their chins being fixed on a rest during the experiment to ensure a similar viewing distance around 45 cm between the eyes and the iPad Air 2. An iPad Air 2 was placed on a 45° viewing table which was placed at the center of the booth, as shown in Figure 2. For understanding the visual comfort of different text-background lightness combinations, 20 text-background combinations were produced. The 20 text-background combinations were composed by all possible combinations of five achromatic colours, as listed in Table 2. Based on the 20 text-background combinations, 190 paired comparisons were generated, considering all possible paired comparisons of these 20 text-background combinations. A total of 20 of the 190 paired comparisons were presented twice for testing the repeatability, meaning 210 paired comparisons in total were conducted by each observer under each surround. Each observer was asked to pick one that was more comfortable to read the text from the two text-background combinations, as shown in Figure 3. Thus, each observer made forced-choices for a total of 630 paired comparisons (210 paired comparisons in a random order × 3 surrounds) in terms of visual comfort.

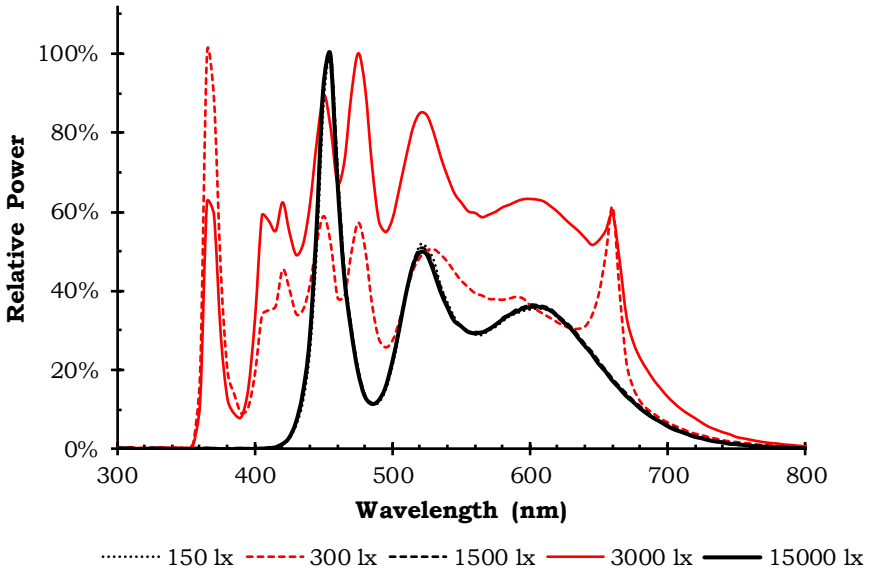

Figure 1 – The relative spectral power distributions (SPDs) of the light sources

Table 1 – Colorimetric characteristics of the light sources

Light source / Illuminance (lx)	CCT (K)	CRI R_a	D_{uv}
150	6475	97	0.001
300	6547	95	0.0039
1500	6454	95	-0.001
3000	6533	98	0.0041
15000	6471	98	-0.002

Figure 2 – The photograph of the experimental setup

Table 2 – Colorimetric characteristics of the five achromatic colours

Achromatic color **Color**	**Luminance (cd/m^2)**	***L****	**(x, y)**
Black	0.7	1.6	(0.311,0.328)
Dark grey	18.1	25.2	(0.307,0.327)
Medium grey	77.3	50.9	(0.306,0.326)
Light grey	196.5	75.3	(0.308,0.327)
White	402.7	100.0	(0.307,0.326)

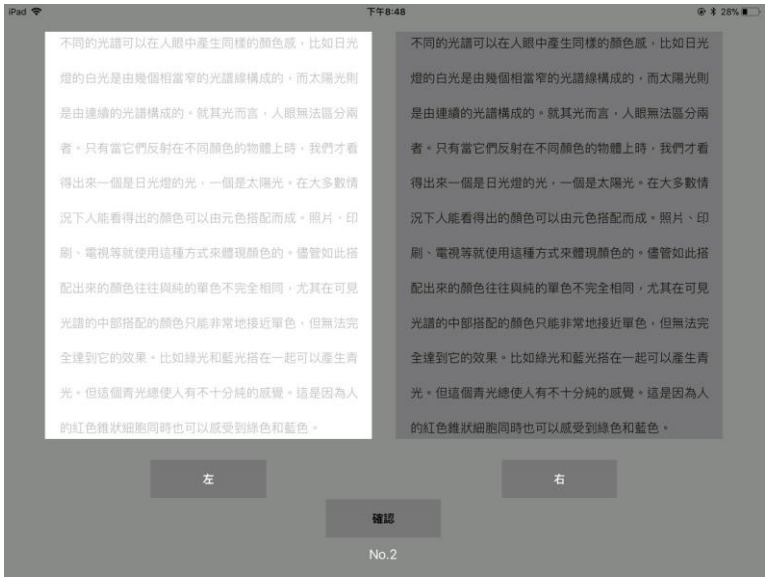

Figure 3 – A screenshot of the paired-comparison presented on the iPad Air 2

3 Results

The repeatability test result for a total of 2 640 paired comparisons presented twice shows that in general the observers made the same judgements for 84.4 % of the replicated trials. This means that the psychophysical experiment was highly repeatable and stable for the 44 observers. The interval scales of visual comfort were determined by the results of paired comparison experiment using Thurstone case V method [Thurstone1994]. The higher the interval scale, the more visual comfortable judged by the observers. When the ambient illuminance below 1 500 lx, the tendency of visual comfort interval scale did not seem to vary with the ambient illuminance. When the ambient illuminance above 1 500 lx, the tendency of visual comfort interval scale also did not seem to vary with the ambient illuminance. However, according to Pearson correlation coefficients (i.e., always below 0.7) between the judgments below those the 1 500 lx conditions (i.e. Dark, 150 lx, 300 lx and 1 500 lx) and the judgments above those the 1 500 lx conditions (i.e. 3 000 lx and 15 000 lx), as shown in Table 3, it is appropriate to say that in general the impact of ambient illuminance on visual comfort was great, especially for the e-reading visual comfort between a dark surround and exterior illuminance levels.

Moreover, though the illuminance levels were found to have little impact on visual comfort for lightness difference, the observers' judgement scale did not always show the same tendency for the background colour. When the ambient illuminance below 1 500 lx, with the same lightness difference for text-background combinations, the visual comfort for the text-background combinations with the black background were assessed more comfortable than the text-background combinations with the white background under lower illuminance level (i.e. Dark, 150 lx, 300 lx and 1 500 lx), as shown in Figure 4 (a)-(d). In contrast, with the same lightness difference for text-background combinations, the text-background combinations with the white background were assessed more comfortable than the text-background combinations with the black background under high illuminance level (i.e. 3 000 lx and 15 000 lx), as shown in Figure 4 (e)-(f).

Table 3 – Correlation between different illuminance levels

Correlation coefficient					
	Dark	**150 lx**	**300 lx**	**1500 lx**	**3000 lx**
150 lx	**0.966**				
300 lx	**0.820**	**0.715**			
1500 lx	**0.954**	**0.906**	**0.918**		
3000 lx	**0.497**	**0.320**	**0.878**	**0.659**	
15000 lx	**0.548**	**0.375**	**0.866**	**0.708**	**0.967**

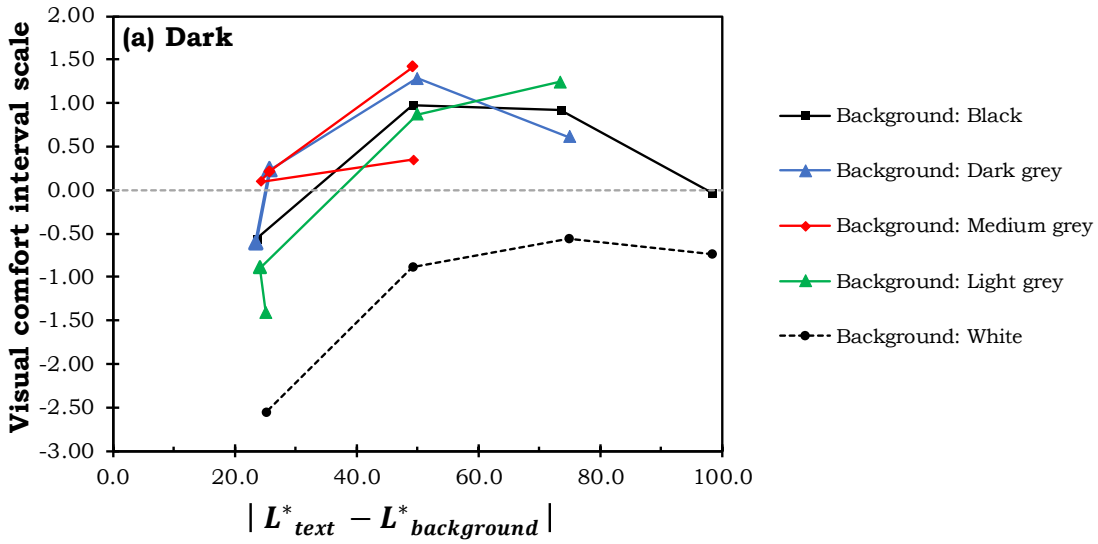
(a) Dark
Visual comfort interval scale
2.00
1.50
1.00
0.50
0.00
-0.50
-1.00
-1.50
-2.00
-2.50
-3.00
0.0
20.0
40.0
60.0
80.0
100.0
$|L^*_{text} - L^*_{background}|$
Background: Black
Background: Dark grey
Background: Medium grey
Background: Light grey
Background: White

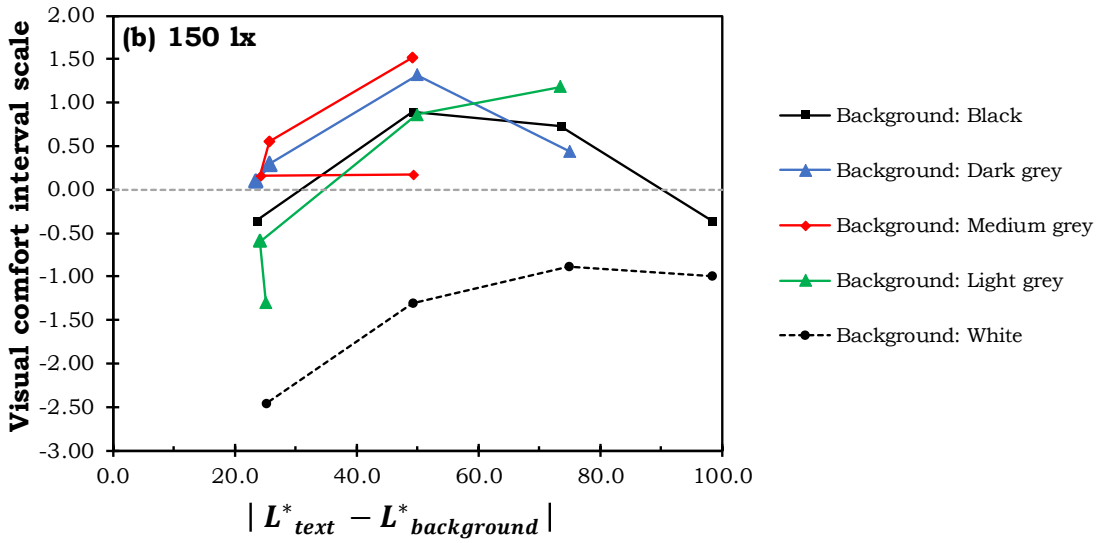
(b) 150 lx
Visual comfort interval scale
2.00
1.50
1.00
0.50
0.00
-0.50
-1.00
-1.50
-2.00
-2.50
-3.00
0.0
20.0
40.0
60.0
80.0
100.0
$|L^*_{text} - L^*_{background}|$
Background: Black
Background: Dark grey
Background: Medium grey
Background: Light grey
Background: White

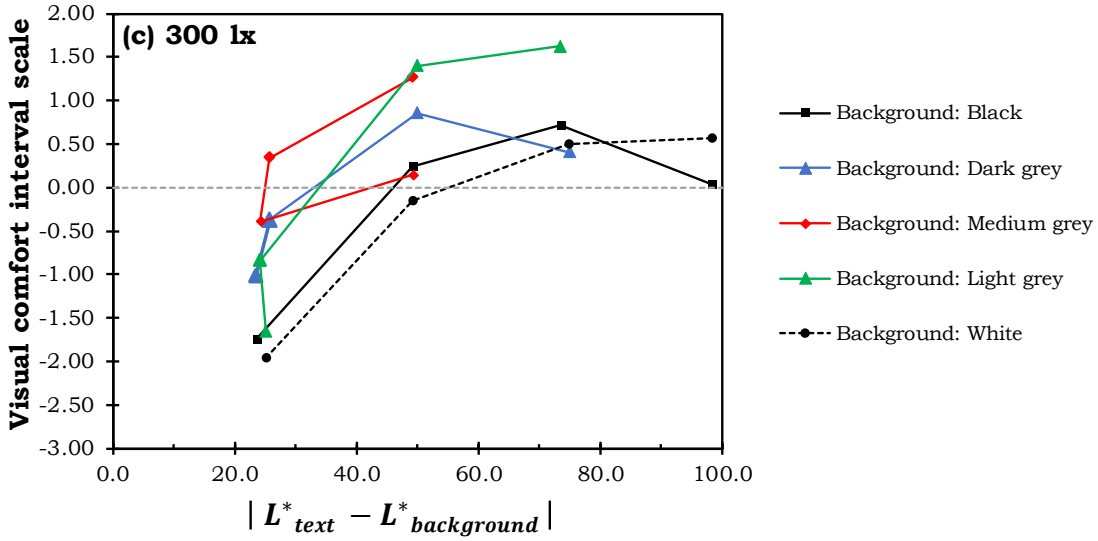
(c) 300 lx
Visual comfort interval scale
2.00
1.50
1.00
0.50
0.00
-0.50
-1.00
-1.50
-2.00
-2.50
-3.00
0.0
20.0
40.0
60.0
80.0
100.0
$|L^*_{text} - L^*_{background}|$
Background: Black
Background: Dark grey
Background: Medium grey
Background: Light grey
Background: White

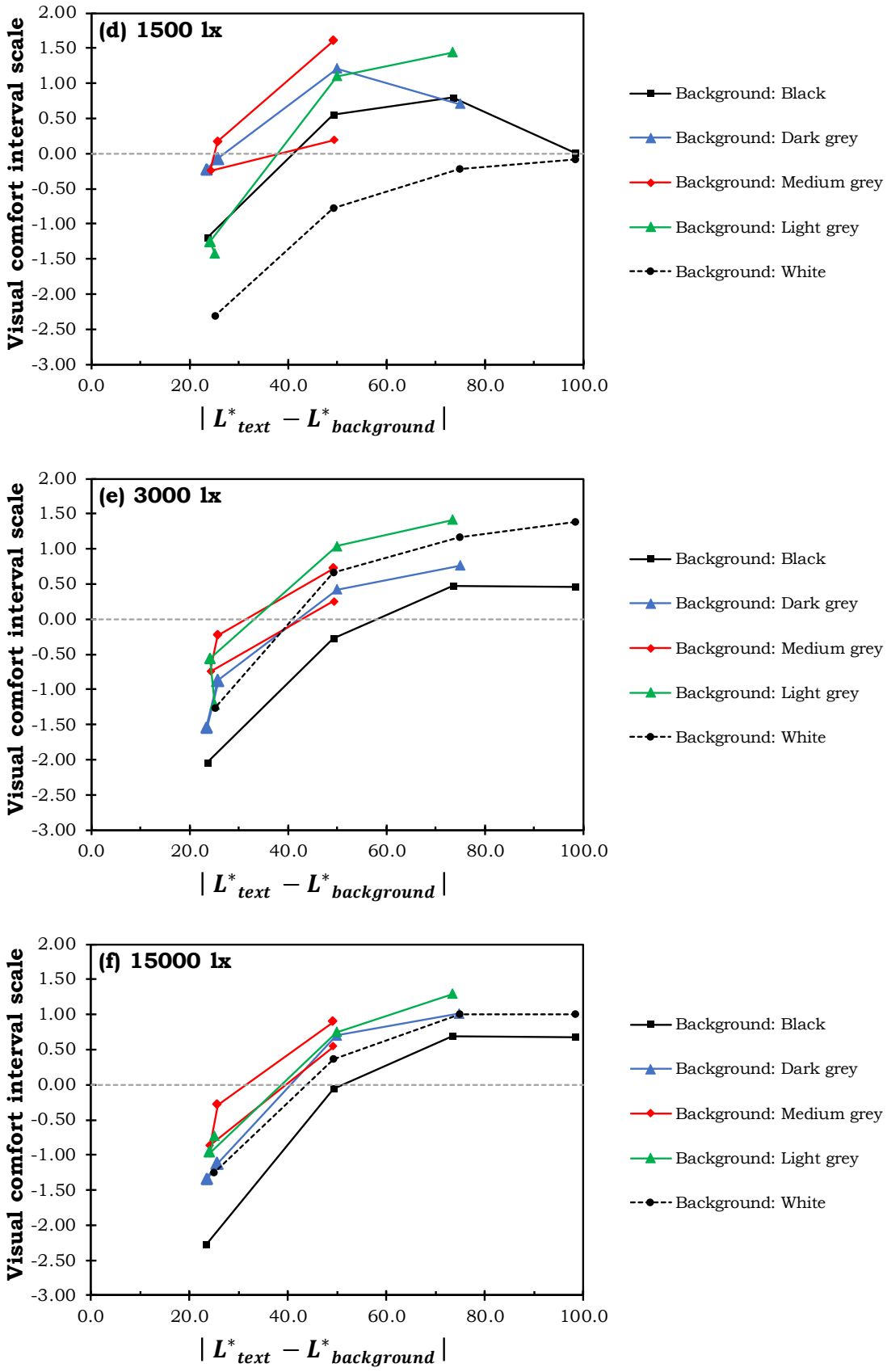

Figure 4 – Visual comfort Interval scale of the 20 text-background combinations evaluated by the observers under each illuminance level (a) Dark; (b) 150 lx; (c) 300 lx; (d) 1 500 lx; (e) 3 000 lx; (f) 15 000 lx

4 Conclusions

A paired comparison psychophysical experiment was conducted to investigate the visual comfort for e-reading under six ambient illuminance levels, including a dark surround, 150 lx, 300 lx, 1 500 lx, 3 000 lx and outdoor illuminance of 15 000 lx. The findings suggest that the observers tended to use different viewing mode for e-reading in interior environments and exterior environments. The experimental results of the study may provide a new guideline for user interface design.

Acknowledgments

This work was supported in part by The Hong Kong Polytechnic University and the Ministry of Science and Technology, Taiwan (MOST 109-2410-H-263-001).

References

Chen MT, Lin CC. 2004. Comparison of TFT-LCD and CRT on visual recognition and subjective preference. Int. J. Ind. Ergonom. 34:167-174.

Lin CC, Huang KC. 2006. Effects of ambient illumination and screen luminance combination on character identification performance of desktop TFT-LCD monitors. Int. J. Ind. Ergonom. 36:211-218.

Na N, Suk HJ. 2015. Adaptive display luminance for viewing smartphones under low illuminance. Opt Express. 23:16912-16920.

Na N, Suk HJ. 2016. Adaptive luminance difference between text and background for comfortable reading on a smartphone. Int. J. Ind. Ergonom. 51:68-72.

Huang HP, Wei MC, Ou LC. 2019. Effect of text-background lightness combination on visual comfort for reading on a tablet display under different surrounds. Color Res Appl. 44:54-64.

Thurstone LL. 1994. A law of comparative judgment. Psychol. Rev. 101:266-270.

International Commission on Illumination
Commission Internationale de l'Eclairage
Internationale Beleuchtungskommission

PO13

OPTIMIZATION OF TRICHROMATIC WHITE LED SPECTRUM FOR DIM LIGHTING CONDITIONS

Hung-Chung Li et al.

DOI 10.25039/x47.2020.PO13

Paper accepted for the 5th CIE Symposium on Colour and Visual Appearance

The paper was selected by the International Scientific Committee (ISC) for presentation at the 5th CIE Symposium on Colour and Visual Appearance, Hong Kong, CN, April 21–22, 2020, which, due to the corona pandemic, could not take place. The paper has not been peer-reviewed by CIE.

CIE Central Bureau
Babenbergerstrasse 9
A-1010 Vienna
Austria
Tel.: +43 1 714 3187
e-mail: ciecb@cie.co.at
www.cie.co.at

PO13

OPTIMIZATION OF TRICHROMATIC WHITE LED SPECTRA FOR DIM LIGHTING CONDITION

Li, H.C.[1], Sun, P.L.[2], Huang, Y.N.[1]
[1] Research Center for Information Technology Innovation, Academia Sinica, Taipei, CHINESE TAIPEI, [2] National Taiwan University of Science and Technology, Taipei, CHINESE TAIPEI
pony780210@citi.sinica.edu.tw

Abstract

Most night-time outdoor and traffic lighting scenarios are in the mesopic range. Because colour gamut in the mesopic conditions is relatively narrow, the general colour rendering index is not suitable for evaluating colour fidelity. Therefore, an optimization of the white LED spectrum based on 3D colour gamut is essential to raise the ability of colour recognition under constant contrast condition for the lighting application. The optimal trichromatic white LED spectra can be obtained by investigating the variance of wavelength positions and peak power density ratios for 10 cd/m^2, 1 cd/m^2, 0.3 cd/m^2, and 0.1 cd/m^2. As a result, a trade-off between mesopic luminance and colour gamut is quite significant. According to the predicted photopic/mesopic luminance level and the gamut volume, the test spectra with the highest Lmes, largest gamut volume (GV), and highest (L_{mes}+GV) are suggested as the optimal white LED spectra under a specific luminance level.

Keywords: Mesopic Vision, White LED, Spectral Optimization, Colour Gamut Estimation

1 Introduction

The luminance level of night-time conditions regularly falls into a mesopic visual range within 0.001 cd/m^2 to 3 cd/m^2. In the early stages of mesopic visual performance research, two methods, which were brightness matching and visual performance-based approaches, were mainly used for establishing the mesopic sensitivity (Eloholma, 2005). The mesopic spectral luminous efficiency could be described with a linear combination of the photopic V(λ) and scotopic V'(λ) spectral luminous efficiency functions. From the previous studies, the design of the white LED spectrum considered the luminance and colour rendering index was solely in the photopic condition where the visual response of humanity was slightly different from the mesopic range. As a result, most researchers have aimed at proposing an appropriate spectrum for mesopic vision currently to meet the visual requirements based on mesopic photometry.

In the mesopic vision, models of mesopic luminous efficiency, such as X-model (Rea, 2004) and MOVE-model (Eloholma, 2006), were derived for calculating mesopic luminance (denoted as Lmes). The X-model was obtained from a reaction time experiment in the mesopic range. In the X-model, a parameter X was used to characterize the ratio between photopic and scotopic luminous efficacy at any luminance. The MOVE-model was proposed by European research consortium MOVE (Mesopic Optimization of Visual Efficiency) as a recommended model for mesopic luminance of road lighting applications. The model was derived from a series of experiments related to visual task performance, such as achromatic contrast threshold, reaction time, and recognition threshold. Despite the similar forms of the X-model and MOVE-model, the major differences of the two models were that the upper luminance limit of the mesopic range, which was considered too low for the X-model and too high for the MOVE-model. Therefore, a modified MOVE-model was later proposed with an appropriate upper luminance limit to meet the street and road lighting conditions (Halonen, 2010). In 2008, Viikari et al. tested the X-model, MOVE-model, and modified MOVE-model by use of visual data acquired from European universities. As a result, the modified MOVE-model described the data best with over half of the situations (Viikari, 2008).

To calculate mesopic luminance, the S/P-ratio of a light source was essential. It was the scotopic lumens divided by photopic lumens as Equation 1 where k_s and k_p were 1699 and 683, respectively, which were the peak value of luminous efficiency in photopic and scotopic ranges. The same light source would have different values for photopic and scotopic lumens because the two conditions' response curves were different. In general, a light source with a higher correlated colour temperature was provided with a higher S/P-ratio (Zan, 2016). If a light source had a higher S/P-ratio, the visual brightness would be relatively higher in the scotopic conditions and likely enhance night-time visual performance and be beneficial to mesopic design (CIE191, 2010). However, if a light source had stronger spectral radiance in about 530 nm, it should be relatively brighter in mesopic vision, but S/P-ratio could not depict it.

$$S/P = \frac{L_s}{L_p} = \frac{\int_{400}^{750} k_s V'(\lambda) S(\lambda) d\lambda}{\int_{400}^{750} k_p V(\lambda) S(\lambda) d\lambda} \tag{1}$$

Shin et al. (Shin, 2004) proposed a mesopic colour appearance model to simulate the variation of colour appearance in the mesopic range and photopic. By adding rod intrusion to the two-stage model (Kaiser, 1996), the mesopic model describes that the opponent process converted the cone responses from L, M, and S to red/green, yellow/blue opponent-colour and luminance channels denoted by L-2M, L+M-S, and L+M, respectively. The model considered the characteristic of the nonlinear shift in spectral luminous efficiency, reduction of saturation at low illuminance levels, and the variations of hue and chroma loci under different illuminance levels from 1 000 lx to 0.01 lx. The experimental results showed that chroma decreases continuously with the decrease of the illuminance level until 0.01 lx. However, it didn't take some complex visual phenomena such as Hunt effect, chromatic adaptation, and background luminous contrast into account.

A comparison of optimal trichromatic and tetrachromatic white LED spectra suggested by Lei et al. and Zan et al. was recently discussed (Li, 2018). The results showed that the performance of both tetrachromatic white LEDs in mesopic luminance and colour gamut volume were not that ideal as those of the trichromatic white LED spectrum. Therefore, the optimization of trichromatic white LED spectra needs an intensive study to achieve the best result.

2 Methods

The approach of trichromatic white LED spectrum optimization is shown in Figure 1. The optimal white LED spectral power distribution (SPDs) for specific luminance level including 10 cd/m^2, 1 cd/m^2, 0.3 cd/m^2 and 0.1 cd/m^2 can be obtained by the following steps: First, individually generate SPDs of trichromatic white LED with 50 000 times based on the data of Philips Color Blast measured by a spectroradiometer (Topcon SR-UL1R) and simulated Gaussian-like function as Equation 2 where *x* and *alpha* represent the peak wavelength and a function of spectral half-width for each component respectively to establish a spectral database. *n* is set as 2 in the study. The Full Width at Half Maximum (FWHM) of red, green, and blue LEDs are 15 nm, 40 nm, 25 nm for Philips Color Blast and 26 nm, 36 nm, 14 nm for simulated Gaussian-like function respectively. The trichromatic white LED spectra which the Duv are below 0.02, and the correlated colour temperature (CCT) between 1 600 K and 10 000 K are selected with the random shifts within 50 nm and ratios from 0.1 to 1 for red, green and blue LED as the test data. Totally 7 929 and 4 811 test SPDs of Philips Color Blast and simulated Gaussian-like function are collected. For consistency, we initialize the peak wavelength of red, green, and blue LED to 600 nm, 520 nm, 430 nm. Second, apply an equal-energy white spectrum and input a specific luminance level to calculate the total radiance of the spectrum in 400 nm to 700 nm range. If the luminance level is below 5 cd/m^2, the modified MOVE-model is adopted to calculate the power of the spectrum. Conversely, only the photopic luminosity function is used. Third, input a series of test SPDs and acquire the absolute radiant power based on the same total radiance with the equal-energy white spectrum to calculate the photopic, scotopic, and mesopic luminance. Judd modified tristimulus values X_{Judd}, Y_{Judd}, Z_{Judd}, and CIE V'(λ) are obtained by the integral of test spectra,

spectral reflectance, Judd modified colour matching functions, and the scotopic luminous function. Then the tristimulus values are converted to the spectral responses of the cones, L, M and S. The scotopic luminance Y' is also calculated. Next, the L, M, and S responses and luminance Y' are regarded as the inputs for the Shin's mesopic colour appearance model. Based on the experimental results from Shin's study, the weighting coefficients under a specific luminance level can be calculated with an interpolation process and divided by a solid angle between the range of 1 000 lx and 0.01 lx. The mesopic/photopic luminance acquired from test SPDs should be converted to the illuminance unit first for using the mesopic colour appearance model.

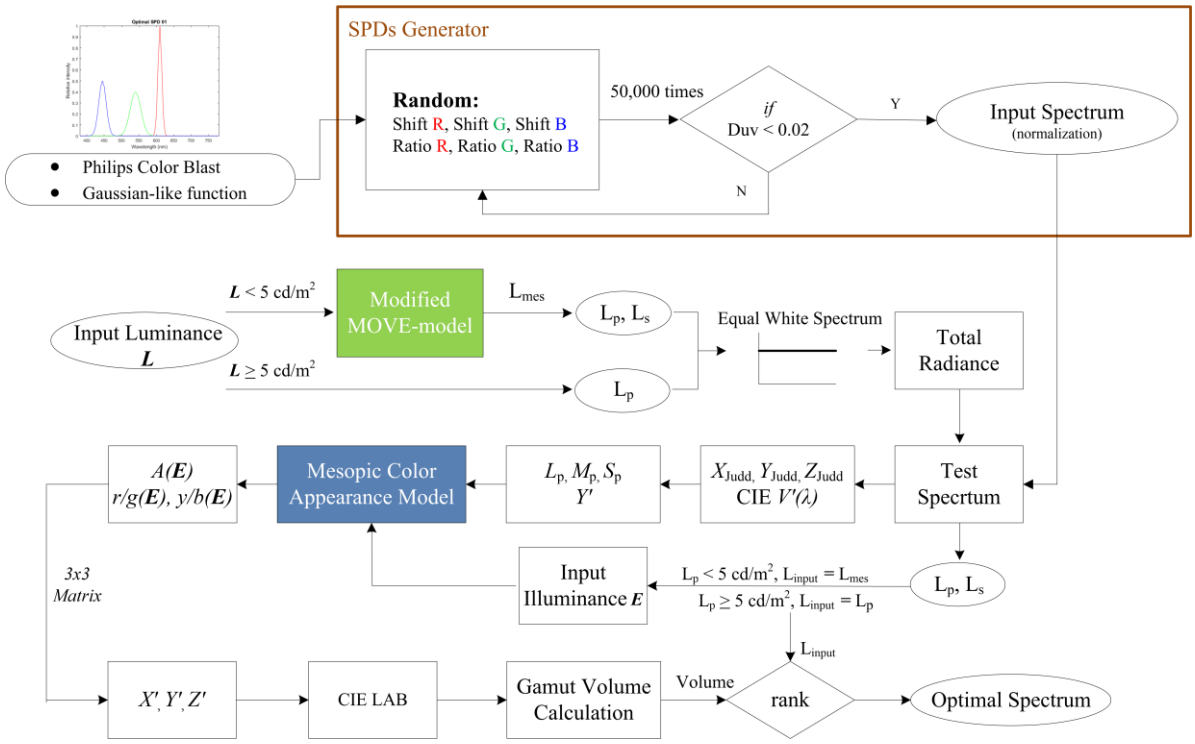

Figure 1 – Flow chart of trichromatic white LED spectrum optimization

$$SuperGaussian(x) = \exp\left(\frac{-0.5 \cdot abs(x)^n}{alpha^n}\right),\ alpha = \mathrm{FWHM} \cdot \frac{\sqrt{2\ln(2)}}{2} \tag{2}$$

After simulating the colour appearance A(E), r/g(E), y/b(E) under a specific luminance level, the simulated tristimulus values X', Y', Z' were obtained by a 3x3 transformation matrix and converted to CIE LAB colour space for its gamut volume calculation. The gamut volume is the summation of all tetrahedron's volume where the tetrahedra are determined by 3D Delaunay triangulation of the colour samples, and the unit of gamut volume is LAB cube. Finally, according to the predicted photopic/mesopic luminance level and the gamut volume, the test spectra with the highest L_{mes}, largest gamut volume (GV), and highest (L_{mes}+GV) are selected as the optimal white LED spectra under a specific luminance level.

3 Results

3.1 Characteristics of trichromatic white LED spectra

To better determine the characteristic of the trichromatic white LED spectrum on mesopic luminance and gamut volume, the spectra with the variance of peak wavelength shifts and the different powers of three components are investigated under 10 cd/m^2 and 1 cd/m^2 luminance levels. Note that the luminance level refers to the luminance of an equal energy white. The test SPDs are normalized to have the same total radiance to the equal energy white. Due to

the similar characteristic of the simulated Gaussian-like function dataset, only the results of Philips Color Blast are present. As shown in Figure 2, the test spectrum where the blue, green, red LED located at 430 nm, 520 nm, 600 nm are shifted to 480 nm, 570 nm, 650 nm with 5 nm spectral interval.

The results indicate that the mesopic luminance would increase with the shifts of blue LED from the shorter wavelength to the longer one, but the maximum gamut volume could be achieved at a particular wavelength position under these two luminance levels. With the shifts of green LED, the gamut volume decreases acutely, but the highest mesopic luminance appears. However, the performance of mesopic luminance in the aspect of the red LED is entirely different from that of the blue LED. Besides, the two lighting levels show an identical tendency. The impacts of the RGB-LED ratio (i.e., the rate of the maximum powers of the blue, green and red LED) on mesopic luminance and gamut volume are also studied, and the results are shown in Figure 3 where the mesopic luminance increases with a higher ratio of green and red LED. By providing higher powers of blue and red LED can extend the range of colour gamut volume.

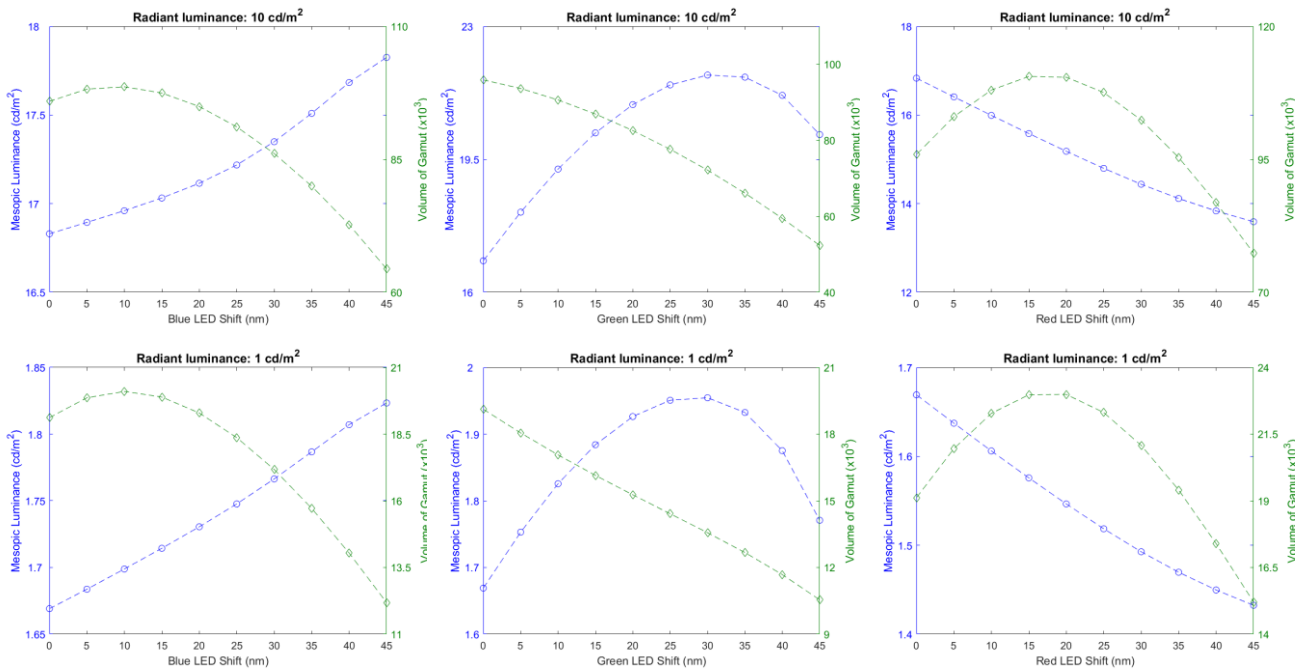

Figure 2 – Characteristic of luminance and gamut volume when shifting peak wavelength of LEDs (left to right: Blue, Green, and Red)

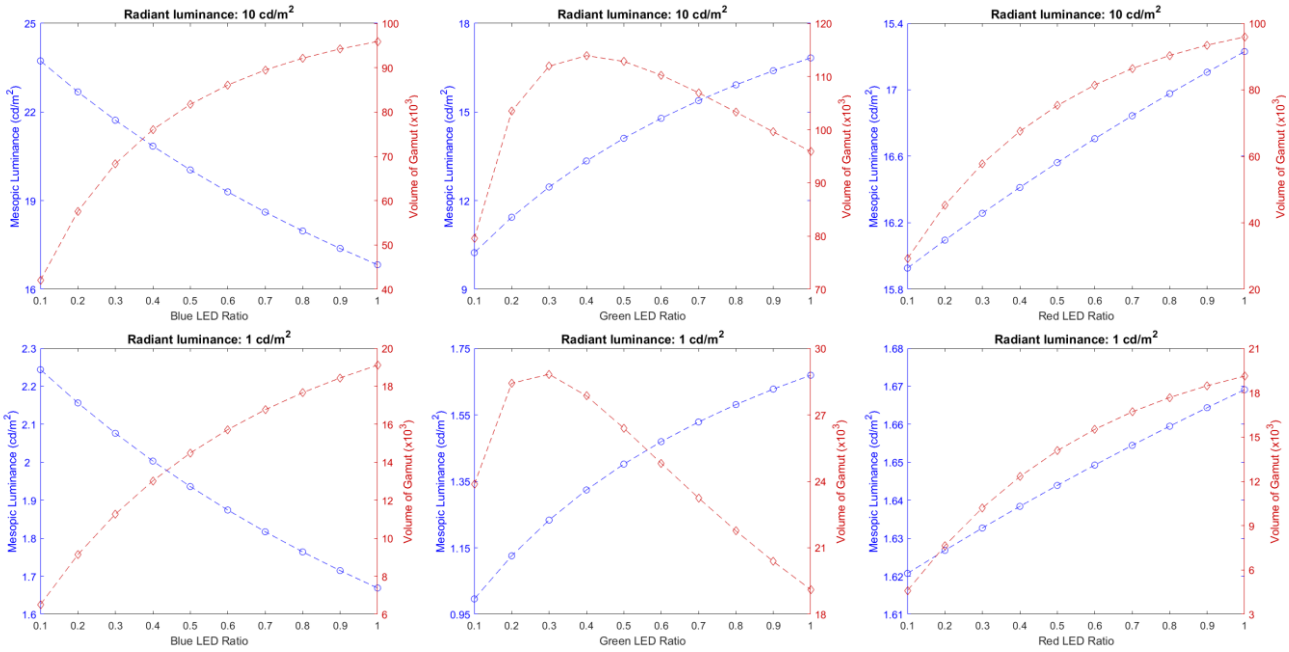

Figure 3 – Characteristic of luminance and gamut volume when changing the ratios of LEDs (left to right: Blue, Green, and Red)

3.2 Optimal trichromatic white LED spectra

Based on the white LED optimization method mentioned above, the optimal trichromatic white LED spectra are derived for 10 cd/m^2, 1 cd/m^2, 0.3 cd/m^2, and 0.1 cd/m^2 luminance levels, respectively. Due to the consideration of the constraint on computing, 3 000 kinds of test SPDs for each dataset are tested in this study. In the theoretical simulation, the spectral reflectance of 1 269 matt Munsell colour chips and the mesopic colour appearance model are used to optimize the white LED spectrum. The different shifts and ratios of red, green, and blue LED are the variables to simulate their gamut volumes in the same radiant quantity condition. The 24 optimal spectra and a colour gamut of the spectrum, which simultaneously provide relatively higher L_{mes} and larger colour gamut (L_{mes}+GV) under four lighting levels, are shown in Figures 4 and 5. Table 1 and Table 2 lists the peak wavelength and the ratios of LEDs. Also, their mesopic luminance (L_{mes}), gamut volume (GV), and S/P-ratio can be seen in Table 3 and Table 4.

Table 1 – The information of optimal white LED spectra (Philips Color Blast)

(cd/m^2)	Peak Wavelength (nm)								
	L_{mes}+GV			L_{mes}			GV		
	Blue	Green	Red	Blue	Green	Red	Blue	Green	Red
10	445	545	620	445	570	605	435	535	645
1	445	545	620	445	570	605	435	525	640
0.3	455	540	620	480	570	605	435	525	640
0.1	460	525	620	475	530	605	445	525	640
(cd/m^2)	**Ratio**								
	L_{mes}+GV			L_{mes}			GV		
	Blue	Green	Red	Blue	Green	Red	Blue	Green	Red
10	0.4	0.6	0.8	0.1	0.6	1.0	0.8	0.5	1.0
1	0.4	0.6	0.8	0.1	0.6	1.0	0.4	0.3	0.5
0.3	0.6	0.7	0.8	0.1	0.5	1.0	0.4	0.3	0.5
0.1	0.4	0.5	0.6	0.1	0.2	0.7	0.5	0.4	0.6

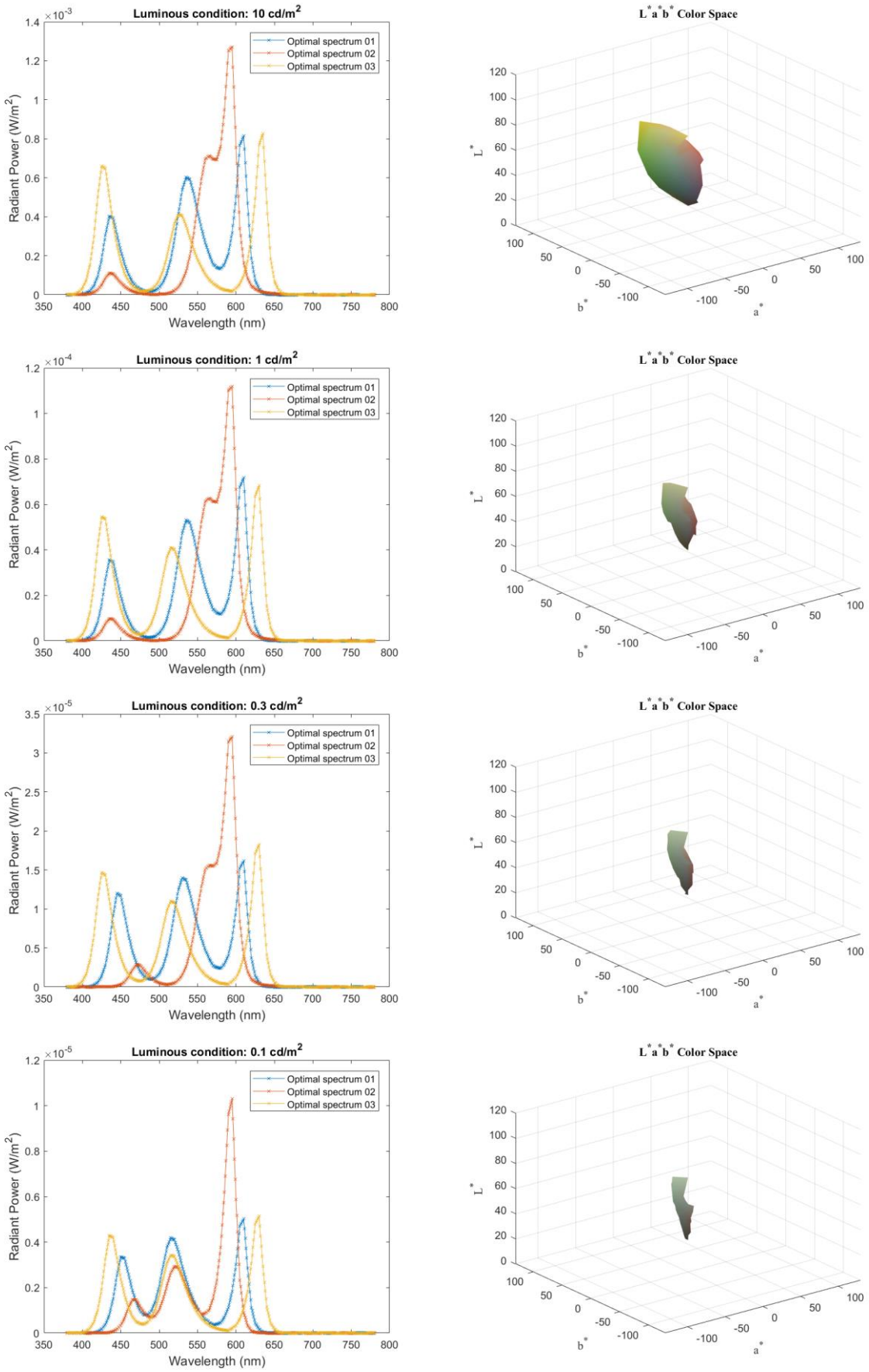

Figure 4 – Illustration of SPDs (left) and colour gamut (right) of SPD (L_{mes}+GV) under 10 cd/m^2, 1 cd/m^2, 0.3 cd/m^2 and 0.1 cd/m^2 luminance levels (Philips Color Blast)

For maximizing the $L_{mes,}$ the optimal spectra derived from Philips Color Blast and Gaussian-like function with similar peak power density ratio of blue, green and red LEDs are recommended for 10 cd/m^2, 1 cd/m^2 and 0.3 cd/m^2 whereas the SPD with higher S/P-ratio for 0.1 cd/m^2 is different. The optimal spectra with higher S/P-ratio and CCT can improve the colour perception, especially under dim lighting conditions. Furthermore, a trade-off between mesopic luminance and colour gamut was quite evident.

Table 2 – The information of optimal white LED spectra (Gaussian-like function)

(cd/m^2)	**Peak Wavelength (nm)**								
	L_{mes}+GV			L_{mes}			GV		
	Blue	Green	Red	Blue	Green	Red	Blue	Green	Red
10	445	555	610	455	570	605	435	535	625
1	445	540	610	455	570	605	435	535	625
0.3	460	540	615	470	570	610	435	535	625
0.1	475	525	615	465	525	605	455	525	625
(cd/m^2)	**Ratio**								
	L_{mes}+GV			L_{mes}			GV		
	Blue	Green	Red	Blue	Green	Red	Blue	Green	Red
10	0.3	0.5	0.8	0.1	0.5	0.9	0.6	0.4	1.0
1	0.2	0.3	0.6	0.1	0.5	0.9	0.6	0.4	1.0
0.3	0.4	0.5	0.9	0.2	0.8	1.0	0.6	0.4	1.0
0.1	0.5	0.4	0.7	0.2	0.3	0.6	0.5	0.4	0.9

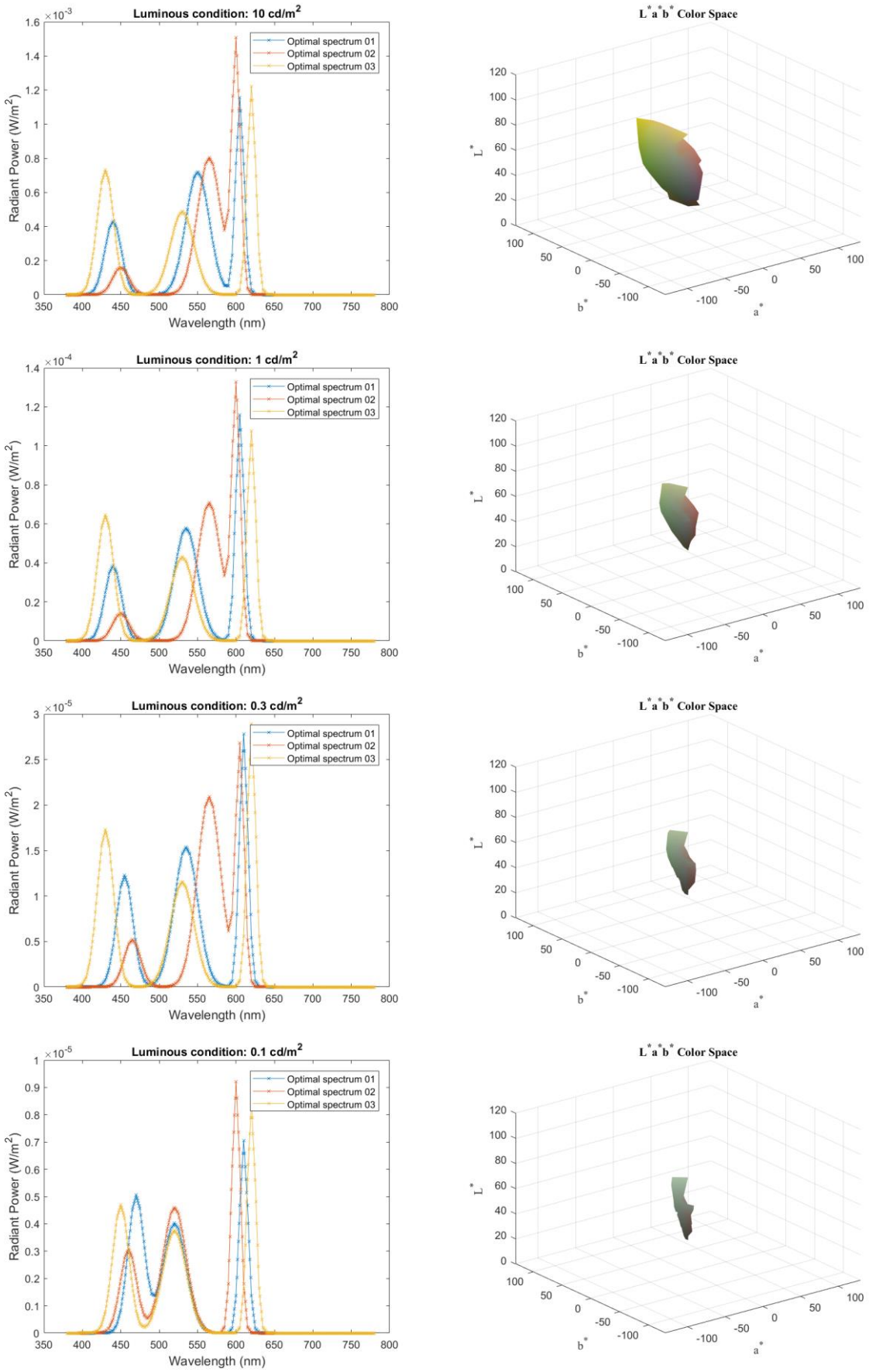

Figure 5 – Illustration of SPDs (left) and colour gamut (right) of SPD (L_{mes}+GV) under 10 cd/m^2, 1 cd/m^2, 0.3 cd/m^2 and 0.1 cd/m^2 luminance levels (Gaussian-like function)

Table 3 – Mesopic luminance (L_{mes}), gamut volume (GV) and S/P-ratio of optimal spectra (Philips Color Blast)

(cd/m^2)	Predicted L_{mes}			Gamut volume (x10^3)			S/P-ratio		
	L_{mes}+GV	L_{mes}	GV	L_{mes}+GV	L_{mes}	GV	L_{mes}+GV	L_{mes}	GV
10	22.36	29.36	13.23	90.79	24.80	128.83	1.55	0.65	2.26
1	2.03	2.55	1.33	17.30	3.97	29.52	1.55	0.65	2.68
0.3	0.57	0.66	0.41	7.48	1.12	15.24	2.02	0.71	2.68
0.1	0.18	0.19	0.15	3.06	1.00	4.59	2.70	1.39	2.95

Table 4 – Mesopic luminance (L_{mes}), gamut volume (GV) and S/P-ratio of optimal spectra (Gaussian-like function)

(cd/m^2)	Predicted L_{mes}			Gamut volume (x10^3)			S/P-ratio		
	L_{mes}+GV	L_{mes}	GV	L_{mes}+GV	L_{mes}	GV	L_{mes}+GV	L_{mes}	GV
10	24.31	28.42	15.05	80.78	33.78	134.35	1.25	0.71	2.11
1	2.02	2.47	1.44	18.65	5.82	30.26	1.70	0.71	2.11
0.3	0.57	0.65	0.43	7.80	2.923	14.81	2.05	0.86	2.11
0.1	0.18	0.19	0.16	3.28	2.47	5.00	3.40	2.48	3.07

By applying more simulated spectral data, the optimization method of the trichromatic white LED spectrum can well find the solutions to raise the mesopic luminance (L_{mes}) and enlarge the colour gamut volume (GV). The results show that the green component is a benefit for mesopic luminance, and the red and blue LEDs influence the range of colour gamut most. Under 0.1 cd/m^2 lighting condition, the green channel of the optimal spectrum producing the highest mesopic luminance shifts to the shorter wavelength position following the conversion of mesopic luminous efficiency from photopic to scotopic vision. Figures 6 and 7 are the simulated images of mesopic colour reproduction using the optimal spectra. The information of Duv, CCT, and colour rendering properties (CRI, R_f and, R_g) are listed in Table 5. The optimal spectra (L_{mes}+GV) can also present the acceptable colour performance for mesopic conditions. However, the majority of the white LED spectrum is optimized based on luminous efficiency and colour rendering index mostly in the photopic vision, which shows a wider colour gamut than in mesopic vision. For dim lighting conditions, the conventional colour rendering properties such as CRI and IES TM-30-15 cannot express the colour variation with the decreasing of illuminance.

Table 5 – CCT, Duv and colour rendering properties of (L_{mes}+GV) white LED spectra

(cd/m^2)	Philips Color Blast					Gaussian-like function				
	CCT(K)	Duv	CRI	R_f	R_g	CCT(K)	Duv	CRI	R_f	R_g
10	4,579	0.0162	68	66	97	4,332	0.0167	49	47	84
1	4,579	0.0162	68	66	97	4,770	0.0183	72	68	102
0.3	5,977	0.0145	77	75	99	5,643	0.0149	82	77	104
0.1	6,665	0.0145	81	76	101	8,023	0.0185	59	53	89

(a)

(b)

(c)

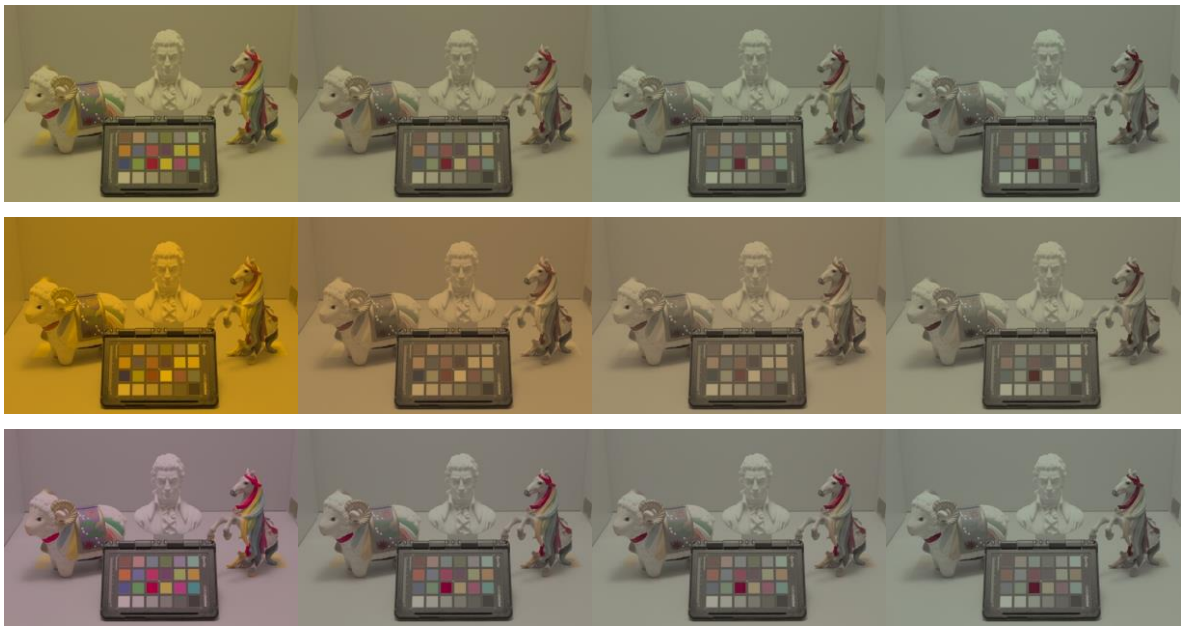

Figure 6 – Simulated images of optimal spectra (Philips Color Blast) under four lighting levels (left to right: 10 cd/m^2, 1 cd/m^2, 0.3 cd/m^2 and 0.1 cd/m^2, (a): L_{mes}+GV (b): L_{mes} (c): GV)

(a)

(b)

(c)

Figure 7 – Simulated images of optimal spectra (Gaussian-like function) under four lighting levels (left to right: 10 cd/m^2, 1 cd/m^2, 0.3 cd/m^2 and 0.1 cd/m^2, (a): L_{mes}+GV (b): L_{mes} (c): GV)

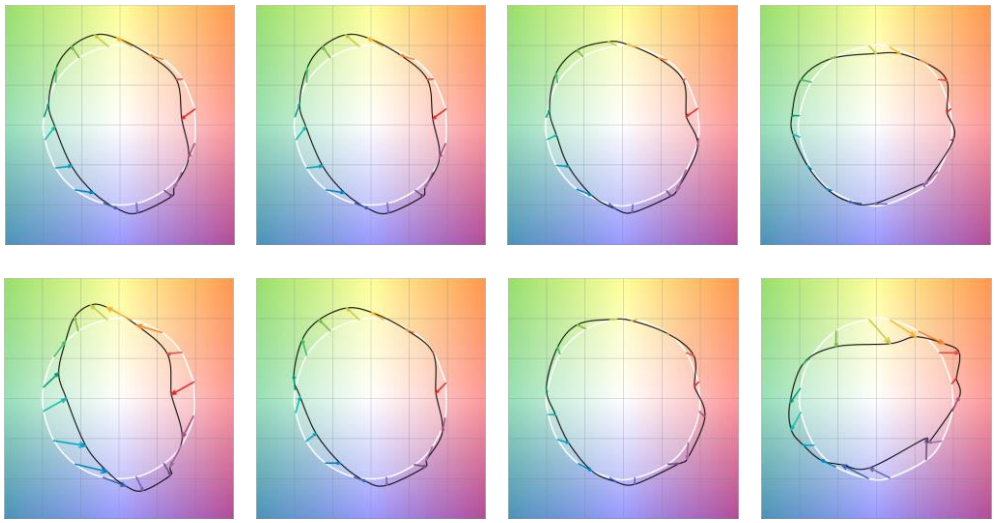

Figure 8 – Colour Vector Graphic of optimal trichromatic white LED (L_{mes}+GV) (top: Philips Color Blast, bottom: Gaussian-like function) for four lighting levels (left to right: 10 cd/m^2, 1 cd/m^2, 0.3 cd/m^2 and 0.1 cd/m^2)

4 Conclusions

In the study, the RGB-LED spectra of Philips Color Blast and simulated by applying Gaussian-like function are tested for better knowing the characteristics of white LED spectra. To obtain mesopic luminous, S/P-ratio of a light source and its photopic luminous are needed. The theoretical simulation uses the mesopic colour appearance model to investigate the gamut volume under optimal white LED spectra. An optimization theory based on the modified MOVE-model and a mesopic colour appearance model is applied to optimize trichromatic white LED spectra for lighting design. Three kinds of white LED spectra with acceptable Duv are recommended for improving visual perception for each luminance level from two datasets. From the simulated results, the SPDs significantly influences the predicted mesopic luminance and 3D colour gamut. The predicted mesopic luminance increases for a blue LED by shifting the peak wavelength to a long position. Besides, the higher power density ratio of blue and red LED contributes to better performance of colour gamut. Comparing our results with the previous study, the optimal spectra we proposed can produce higher mesopic luminance but not for colour gamut volume because of the trade-off between these two features. However, the 24 optimal spectra are the results of local optimization. For future work, the global optimization for trichromatic white LED spectra can be discussed with parallel computing, and a visual experiment is necessary to verify the effect of lighting applications.

References

Eloholma, M., Viikari, M., Halonen, L., Walkey, H., Goodman, T., Alferdinck, J. W. A. M., ... & Várady, G. 2005. Mesopic models—from brightness matching to visual performance in night-time driving: a review. *Lighting Res. Technol.*, 37(2), 155-173.

Rea, M. S., Bullough, J. D., Freyssinier-Nova, J. P., & Bierman, A. 2004. A proposed unified system of photometry. *Lighting Res. Technol.*, 36(2), 85-109.

Eloholma, M., & Halonen, L. 2006. New model for mesopic photometry and its application to road lighting. *Leukos*, 2(4), 263-293.

Halonen, L., & Puolakka, M. 2010. CIE and mesopic photometry. CIE NEWS, 1-2.

Viikari, M., Ekrias, A., Eloholma, M., & Halonen, L. 2008. Modeling spectral sensitivity at low light levels based on mesopic visual performance. Clinical ophthalmology (Auckland, NZ), 2(1), 173.

Zan, L., Lin, D., Zhong, P., & He, G. 2016. Optimal spectra of white LED integrated with quantum dots for mesopic vision. *Optics Express*, 24(7), 7643-7653.

CIE 2010. CIE 191:2010. *Recommended System for Mesopic Photometry Based on Visual Performance*. Vienna: CIE.

Shin, J., Matsuki, N., Yaguchi, H., & Shioiri, S. 2004. A color appearance model applicable in mesopic vision. *Optical review*, 11(4), 272-278.

Kaiser, P. K., & Boynton, R. M. 1996. Human color vision.

Li, H. C., Huang, Y. N., & Sun, P. L. 2018. A comparison of optimal white LED spectra under mesopic condition. Optics & Photonics Taiwan International Conference.

Illuminating Engineering Society of North America. 2015. *IES TM-30-15, IES Method for Evaluating Light Source Color Rendition*. Illuminating Engineering Society of North America.

Li, H. C., Sun, P. L., & Ronnier Luo, M. 2016. Optimization of White LED Spectrum under Mesopic Condition Based on 3D Color Gamut. 4th CIE Symposium on Color and Visual Appearance, Prague, Czech Republic.

International Commission on Illumination
Commission Internationale de l'Eclairage
Internationale Beleuchtungskommission

PO17

A COMPARISON OF COLOUR APPEARANCE IN VIRTUAL REALITY BETWEEN DIFFERENT SCREEN RESOLUTIONS

Chi-Han Ma et al.

DOI 10.25039/x47.2020.PO17

Paper accepted for the 5th CIE Symposium on Colour and Visual Appearance

The paper was selected by the International Scientific Committee (ISC) for presentation at the 5th CIE Symposium on Colour and Visual Appearance, Hong Kong, CN, April 21–22, 2020, which, due to the corona pandemic, could not take place. The paper has not been peer-reviewed by CIE.

CIE Central Bureau
Babenbergerstrasse 9
A-1010 Vienna
Austria
Tel.: +43 1 714 3187
e-mail: ciecb@cie.co.at
www.cie.co.at

PO17

A COMPARISON OF COLOUR APPEARANCE BETWEEN DIFFERENT RESOLUTION IN VIRTUAL REALITY

Ma, C.[1], Huang, H.[2], Ou, L.[1]
[1] National Taiwan University of Science and Technology, Taipei, CHINESE TAIPEI
[2] Chihlee University of Technology, New Taipei City, CHINESE TAIPEI
karena6041@gmail.com

Abstract

This study compares colour appearance in virtual reality between different levels of display resolution. A total of 24 test colours selected from CIELAB space including 5 hue regions: red (with a hue angle of 20°), yellow (90°), green (164°), blue (245°) and purple (320°). 16 observers participated in this experiment. High correlation was found between perceived lightness and CIECAM02 J, between perceived hue quadrature and CIECAM02 H, and between perceived colourfulness and CIECAM02 M with a correlation coefficient of 0.88, 0.99 and 0.81, respectively.

Keywords: Colour appearance, Virtual reality, CIECAM02

1 Introduction

Many types of virtual reality (VR) devices are used in our daily life, among which the most convenient one is the mobile VR headset - putting a mobile phone in the headset and then starting the VR experience anywhere. It is unclear whether there is any difference in colour appearance between colours seen in a VR environment and those in the real world, and thus it is desired to investigate the appearance of colour in VR space. In a previous study, we have conducted such a comparison between perceived colour appearance in VR and the predicted values by CIECAM02. The experimental results show high predictive performance of CIECAM02 for colour appearance in the VR environment for lightness and hue quadrature, but relatively lower correlation was found for colourfulness. We had a hypothesis that maybe the reason for this result was due to the fact that the display resolution of the mobile phone used in the experiment was too low, and that if we can increase the display resolution, we may get a different result. In that previous study, we used an iPhone 6 in the experiment, with a PPI of 326, and this time we used an iPhone XS, with a PPI of 458, in an attempt to investigate whether the display resolution will affect the experimental results or not.

2 Experimental Methods

A psychophysical experiment of colour appearance was conducted in this study. We used 3DS MAX software to create a 3-dimensional interior space which was then transformed into VR images. An iPhone XS was used to present the VR images in this study. The phone had a 5.8 inch screen, with a resolution of 2 436 pixels by 1 125 pixels, i.e. 458 ppi. A MINISO Simple 3D VR Glasses was also used in this experiment.

2.1 VR Environment

The size of VR space was 220 (width) by 255 (depth) by 200 (height). All of the objects, including the walls and a desk, in this VR space had a colour of medium grey, except the three colour patches on the main wall. Three colour patches were presented side by side on the wall, with a perceived size of patches on the left side and the right side of 21.25 cm by 21.25 cm. The colour patch in the middle, i.e. the test colour, had a perceived size of 37.5 cm by 37.5 cm. The layout for the three colour patches is shown in Figure 1. The left patch was the reference white, with an adopted lightness value of 100. The one on the right was the reference colourfulness, with an adopted colourfulness value of 40. The luminance of the reference white was

286.53 cd/m^2, with (x, y) = (0.3177, 0.3384). The perceived viewing distance between the observer's eyes and the main wall was 214 cm.

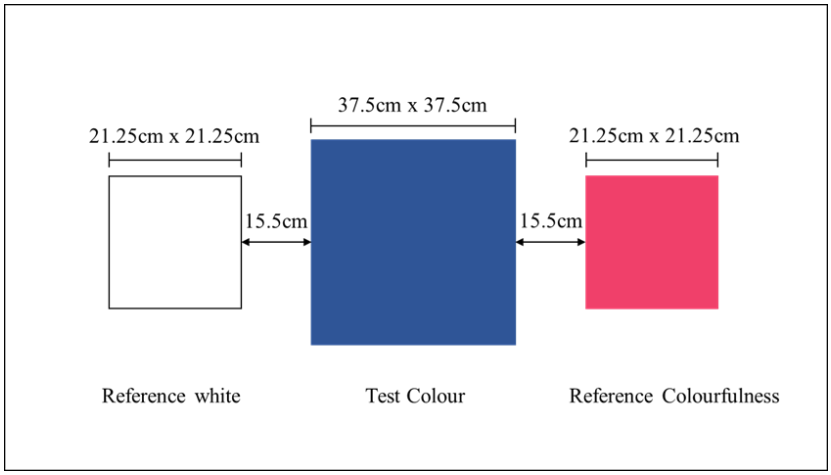

Figure 1 – The layout for colour appearance in virtual reality experiment

2.2 Colour Samples

24 colours were selected from CIELAB space to be used as the test colour samples in this study. Figure 2 (a)-(c) show the distribution of these test colours in CIELAB a*-b*, L*-a* and L*-b*, respectively. These colours included 5 hue regions: red (with a hue angle of 20°), yellow (90°), green (164°), blue (245°) and purple (320°). Each hue region has 4 levels of lightness with chroma, and 4 achromatic colours. 10 of these test colours were repeated in the experiment for repeatability test. Thus, each observer made 34 visual assessments of colour appearance in the experiment.

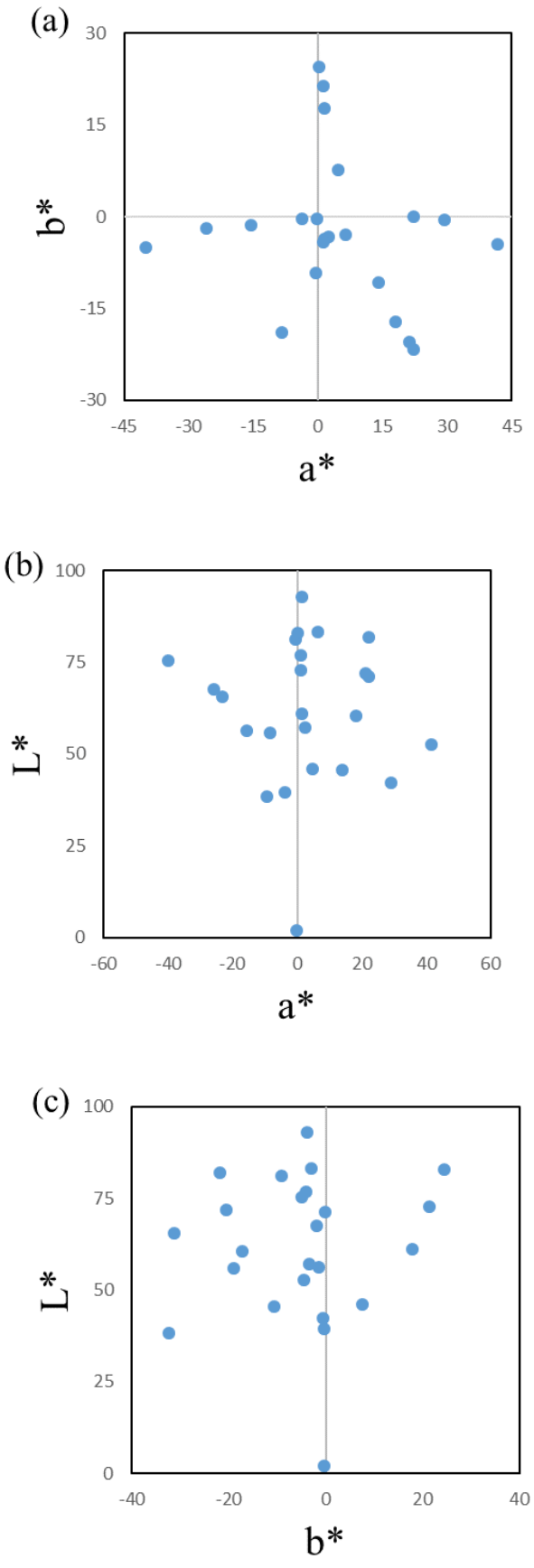

Figure 2 – The 24 test colours of this experiment plotted in (a) CIELAB a*-b*, (b) CIELAB L*-a* and (c) CIELAB L*-b*planes

2.3 Experimental Procedure

Each observer was asked to visually assess each colour sample in terms of lightness, colourfulness and hue quadrature during the experiment. The 34 test colours, including 10 replicated colours, were presented one at a time in random order. After a test colour was assessed, a full screen of medium grey was presented for 30 seconds, after which a next test colour would be shown. The observer needed to wear the VR headset to perform the visual assessments. To prevent them from getting too tired in the eyes due to the VR experience, there was a 10-minute break after the observer has completed 17 test colours, and during the break the observer was encouraged to take off the VR headset to take a rest. The entire experiment lasted about 30 minutes for each observer.

16 observers participated in this experiment, who were all university students with normal colour vision. After the study, none of the observers reported visual discomfort.

3 Results

As a result, high correlation was found between perceived lightness and CIECAM02 J, with a correlation coefficient of 0.88. High correlation was also found between perceived hue quadrature and CIECAM02 H, with a correlation coefficient of 0.99. However, correlation between perceived colourfulness and CIECAM02 M was found to be relatively lower than the other two scales, with a correlation coefficient of 0.81.

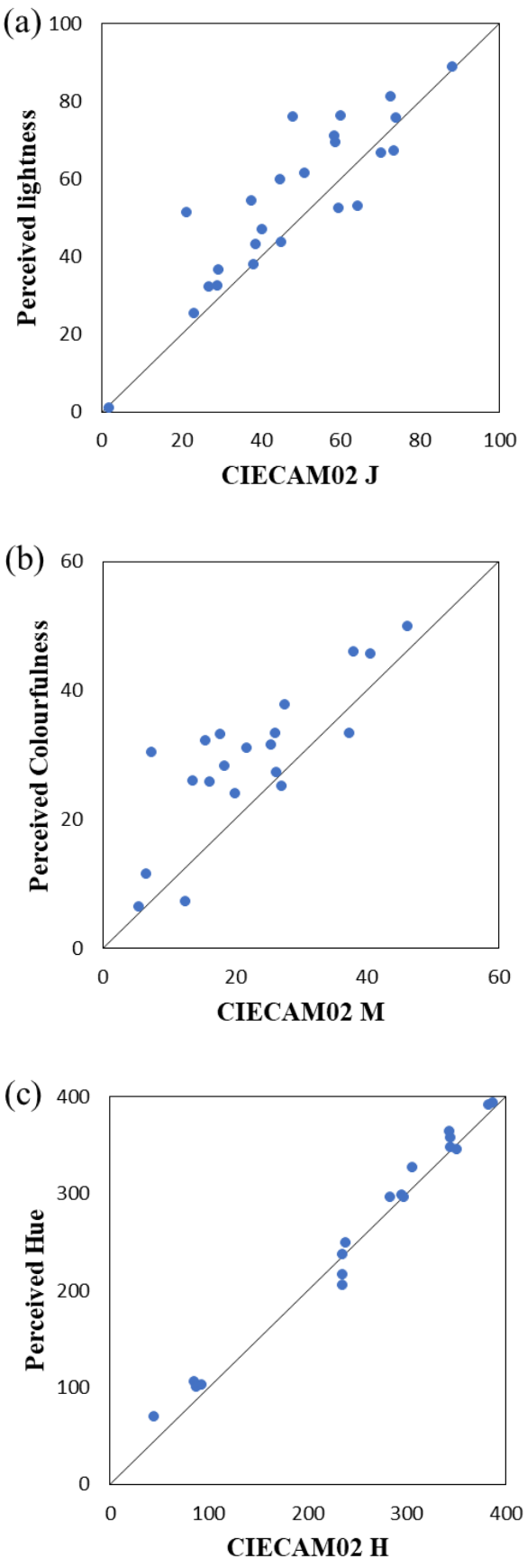

Figure 3–(a) The perceived lightness vs. CIECAM02 J, (b) perceived colourfulness vs. CIECAM02 M, (c) perceived hue quadrature vs. CIECAM02 H

4 Conclusion

Comparing the experimental results with those conducted previously, both have high correlation with CIECAM02, showing good predictive performance of CIECAM02 for VR environment. Apart from hue quadrature, the perceived lightness and perceived colourfulness seem to be higher than the corresponding predicted values by CIECAM02. The scatter graph of perceived colourfulness still shows a somewhat logarithmic curve. Due to these results, maybe the resolution is not the most important factor. Future studies may look into the lighting, colours and some other conditions to increase the quality of VR experience.

Acknowledgments

This work was supported in part by the Ministry of Science and Technology, Taiwan (MOST 109-2410-H-263-001).

References

Fairchild, M.D., 2013. *Color appearance models*. John Wiley & Sons.

Moroney, N., Fairchild, M.D., Hunt, R.W., Li, C., Luo, M.R. and Newman, T., 2002, January. The CIECAM02 color appearance model. In *Color and Imaging Conference* (Vol. 2002, No. 1, pp. 23-27). Society for Imaging Science and Technology.

International Commission on Illumination
Commission Internationale de l'Eclairage
Internationale Beleuchtungskommission

PO19

CONTROLLED SPECTRAL POWER DISTRIBUTION METHOD TO IMPROVE VISUAL ACUITY IN THE MESOPIC AND SCOTOPIC STATES OF VISION, FOR OUTDOOR LIGHTING APPLICATIONS

Rohan Nag

DOI 10.25039/x47.2020.PO19

Paper accepted for the 5th CIE Symposium on Colour and Visual Appearance

The paper was selected by the International Scientific Committee (ISC) for presentation at the 5th CIE Symposium on Colour and Visual Appearance, Hong Kong, CN, April 21–22, 2020, which, due to the corona pandemic, could not take place. The paper has not been peer-reviewed by CIE.

CIE Central Bureau
Babenbergerstrasse 9
A-1010 Vienna
Austria
Tel.: +43 1 714 3187
e-mail: ciecb@cie.co.at
www.cie.co.at

PO19

CONTROLLED SPECTRAL POWER DISTRIBUTION METHOD TO IMPROVE VISUAL ACUITY IN THE MESOPIC AND SCOTOPIC STATES OF VISION, FOR OUTDOOR LIGHTING APPLICATIONS

Nag, R.
Regent Lighting, Bangalore, INDIA
rohan.studsat@gmail.com

Abstract

Rapid transition from conventional to solid state lighting combined with the lack of technical understanding on outdoor lighting applications and human vision perception, poses a serious threat to the nocturnal ecology and the health and safety of human beings. In an experimental setup, by varying the relative spectral power of a luminous source in an outdoor environment; we are able to test and validate a significant increase in responsivity and decrease in metamerism under low and very low lighting conditions.

1 Motivation

In the past decade the world has witnessed an increasing number of companies, emerging in the solid state lighting industry. Under a stiff competitive environment, numerous projects are being executed where, utmost importance is given to achieve and maintain the photopic lux but almost no calculation on the rendering conditions in the mesopic and the scotopic states are ever emphasized. The inability to understand the lighting applications completely, its demands, parameters, etc. along with the failure to leverage the current scientific breakthroughs in the field of solid state control technologies has not only resulted in the increased lighting points & lighting levels causing light pollution from surface scattering & direct spill light, but also reduced human visual acuity in many instances.

The motivation for this technical paper comes from the numerous years spent and the numerous challenges faced through those years, in the fields of light planning, designing, installing and commissioning various lighting applications. Also the recent advancements in human circadian lighting mechanisms and the current quest towards defining the visual adaptation field to quantify the adaptation luminance, have all been a source of inspiration for this paper.

2 Method

To have a comprehensive understanding of the solution, we have shortlisted one of several real world problem statements that will have the maximum impact, if solved. After thorough investigation, we implemented the test procedures at the experimental setup and observed the results over multiple iterations. The problem statement considered, is of the night time poor visibility issue at coastal areas under infrastructure lighting. Unlike the widely known phenomenon of water vapour condensing on airborne salt particles causing fog which scatters light beams from a solid state lighting source, which were intended to uniformly reach the target application surface; the night time sea fog is actually caused when cold air passes over moist warm lands. Experimental setup as depicted in Figure 1. In such a situation, the problem of poor visibility cannot be addressed by the currently used methods of either increasing the luminous intensity intended per unit area of the application or altering the beam angle of the luminaire between wide and narrow beams. The probable solution takes inspiration from the previous lighting technology used in these applications, the high pressure sodium vapour lamps. With a low correlated colour temperature and lower colour rendering index, the HPSV technology had catered to the visibility issue for years but had eventually phased out because of high operational costs and frequent maintenance needs.

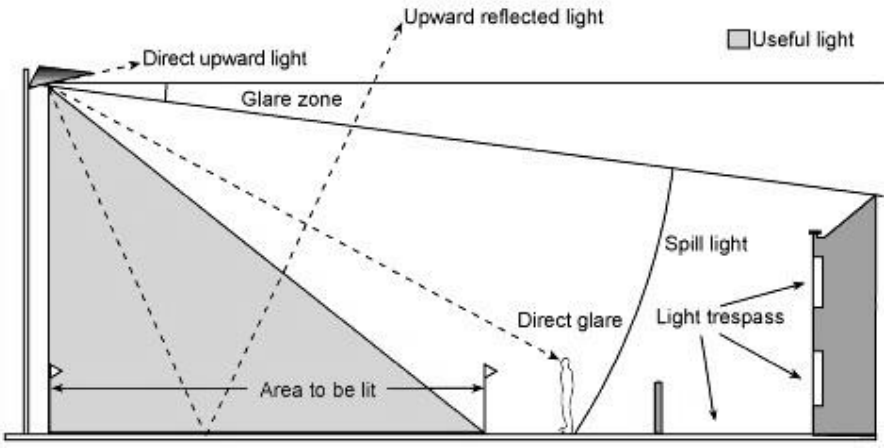

Figure 1 – Infrastructure Lighting Application

The hardware construction of the experimental setup consists of two parts. Three numbers of LED's Red, Green and Blue soldered together on a PCB as a single unit with a dedicated lens on each PCB unit, collectively enclosed in a clear polycarbonate diffuser; forms the optical compartment. The hardware was initially tested with the LED chips, depicted in Figures 2 and 3.

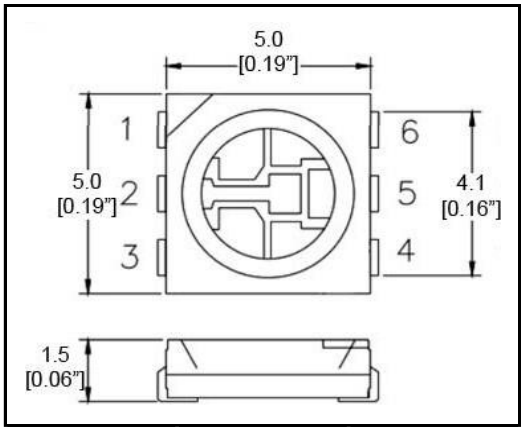

Figure 2 – RGBW LED Chip

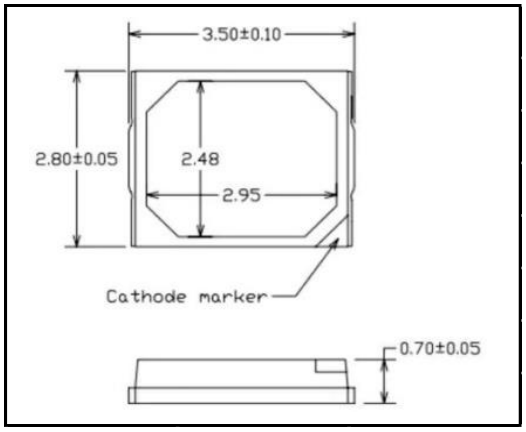

Figure 3 – Tunable LED Chip

The spectral power distribution module with its multichannel control lines to the PCB's are enclosed in the driver compartment, connected to a secure server over a virtual LAN. The software construction consists of a data intake system that draws real-time data from an astronomical clock and a local weather station. The data is assembled on a single platform and analysed by a centrally housed algorithm. In every ten minutes, the spectral power control data for various zones of the application is transmitted wirelessly.

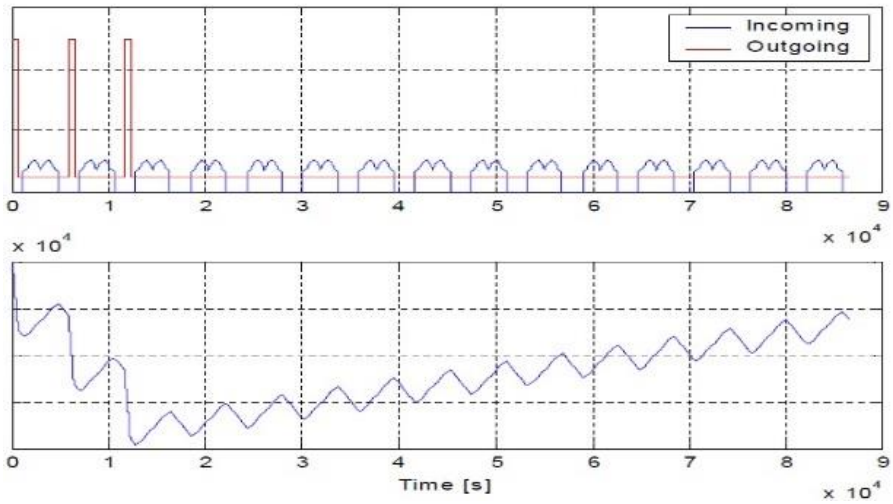

Figure 4 – Test Indicating Increase in Responsivity on the Simulator

To better understand the suitable applications of this technology, we conducted an experiment between two different lighting designs with the use of the same SPD unit. Below Figure 5 depicts the direct lighting application and the Figure 6 depicts the volumetric lighting application (light sources placed at equal but angular locations)

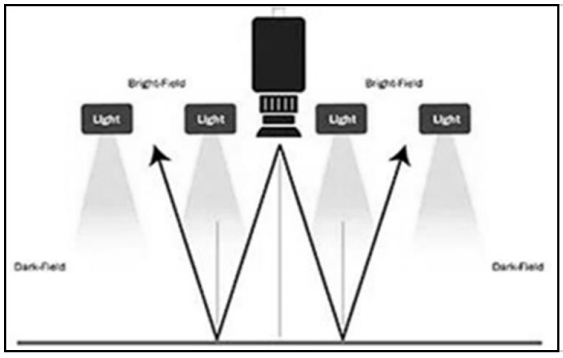

Figure 5 – Direct Application

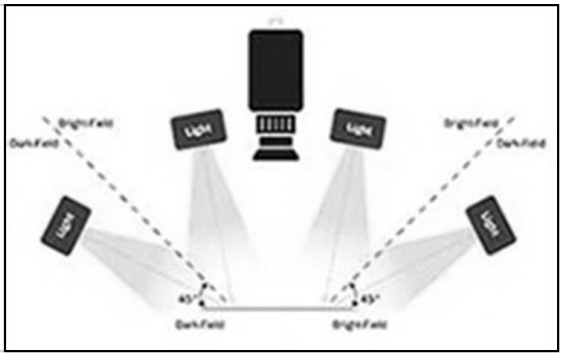

Figure 6 – Volumetric Application

Four different beams were selected for each application. A wide, narrow, dual asymmetric and asymmetric beams. Each beam was used for several hours to study the transitions between the mesopic to scotopic and scotopic back to mesopic states.

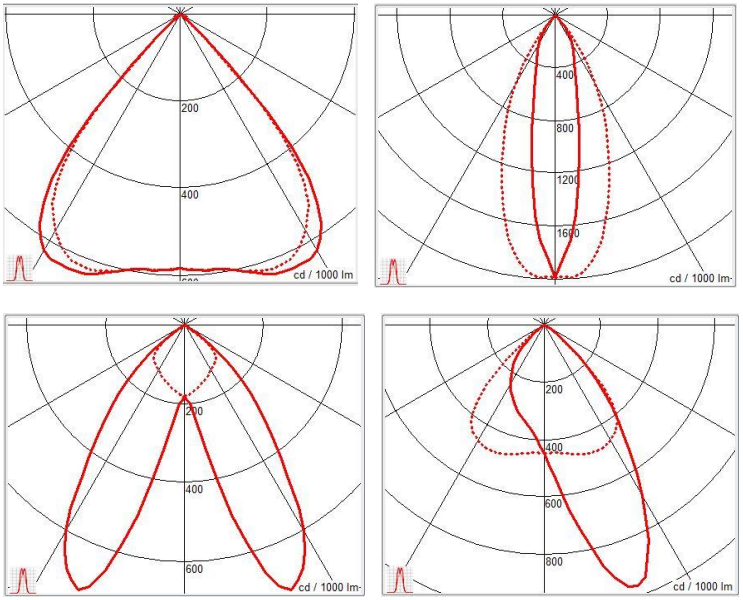

Figure 7 – Four Different Beams Applied

With the completion of the initial experiment, we were able to plot the resultant data and draw our conclusions; formulate our aim for the next set of experiments and parameters to consider.

3 Results

The experimental setup was simulated and run from dusk to dawn, continuously for a week. We observed the gradual change in $W \cdot m^{-2} \cdot nm^{-1}$ for different application zones depending upon the variable input data set. The intensity was intentionally varied under harsh weather conditions, as to enter the mesopic 0.01 cd/m^2 to 3 cd/m^2 state of vision, then the scotopic 10^{-3} cd/m^2 to 10^{-6} cd/m^2 state of vision and back to the mesopic state of vision. The experiment was repeated several times and the observations were tabulated. Improvements in the backend algorithm was done repeatedly after every round of experimentation. Currently we are attempting to narrow down on the results for a better understanding of the human vision perception and phenomenon. The plotted results from the experiment is described in the Chart 1, below. We now understand that direct lighting application has a higher rate of responsivity vs the volumetric application, since the spectrally tuned wave gets heavily distorted with the increase in overall distance from the source; because of scattering.

Chart 1 – Difference in Measured Responsivity

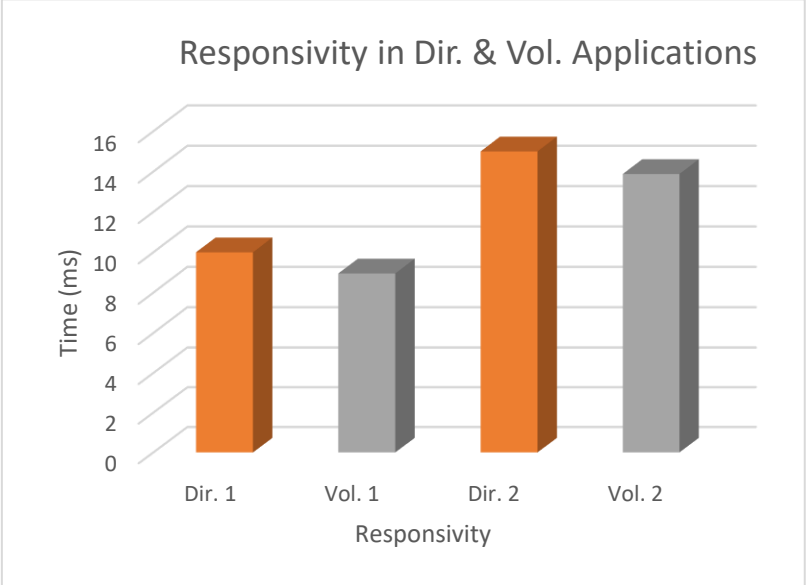

The above discussed procedure was also tested with a different control parameter set, for a heavy manufacturing industry; to address the issue of metamerism on the assembly floor. Significant increase in the quality of workmanship was observed.

4 Conclusion

From the above experimental setup and the subsequent understanding gathered over a period of few months, we can deduce that; implementing a controlled spectral power distribution method in outdoor lighting fixtures, helps in improving human vision without causing harm to the nocturnal ecosystem. The sole intention of writing this scientific paper is to propose, debate and discuss the very need for a deeper understanding of the mesopic and its transition to and from the scotopic state of human vison and the conditions governing them. We find ourselves in full confidence that a mesh network of intelligent spectral power distribution units can be implemented in different lighting applications, world across to reduce risks and improve overall wellbeing. We hope that the spirit of scientific enquiry in this field will generate feedback and criticism; from which we shall draw the ways of improvement of this technology, in the near future.

International Commission on Illumination
Commission Internationale de l'Eclairage
Internationale Beleuchtungskommission

PO39

COLOR MATCHING CONSIDERATION ON THE EFFECT OF IPRGC FOR COLOR REPRODUCTION ON DISPLAY DEVICE

Kota Akiba et al.

DOI 10.25039/x47.2020.PO39

Paper accepted for the 5th CIE Symposium on Colour and Visual Appearance

The paper was selected by the International Scientific Committee (ISC) for presentation at the 5th CIE Symposium on Colour and Visual Appearance, Hong Kong, CN, April 21–22, 2020, which, due to the corona pandemic, could not take place. The paper has not been peer-reviewed by CIE.

CIE Central Bureau
Babenbergerstrasse 9
A-1010 Vienna
Austria
Tel.: +43 1 714 3187
e-mail: ciecb@cie.co.at
www.cie.co.at

PO39

COLOUR MATCHING CONSIDERATION ON THE EFFECT OF IPRGC FOR COLOUR REPRODUCTION ON DISPLAY DEVICE

Akiba, K.[1], Tanaka, M.[2], Horiuchi, T.[1]
[1] Graduate School of Science and Engineering, Chiba University, Chiba, JAPAN
[2] College of Liberal Arts and Sciences, Chiba University, Chiba, JAPAN
midori@chiba-u.jp

Abstract

At the beginning of this century, intrinsically photoreceptive retinal ganglion cells (ipRGCs), new photoreceptors different from cones and rods, were discovered. The aim of this study was to experimentally verify the influence of ipRGCs on the colour reproduction of a display. In the experiment, we performed perceptual colour matching between colour patches and displays. Although colorimetric reproduction of the colour patch was used for the initial image of the display, the colour matching results were largely out of colorimetric colour reproduction. Since this result suggests that ipRGCs may affect colour reproduction of displays, a correction equation that accounts for the influence of ipRGCs was derived. Applying this correction formula improved the results. It is considered possible to accurately display the colour of a real object on a display using a correction equation that accounts for the effect of ipRGCs.

Keywords: ipRGC, colour reproduction, colour perception, display

1 Introduction

At the beginning of this century, cones and photoreceptors other than rods were discovered in the retina of mammals and were named “intrinsically photosensitive retinal ganglion cells” (ipRGCs) [1]. The ipRGC is a special ganglion cell containing the visual substance melanopsin. The spectral sensitivity function [2] shown in Figure 1 was defined by the Commission Internationale de l´Eclairage (CIE) in 2018 and had a peak at around 490 nm. The ipRGC affects non-imaging functions, such as regulation of the circadian rhythm and pupillary light reflection, compared to imaging functions that form the image of an object, such as cones and rods [3]. However, recent studies have reported that ipRGC affects human visual perception through changes in the amount of stimulation for visual perception. For example, to verify the effect of ipRGC on visual perception, we used the silent-substitution method, which changes only the amount of stimulation to ipRGC without changing the amount of stimulation to the cone by manipulating the shape of the spectral distribution [4]. Considering a method for stimulating only melanopsin cells, colour stimuli were created using a light-emitting diode (LED) mounted on an integrating sphere as a light source, and experiments were performed. Figure 1 shows the sensitivity of the long, medium, short-wavelength (LMS) cone and the ipRGC overlap. All these reported experiments were performed in a tightly controlled environment.

In current displays, colour reproduction is performed colorimetrically based on the perception amount of the LMS cone in photopic vision. However, previous studies have suggested that ipRGC may affect visual perception. If ipRGCs influence colour perception, in addition to the amount perceived by the LMS cone, it is necessary to consider the effect of ipRGC on the colour reproduction of display devices. In our previous study [5], we attempted to analyze a fundamental colour matching experiment in which patches and display reproduction colours were visually juxtaposed. It indicated that ipRGCs might contribute to the colour vision pathway. However, since the stimuli were visually placed side by side, observing them with a single eye was necessary.

The aim of this study was to verify the effect of ipRGCs on the display in an experimental environment where patches and display reproduction colours were physically juxtaposed. Furthermore, when it was suggested that the colour reproduction of a display is different from

that of a conventional display, we constructed a model for evaluating the colour reproduction accuracy of a new display constructed using the values obtained from the experimental results.

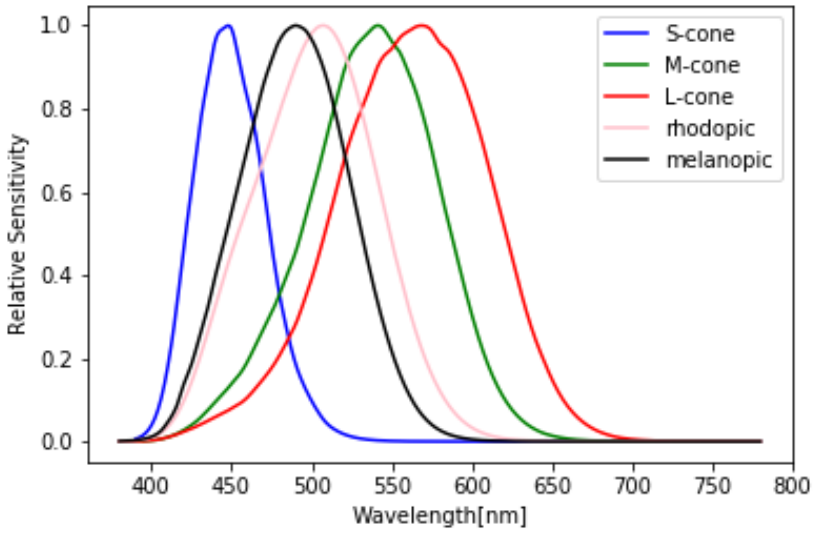

Figure 1 – Relative sensitivity of S-, M-, and L-cones and rhodopic and melanopic irradiance

2 Experiments

In the experiment, perceptual colour matching was performed between colour patches, and the colour patches were reproduced on a display under 6 000 K by 4 500 lx LED illumination. The spectral distributions of both colour stimuli were different. Therefore, matching results were expected without the smallest colour difference in the case that the ipRGCs influence colour perception. To control the influence of rods, we used a high-brightness liquid crystal display (SHARP PN-A601) after colour calibration. Drawing papers toned by Japan Colour Enterprise Co., Ltd. to the colour of the X-Rite ColorChecker were used as the real colour patches. Seven colours (red, blue, moderate red, blue sky, magenta, cyan, and white) with comparatively high reproducibility from 24 colour patches were used as the colour stimuli in this experiment. Many short- and long-wavelength components containing a colour were selected in addition to confirming the effect at approximately 490 nm, which is the peak visibility of ipRGCs. The CIE1976 ΔE colour difference was an average of 1.42 and a maximum of 3.15 (cyan).

In the experiment, colour matching was performed between a colour patch and a reproduced image on a high-brightness display. Since the spectral distributions of both colours are different, it is hypothesized that if ipRGC affects colour perception, the colour difference will not always be minimal. Figure 2 shows the experimental environment. The subjects were six observers (5 men and 1 woman) with normal colour vision. The experiment was performed twice to evaluate the stability of the results. The viewing distance from the observer to the display and colour patch was set at 150 cm, and the experimental environment was designed in a way that both stimuli could be physically juxtaposed and observed with both eyes. The viewing angle of each colour stimulus was 3.4°. It was shielded from light by a black paper, except for the part showing the colour of the display. The colour matching procedure was performed by independently adjusting the hue, saturation, and lightness. The colorimetric reproduction colour with the smallest colour difference was displayed for each stimulus as the initial colour. The experiment was performed after the training process for the observers to become accustomed to toning. The adjusted colour on the display device was measured using a spectroradiometer (KONICA MINOLTA CS-2000) after the colour matching experiment.

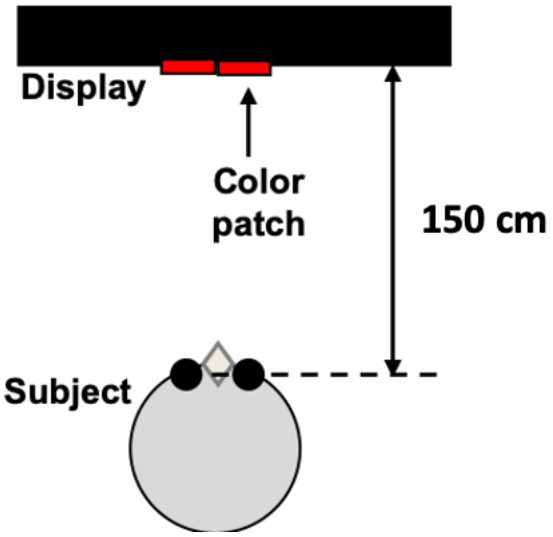

Figure 2 – Experimental environment

3 Results and discussion

The CIE 1976 Delta E colour difference between the reproduced colour and the colour patch was calculated after colour matching. The outliers for each colour of the experimental results were derived using the Smirnov–Grubbs test. Figure 3 shows the average statistical results of two experiments performed by six observers for each colour stimulus, together with the colour difference of colorimetric colour reproduction (initial colour). The deviation in the figure indicates the standard deviation. As shown in Figure 3, the colour difference average of the seven colours of colorimetric colour reproduction was 1.4, and it changed to 3.9 after colour matching. In particular, the errors for the blue and white patches were large, and variations were observed among the observers.

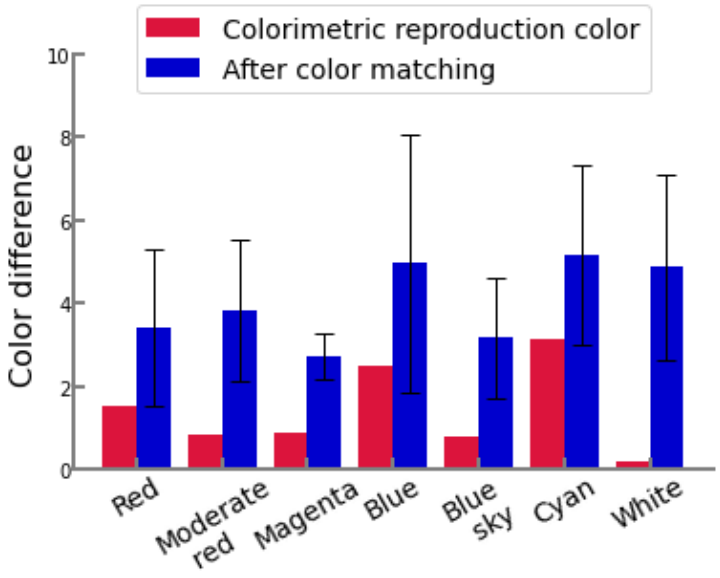

Figure 3 – Average colour difference among the six observers

The ratio of colour difference, i.e. ΔL*:Δa*:Δb*, was 0.26:0.30:0.44. Focusing on the blue stimulus overlapping with the sensitivity of ipRGCs, the colour difference ratio was 0.12:0.36:0.52, and the colour difference of b* was large. This result indicates that ipRGCs may also contribute to the colour vision pathway.

The RGB colour-matching function of CIE1931 was derived from colour matching experiments using Guild and Light. Because this colour-matching function includes negative terms, the CIE1931 XYZ colour matching function was derived by basis transformation, which assumes that the LMS signals are independent. However, we hypothesized that the LMS signal would reach the ganglion cells and that the LMS signal would be biased by ipRGCs in the ganglion cells. Therefore, the correction formula of CIE XYZ obtained by correcting each value of CIE XYZ with the ipRGC absorption rate was derived by regression with the dependent variable as "CIE XYZ of a real colour patch" and the independent variables as "ipRGC absorption rate" and "CIE XYZ of the reproduced colour on the display after colour matching." Here, for the regression, 189 datasets obtained by removing the outliers from the XYZ data observed 12 times for the seven colour stimuli were used. The ipRGC absorption rate was calculated using the spectral sensitivity of ipRGC [2] and spectral distribution of the reproduced colours on the display. The modified XYZ values, XYZ_{ipRGC}, are derived by the ipRGC effect as follows:

$$XYZ_{ipRGC} = -9.479 + 107.5 \times ipRGC + 0.9277 \times XYZ_m \quad -(1)$$

where XYZ_m represents the CIE XYZ values of the reproduced colour on the display device after the colour matching, including the impact of ipRGCs. The variable $ipRGC$ is the ipRGC absorption rate of the reproduced colour. By adopting the modified XYZ values, Figure 4 presents the average colour difference among the six observers. According to the description in the figure, after applying the modified XYZ values, the CIE Delta E colour difference after colour matching worsened to an average of 5.6. The ratio of colour difference was 0.22:0.31:0.47.

Since the absorbance spectrum of ipRGCs has a peak on the short wavelength side, we modified only the Z-value of the display after colour matching. Figure 5 shows the average colour difference among the six observers. The colour difference using the correction formula improved to an average of 3.5 for the seven colours. In particular, improved results were obtained for the colour stimuli containing many short wavelength components. This suggested that the absorption component of ipRGCs affected the z-value in the tristimulus values.

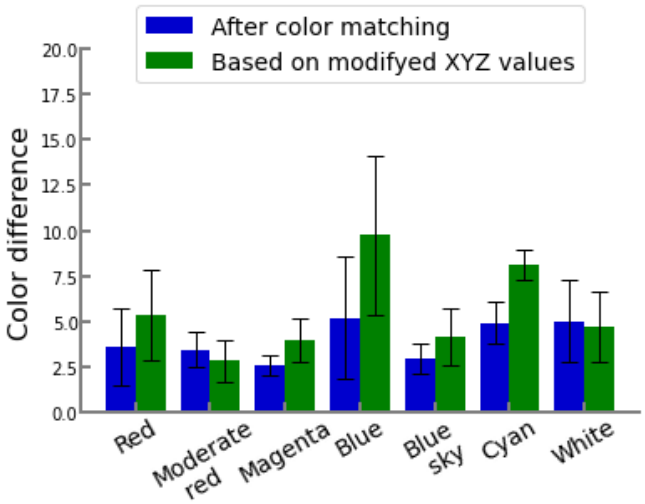

Figure 4 – Average colour difference among the six observers after applying the modified XYZ values

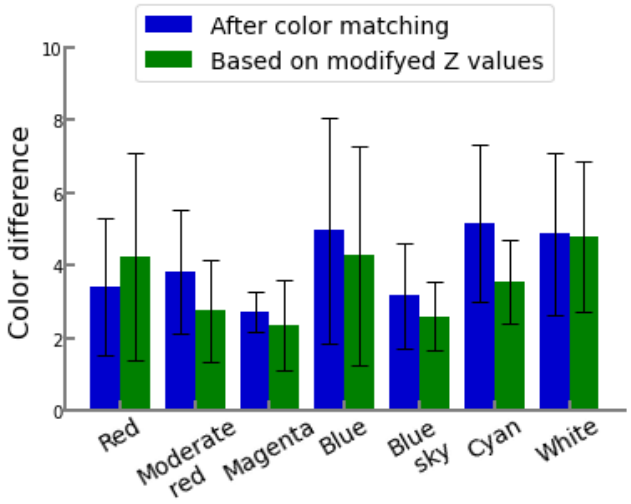

Figure 5 – Average colour difference among the six observers after applying the modified Z value

4 Conclusions

In the colour matching experiment using a high brightness display, colour perception of the display was influenced by ipRGCs. This effect could be confirmed even when colour matching was performed for the juxtaposed stimuli in the same way as in the previous study that included a single eye. We assumed that the LMS signal was biased by ipRGCs in the ganglion cells. The study also provided a derivation of the correction formula of CIE XYZ acquired by correcting XYZ values with the ipRGC absorption rate. In particular, by considering the CIE Z value, the colour difference improved and suggested the necessity of ipRGCs in colour perception of displays.

Further analysis is required to derive a more appropriate correction formula while considering the effect of ipRGCs on the perceptual model. In general, it is expected that the sensitivity of ipRGCs and cone sensitivity depend on the observer; therefore, we need to consider an experimental design that takes this into consideration.

Acknowledgment

This work was supported by JSPS KAKENHI Grant Number 19K12038.

References

1. D.M. Berson, F.A. Dunn, and M. Takao “Phototransduction by Retinal Ganglion Cells That Set the Circadian Clock” SCIENCE, vol 295, 8 February 2002
2. CIE System for Metrology of Optical Radiation for ipRGC-Influenced Responses to Light (2018)
3. S. Hattar, H.-W. Liao, M. Takao, D.M. Berson, and K.-W. Yau “Melanopsin-Containing Retinal Ganglion Cells: Architecture, Projections, and Intrinsic Photosensitivity” SCIENCE, vol 295, 8 February 2002
4. T.M. Brown, S. Tsujimura, A.E. Allen, J. Wynne, R. Bedford, G. Vickery, A. Vugler, and R.J. Lucas “Melanopsin-Based Brightness Discrimination in Mice and Humans” Current Biology, 22, pp.1134- 1141 (2012)
5. K. Akiba, M. Tanaka, and T. Horiuchi “Experimental consideration on the effect of ipRGC for color reproduction on display device” International Color Association, Buenos Aires, Argentina, October 2019

International Commission on Illumination
Commission Internationale de l'Eclairage
Internationale Beleuchtungskommission

PO40

EFFECT OF LIGHTING ON READABILITY OF COLOUR PRINTING FOR VARIOUS AGES

Natsuki Murakami et al.

DOI 10.25039/x47.2020.PO40

Paper accepted for the 5th CIE Symposium on Colour and Visual Appearance

The paper was selected by the International Scientific Committee (ISC) for presentation at the 5th CIE Symposium on Colour and Visual Appearance, Hong Kong, CN, April 21–22, 2020, which, due to the corona pandemic, could not take place. The paper has not been peer-reviewed by CIE.

CIE Central Bureau
Babenbergerstrasse 9
A-1010 Vienna
Austria
Tel.: +43 1 714 3187
e-mail: ciecb@cie.co.at
www.cie.co.at

PO40

EFFECT OF LIGHTING ON READABILITY OF COLOUR PRINTING FOR VARIOUS AGES

Murakami, N.[1], Iwata, T.[2], Sakuma, R.[1], Nishihara, K.[3]
[1] Graduate school engineering of Tokai University, Kanagawa, JAPAN
[2] Tokai University, Kanagawa, JAPAN
[3] Misawa Reform Co., Ltd, Tokyo, JAPAN
nackun919@gmail.com

Abstract

In recent years, LED lighting has spread rapidly and has been used in various places. Also, there has been an increase in colour printing on posters, in advertisements and on packaging using various colour for alphabetic characters and background. It is a concern that elderly people with ageing eyes which cannot read the colour characters on the colour background easily under some colour lighting. A subjective experiment was conducted on the readability of colour printing lit by different CCT lamps. The colour differences calculated by CIEDE2000 formula was smaller than the colour differences calculated by CIE76 formula under all conditions. The subject experiments showed that the readability of colour printing could not be predicted by the colour difference calculated by the CIEDE2000 formula. As a result of examination using tristimulus values, it was suggested that accurate readability evaluation can be predicted by considering colour constancy.

Keywords: LED lighting, Colour printings, Readability, Colour difference, Tristimulus value

1 Introduction

In recent years, LED lighting has spread rapidly and has been used in various places. The common type of LED lighting is the combination of blue LEDs with yellow and red phosphors to produce white light. Recently, the type that uses red, green, blue, and white LEDs (called RGBW) is also available. Light with various colours can be emitted from this type of LED.

Also, colour printing using various colours for alphabetic characters and background, has increased on posters, in advertisements and on packaging. As people age, the lens selectively absorbs shorter-wavelength light because of accumulation of yellow pigments in the lens (Salvi et al., 2006). It is a concern that elderly people with ageing eyes which have low transmittance for shorter wavelengths cannot read the colour characters on the colour background easily under some colour lighting.

A previous study (Komori, 2019) on the readability of colour printing using a paired comparison method showed the difference in readability between ages. However, the CIE76 colour difference model showed low correlation with readability.

The purpose of our study is to develop a method which can predict readability of colour printing under different light for various ages using the latest colour difference formula and 7-point scale. In this paper, the term “readability” refers to the visibility of the target.

2 Previous research on colour discrimination

2.1 Identification of colour

The colour appearance model is based on the tristimulus values *XYZ*, which are calculated by the spectral distribution of the light source: $I(\lambda)$, the spectral reflectance of the target colour: $\rho(\lambda)$, and the colour matching functions of the observer: $x(\lambda)$, $y(\lambda)$, $z(\lambda)$. The tristimulus values *XYZ* are calculated from Equations (1) to (3).

$$X = \int I(\lambda)\rho(\lambda)\overline{x_{age}}(\lambda)d\lambda \quad (1)$$

$$Y = \int I(\lambda)\rho(\lambda)\overline{y_{age}}(\lambda)d\lambda \quad (2)$$

$$Z = \int I(\lambda)\rho(\lambda)\overline{z_{age}}(\lambda)d\lambda \quad (3)$$

where

$I(\lambda)$ is the spectral distribution of the light source

$\rho(\lambda)$ is the spectral reflectance of the target colour

$x_{age}(\lambda)$, $y_{age}(\lambda)$, $z_{age}(\lambda)$ are the colour matching functions of the observer

2.2 Colour difference

The colour difference ΔE^*_{ab} calculated by the CIE76 formula is the first colour difference of CIE. ΔE^*_{ab} is calculated by equation (4) based on the coordinates of two points in the CIELAB colour space obtained by converting the coordinates of the CIEXYZ colour space.

$$\Delta E^*_{ab} = \sqrt{(L^*_1 - L^*_2)^2 + (\Delta a^*_1 - \Delta a^*_2)^2 + (\Delta b^*_1 - \Delta b^*_2)^2} \quad (4)$$

where

L^*_1, L^*_2 are the brightness of two points

a^*_1, a^*_2, b^*_1, b^*_2 are the coordinates representing hue and chroma

However, it was pointed out that the CIE76 formula had a low correlation with the visual sense (M.R.Luo et. al, 2001), so the CIEDE2000 formula was proposed as a new colour difference formula. There are elliptical colour identification areas in the CIELAB colour space (MacAdam, 1970). However, ΔE^*_{ab} is shown as a perfect circle on the chromaticity diagram (Tanaka et. al, 2014). It is considered to be the cause of the deviation from the human colour identification range. ΔE_{00} calculated by the CIEDE2000 formula was improved by weighting the deviation of ΔE^*_{ab} in consideration of brightness, chroma, and hue (M.R.Luo et. al, 2001). ΔE_{00} is calculated by equation (5) based on the LCH colour space converted from the CIELAB colour space.

$$\Delta E_{00} = \sqrt{\left(\frac{\Delta L'}{k_L S_L}\right)^2 + \left(\frac{\Delta C'}{k_C S_C}\right)^2 + \left(\frac{\Delta H'}{k_H S_H}\right)^2 + R_T\left(\frac{\Delta C'}{k_C S_C}\right)\left(\frac{\Delta H'}{k_H S_H}\right)} \quad (5)$$

where

$\Delta L'$ is the brightness difference

$\Delta C'$ is the chroma difference

$\Delta H'$ is the hue difference

R_T is the revolution coefficient for the calculation of blue colour differences

S_L, S_C, S_H are scaling factors

k_L, k_C, k_H are weighting parameters

3 Methods

3.1 Conditions

3.1.1 The spectral distribution of the light source: $I(\lambda)$

The spectral distribution of each colour temperature (2 500 K, 5 000 K, 8 000 K) of the light source used in the experiment was measured by the spectral illuminance meter CL-500A (KONICAMINOLTA). Figure 1 shows the spectral distribution of the light sources used in the experiment.

3.1.2 The spectral reflectance of the target colour: $\rho(\lambda)$

The spectral reflectance of the colours of the visual targets (combination of colour characters and colour background) used in the experiment were measured by spectrophotometer CM-d700 (KONICAMINOLTA). Each target was a combination of two of seven colours (colour1: yellow, colour2: red, colour3: light blue, colour4: light yellow, colour5: pink, colour6: light green, colour7: purple). Figure 2 shows the spectral reflectance of the colours of the visual targets.

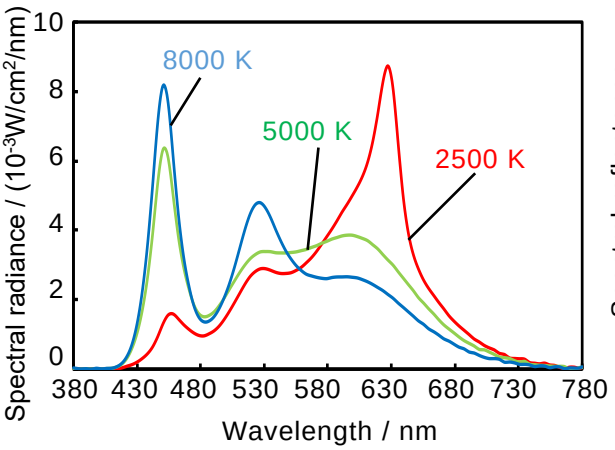

Figure 1 – Spectral distribution

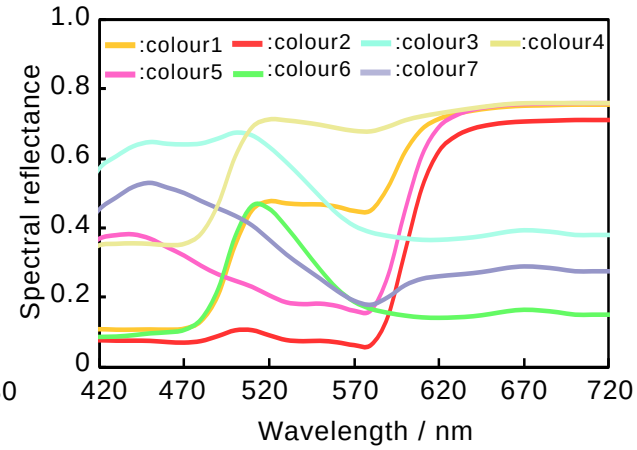

Figure 2 – Spectral reflectance

3.1.3 The colour matching functions of observer: $x(\lambda)$, $y(\lambda)$, $z(\lambda)$

The colour matching function of the person in their 20s was assumed as the CIE1931 2-deg function, and the colour matching function of the person in their 70s was calculated using the visual sensitivity of a person in their 70s of JIS (JIS, 2010). Also, the colour matching functions simulating the person in their 70s were calculated from the transmittances of special goggles (Figure 3) simulating an elderly person's eye. Figure 4 shows the colour matching function of the people in their 20s, 70s, and simulated 70s.

Figure 3 – Special goggle

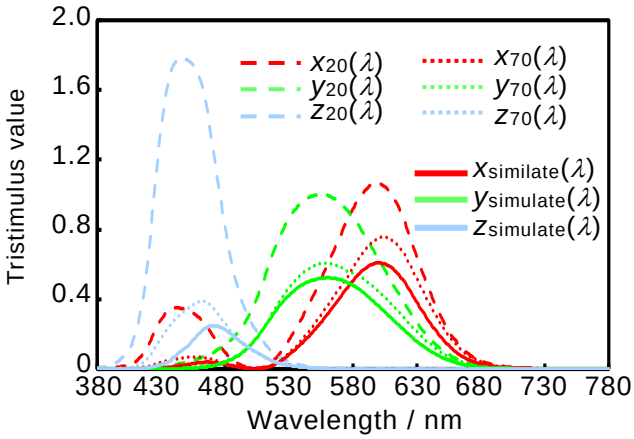

Figure 4 – Colour matching function

3.1.4 The decision of the visual targets

The six visual targets were selected based on the colour differences between the background and the alphabetic characters. The size of the visual targets was 100 mm × 110 mm, and the characters were set to 24 points so that the size was large enough to read for the elderly. Table 1 shows the colour combinations (the colour of alphabetic characters and the colour of background) of the six visual targets (A to F) shown in Figure 5.

Table 1 – Colour combinations of six visual targets

The visual target	Characters	Background	The visual target	Characters	Background
A	colour 3	colour 2	D	colour 5	colour 6
B	olour 2	colour 3	E	colour 4	colour 3
C	colour 6	colour 5	F	colour 7	colour 1

Figure 5 – Six visual targets

3.2 Experiment set-up

An experimental booth (width 800 x depth 600 x height 900 mm) was set up and LED lighting was installed. PHILIPS Hue with changeable colour temperature was used as the light source, and the colour temperatures were 2500 K (Ra 94), 5000 K (Ra 94), and 8000 K (Ra 94). The illuminance on the target was kept at 500 lx. Special goggles were used to simulate an elderly person's eye of lower transmittance of shorter wavelengths. The transmittance of the goggles at 450nm was 24.3% while that at 550nm was 55.4%. Figure 3 shows the special goggles used in the experiment. The subjective experiment was conducted under six conditions (three colours of light with and without goggles). Figure 6 shows subjects during the experiment.

Figure 6 – Subjects during the experiment

3.3 Procedure

Eighteen Japanese students (between 21 and 22 years old) participated as subjects. In order to exclude colour blind subjects, Ishihara-style colour blindness tests (Ishihara, 2014) were conducted. Figure 7 shows the Ishihara-style colour blindness test. As a result of the Ishihara-style colour blindness tests, all subjects had normal colour vision. The subjects acclimated themselves to darkness for a few minutes then looked at the visual target in the booth and assessed the readability using a 7-point scale (-3: very difficult to read, -2: difficult to read, -1: slightly difficult to read, 0: neither, 1: slightly easy to read, 2: easy to read, 3: very easy to read). The readability of 6 visual targets was evaluated under six conditions (three colours of light with and without goggles).

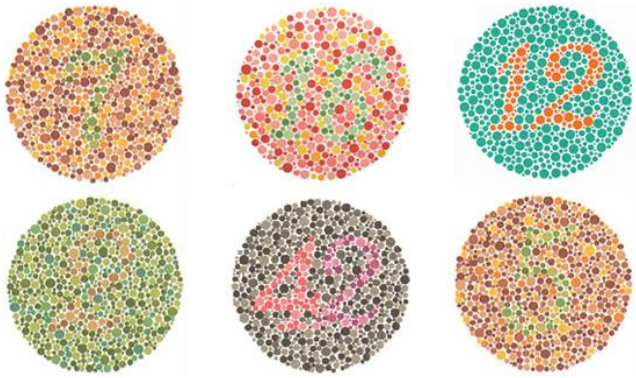

Figure 7 – Ishihara-style colour blindness test

4 Result

4.1 Comparison of the CIE76 formula and the CIEDE2000 formula

Under all conditions, ΔE_{00} calculated by the CIEDE2000 formula was smaller than ΔE^*_{ab} calculated by the CIE76 formula. Figure 8 shows the relationship between ΔE^*_{ab} and ΔE_{00} under all conditions.

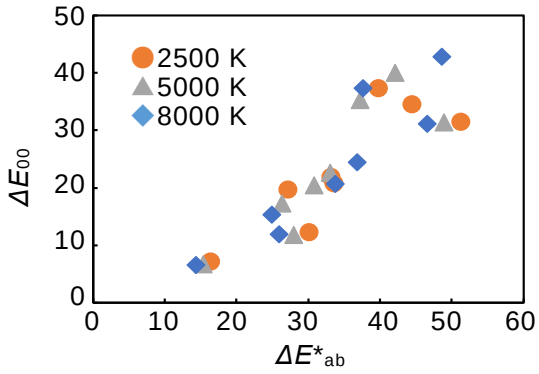

Figure 8 –Relationship between ΔE^*_{ab} and ΔE_{00}

The effect of colour temperature on the colour difference (ΔE_{00} and ΔE^*_{ab}) was examined and it was different for each target. In some conditions, ΔE_{00} and ΔE^*_{ab} showed a similar tendency, e.g. both ΔE_{00} and ΔE^*_{ab} of the visual target E decreased as colour temperature increased with and without goggles, as shown in the left graph of Figure 9. On the other hand, ΔE_{00} and ΔE^*_{ab} are affected differently by colour temperature, as shown in the right graph of Figure 9.

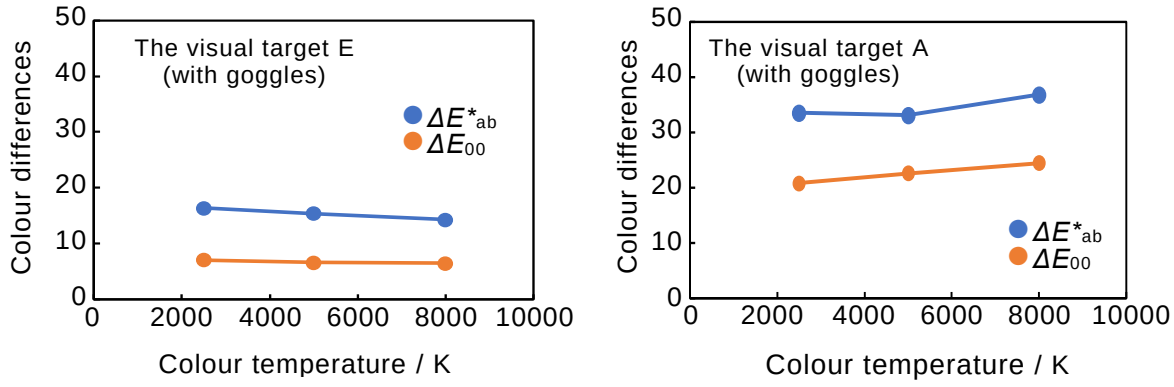

Figure 9 – Examples of the effect of colour temperature on colour difference

4.2 Colour difference and readability evaluation

Figure 10 shows colour difference ΔE_{00} and the evaluation of readability. When the goggles were not worn, zero and more of the evaluation of readability was obtained under most visual targets and conditions. In addition, the correlation between the colour difference ΔE_{00} and the evaluation of the readability was low with and without the goggles. In some conditions, the readability evaluation was significantly different even when the difference in ΔE_{00} was small. Since the colour difference ΔE_{00} is an index that mainly distinguishes two very similar colours so it is considered that ΔE_{00} cannot predict the readability of colour characters on a colour background.

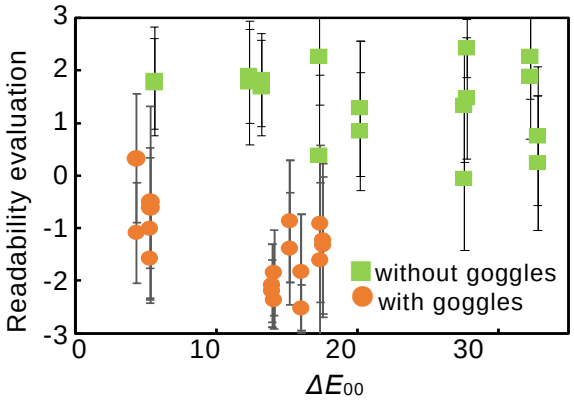

Figure 10 – Colour difference and readability evaluation

4.3 Factors determining readability

4.3.1 Tristimulus value difference

Since the evaluation of readability could not be predicted by the colour difference ΔE_{00}, this paper tried to predict the evaluation of readability using the difference between the tristimulus values of the colour of the characters and the colour of the background (ΔX, ΔY, and ΔZ). Multiple regression analysis was performed with the differences of tristimulus values ΔX, ΔY, and ΔZ as the explanatory variables and the evaluation of readability as the objective variable. Multicollinearity was excluded. Table 2 shows the results of the multiple regression analysis. Although the multiple correlation coefficient was 0.76, the difference between the predicted value of the readability and the actual evaluation of the readability was large when the readability evaluation was high. Figure 11 shows the relationship between the readability evaluation and the predicted evaluation.

Table 2 – Multiple regression analysis of readability evaluation and ΔX, ΔY, and ΔZ

Variable	Partial regression coefficient	Standard partial regression coefficient	Significant
ΔX	11.71	0.24	*
ΔY	15.97	0.24	
ΔZ	17.69	0.59	**
Constant term	-1.78		**
			** : P < 0.01 * : P < 0.05

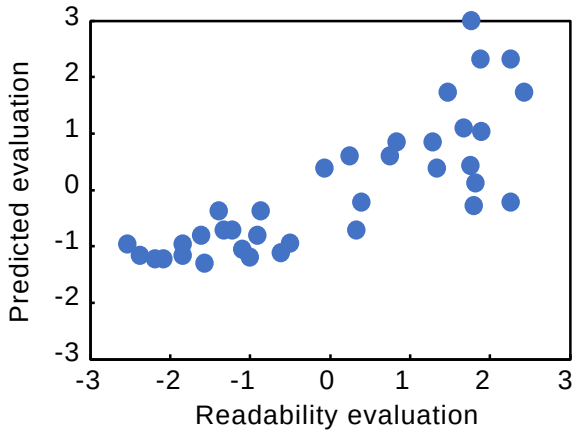

Figure 11 – Readability evaluation and prediction evaluation

4.3.2 Consideration of other factors that affect readability

Since the readability could not be predicted by the difference in tristimulus values, it was considered that the other factors had an effect on the readability. Three other factors, (adaptation to the colour of the background, the difference in individual sensitivity, the colour constancy was examined.

(1) Adaptation to the colour of background

Since the two visual targets where the colour combination is the same, but the background colour and the alphabetic character colour are opposite showed different readability, the effect of adapting to the background colour was examined. Multiple regression analysis was performed with the differences of tristimulus values divided by the tristimulus value of the colour of the background ($\Delta X/X_{background}$, $\Delta Y/Y_{background}$, and $\Delta Z/Z_{background}$) as the explanatory variable and the readability evaluation as the objective variable. The multiple correlation coefficient was 0.24, and no effect of the colour of the background was shown. Table 3 shows results of multiple regression analysis of the readability evaluation and $\Delta X/X_{background}$, $\Delta Y/Y_{background}$, and $\Delta Z/Z_{background}$.

Table 3 – Multiple regression analysis of readability evaluation and $\Delta X/X_{background}$, $\Delta Y/Y_{background}$, and $\Delta Z/Z_{background}$

Variable	Partial regression coefficient	Standard partial regression coefficient	Significant
$\Delta X/X_{backgraound}$	-1.16	-0.25	
$\Delta Y/Y_{backgraound}$	-0.03	-0.01	
$\Delta Z/Z_{backgraound}$	0.71	0.30	

(2) Difference in individual sensitivity

Assuming that there is individual difference in the sensitivity of X, Y, and Z, the correlation coefficient between the differences in X, Y, and Z (ΔX, ΔY *and* ΔZ) and the readability evaluation was calculated for each subject. Table 4 shows the results. For all subjects the correlation coefficient between ΔY and the readability evaluation was higher than that between ΔX and the readability or between ΔZ and the readability. However, the correlation coefficients between ΔY and the readability evaluation were low. The individual difference in the X, Y and Z sensitivity could not explain the readability evaluation obtained in this paper.

Table 4 – Correlation coefficient between the difference in the tristimulus values and the readability evaluation

	Correlation coefficient with readability evaluation				*Correlation coefficient with readability evaluation*		
Subject	*ΔX*	*ΔY*	*ΔZ*	Subject	*ΔX*	*ΔY*	*ΔZ*
1	-0.04	0.18	-0.13	10	-0.18	0.25	-0.03
2	-0.16	0.43	0.13	11	-0.04	0.30	-0.02
3	-0.14	0.35	-0.05	12	-0.20	0.25	-0.09
4	-0.03	0.39	0.00	13	-0.05	0.20	-0.13
5	-0.30	0.19	0.04	14	-0.11	0.20	-0.19
6	-0.06	0.09	-0.16	15	-0.12	0.38	-0.03
7	-0.34	0.29	0.09	16	-0.13	0.24	-0.12
8	-0.20	0.40	-0.02	17	-0.18	0.41	-0.06
9	-0.24	0.18	0.17				

(3) Colour constancy

Assuming that there were influence of colour constancy, multiple regression analysis was performed for each light colour with the difference in tristimulus values as the explanatory variables and readability as the objective variable. Table 5 shows the results of multiple regression analysis of the readability evaluation and *ΔX*, *ΔY*, and *ΔZ* for each colour temperature. The multiple correlation coefficients were 0.87 at 2 500 K, 0.83 at 5 000 K, and 0.93 at 8 000 K.

Table 5 – Multiple regression analysis of readability evaluation and *ΔX*, *ΔY*, and *ΔZ* for each colour temperature

Colour temperature	Variable	Partial regression coefficient	Standard partial regression coefficient	Significant
2 500 K	*ΔX*	15.04	0.44	*
	ΔZ	101.50	0.82	**
	Constant term	-2.14		**
5 000 K	*ΔZ*	21.50	0.83	**
	Constant term	-1.24		**
8 000 K	*ΔZ*	30.62	0.94	**
	Constant term	-1.74		**
** : $P < 0.01$ * : $P < 0.05$				

Figure 12 shows the relationship between milled (the reciprocal of the colour temperature) and standard partial regression coefficient. A high correlation between the milled and the standard partial regression coefficient was shown in *ΔX* (*R*=0.99) and *ΔZ* (*R*=1). Since *Z* is based on a S-cone that is sensitive to the shorter wavelength light, *Z* has a large effect when the colour temperature is high.

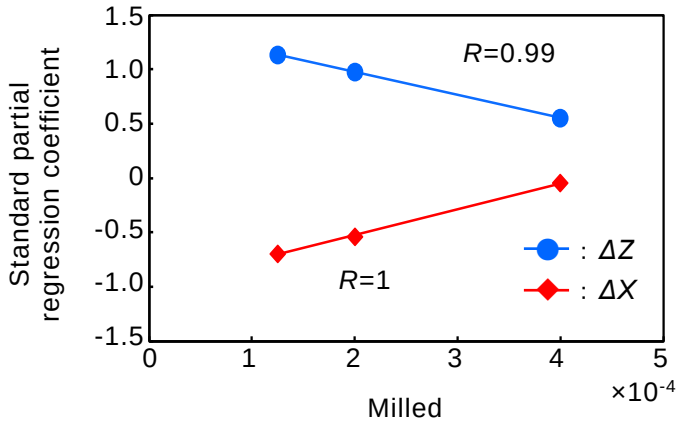

Figure 12 – Correlation between milled and standard partial regression coefficient

From the above results, to take into account colour constancy, each difference in the tristimulus values between the colour of alphabetic characters and that of the background were divided by the tristimulus values of light X_n, Y_n and Z_n. A multiple regression analysis was performed with $\Delta X/X_n$ $\Delta Y/Y_n$ and $\Delta Z/Z_n$ as the explanatory variables and the readability evaluation as the objective variable. The multiple correlation coefficient was 0.62. It was found that colour constancy affected the relationship between the difference between the tristimulus values of the background and the alphabetic characters and the readability evaluation, however, it was not shown by the formula. A Further study is required to develop an index that can predict readability under various conditions.

5. Conclusion

The readability of colour printings was examined using the colour of the light source, the colour of printings, and age as parameters. The colour difference was recalculated with the CIEDE2000 formula and compared with the CIE76 formula. As a result, the colour differences calculated by the CIEDE2000 formula(ΔE_{00}) was smaller than the colour differences calculated by the CIE76 formula(ΔE^*_{ab}) under all conditions. However, the readability could not be predicted with the colour difference calculated by the CIEDE2000 formula(ΔE_{00}). In the examination using the difference between the tristimulus values of the colour of the characters and the colour of the background (ΔX, ΔY, and ΔZ), it was suggested that it is possible to accurately predict the readability evaluation by considering colour constancy. However, there are still some issues to be clarified, such as the difference in the evaluation of the visual target in which the colour of the characters and the colour of the background are reversed.

References

Ishihara, S. 2014. Ishihara-style colour blindness tests 2 International version 38 figures. Tokyo: Handaya store Co., Ltd.

JIS 2010 JIS S0031:2010. *Ergonomics -Accessible design- Specification of age-related luminance contrast for coloured light*.

Komori, M, 2018. Effect of Lighting on colour-letter readability of various age. *Tokyo Branch of The Illuminating Engineering Institute of Japan*.

Luo, R, M. et. al, 2001. The Development of the CIE 2000 Colour-Difference Formula. *CIEDE2000, Colour Research and Application*., 26(5), 340-350.

D, L, MacAdam. 1971. Geodesic Chromaticity Diagram Based on Variances of Colour Matching by 14 Normal Observers. *Applied Optics*., 10(1), 1-7

Salvi, M, S. et. al, 2006. Ageing changes in the eye. *Postgraduate Medical Journal*., 82(971), 581–587

Tanaka, K. Et. al, 2014. Study of Acceptable Colour – Difference Formula of Printed Documents. *Journal of the Imaging Society of Japan*., 53(2), 112-117

International Commission on Illumination
Commission Internationale de l'Eclairage
Internationale Beleuchtungskommission

PO41

DIFFUSENESS OF ILLUMINATION SUITABLE FOR REPRODUCING THE SURFACE APPEARANCE OF OBJECTS

Suzuki Mizushima et al.

DOI 10.25039/x47.2020.PO41

Paper accepted for the 5th CIE Symposium on Colour and Visual Appearance

CIE Central Bureau
Babenbergerstrasse 9
A-1010 Vienna
Austria
Tel.: +43 1 714 3187
e-mail: ciecb@cie.co.at
www.cie.co.at

PO41

DIFFUSENESS OF THE ILLUMINATION SUITABLE FOR REPRODUCING THE SURFACE APPEARANCE OF OBJECTS

Mizushima, S.[1], Mizokami, Y. [1]
[1] Chiba University, Chiba, JAPAN
suzuki-mizushima1125@chiba-u.jp

Abstract

The appearance of an object is influenced by its material and shape, and the lighting conditions. Especially, the diffuseness of lighting involves the appearance of material and surface textures. We investigated the diffuseness of illumination, exhibiting an accurate surface appearance compared to a memorized material recognition under natural light. We also examined the lighting condition for an ideal material appearance. After pre-observing and memorizing the impression of objects under daily lighting environments, observers evaluated the appearance of the objects under different diffuseness lighting conditions. As a result, observers highly rated moderate diffuseness compared to low and high diffuseness conditions. It implies that a very low or high diffuseness, which is unfamiliar, is not suitable for reproducing the accurate or ideal surface appearance. Our results suggest that it is possible to define a diffuseness level for accurate appearance common to objects with different materials. However, materials should be considered for the diffuseness condition for an ideal appearance.

Keywords: Diffuseness of illumination, Material perception, Surface appearance

1 Introduction

The impression of an object changes depending on illumination and many people experience it in everyday life. For example, a product bought under the lighting of the shop may have a different appearance when it is viewed outside. In recent years, with the evolution of solid-state lamps, including light-emitting diodes (LEDs) and organic light-emitting diodes (OLEDs), the development of lighting with various types of intensity, spectral power distribution, and spatial distribution has progressed. Besides, lamps with various shapes such as plate-type and curved designs have also been developed. These lightings could have a great difference in diffuseness from conventional lightings. Then they could have a significant impact on the appearance of objects. For example, Fig. 1 shows the appearance of an object under illumination with different diffuseness. Therefore, it is necessary to consider the surface appearance of objects such as glossiness and roughness when developing and evaluating the lighting environment.

The appearance of an object also largely depends on the material and shape. Studies on texture appearance have been conducted under various material and surface conditions (Fujisaki et al., 2015; Xiao et al., 2016; Ho et al., 2008). However, regarding the colour of an object, Maloney et al. have shown that stable colour perception can be achieved without depending on the roughness and glossiness of the surface.

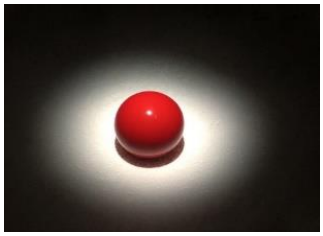

Low diffuseness

High diffuseness

Figure 1 – Object appearance under lighting with different diffuseness

The effect of surface texture has been extensively studied using images rendered using the bidirectional reflectance distribution function (BRDF) (Fleming et al., 2003; Hartung and Kersten., 2002; Langer and Bulthoff., 2001; Maloney 2002; Mingolla et al., 2001; Obein et al., 2004). It is a function that expresses the distribution of reflected light concerning the incident light. Olkkonen & Brainard (2010) showed that the impression of matte objects was stable, but the impression of glossy objects changed when the lighting environment changed.

Lighting conditions that affect an object's appearance are related to how the light hits and how the illumination light spreads. Mizokami et al. (2019) suggested that a rough wavy surface with high frequency tends to appear less glossy and smoother as the diffuseness of the light increase. Moreover, a glossy surface appeared less glossy, and matte one appeared smoother under diffusive light. Yamazoe et al. (2019) showed that the high diffuseness of illumination increases the fidelity of the appearance of an object. However, in their experiment, the diffuseness range was limited to low to middle. Therefore, it was not yet clear how much object's appearance changes, and which diffuseness levels reproduce object's appearance more faithful and ideal. Here, we investigate the diffuseness of illumination suitable for reproducing the object's faithful or ideal surface appearance in a wider diffuseness range.

In Experiment I, we examined lighting conditions which reproduce the faithful and ideal appearance of the objects in four diffuseness levels. In Experiment II, we added a lower diffuseness condition and used a new evaluation method to clarify the lighting conditions suitable for reproducing faithful and ideal appearance.

2 Experiment I

2.1 Environment

A viewing booth was constructed by combining a lighting part and an observation part, imitating a pseudo integrating sphere, as shown in Fig. 2 (a). An observer viewed a stimulus from observation holes, as shown in Fig. 2 (b). The experiment was conducted in a dark room. The lighting part consisted of the combination of an LED lamp (Panasonic EVERLEDS LDA8DA1D; correlated colour temperature, 6 500 K; colour rendering index, Ra 73) with a duct and a Fresnel lens. The observation part was made by a white styrofoam sphere with a diameter of 60 cm to create a high diffuseness lighting condition.

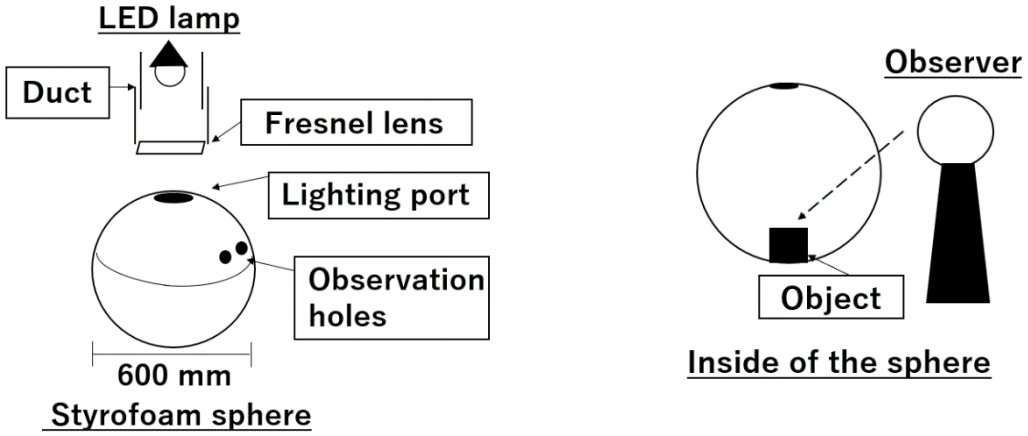

Figure 2 – (a) Viewing booth, (b) side view of the observation part

The diffuseness of illumination was set at four levels (0.40, 0.55, 0.67, and 0.93) by changing the length of the duct and the distance between the LED lamp and the lighting port, as shown in Fig. 3. We used the cubic illuminance measurement defined by Cuttle (2014) and the diffuseness value defined by Xia et al. (2016) as the measurement and evaluation method of diffuseness in our experiment. The horizontal illuminance at the position of a stimulus was unified to 300 lx.

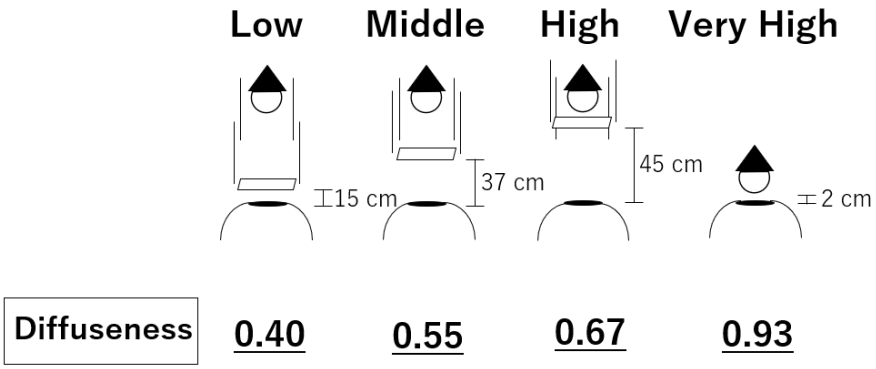

Figure 3 – Four-levels of diffuseness conditions

2.2 Stimulus

Experimental stimuli are polyresin (diameter 3.4 cm, 83 g, sphere, red), fur charm (diameter 7 cm, 8 g, sphere, grey), wood (4.5 cm, 43 g, cube, brown), and stainless steel (2.6 cm, 35 g, cube, silver). Figure 4 shows the experimental stimulus under each illumination.

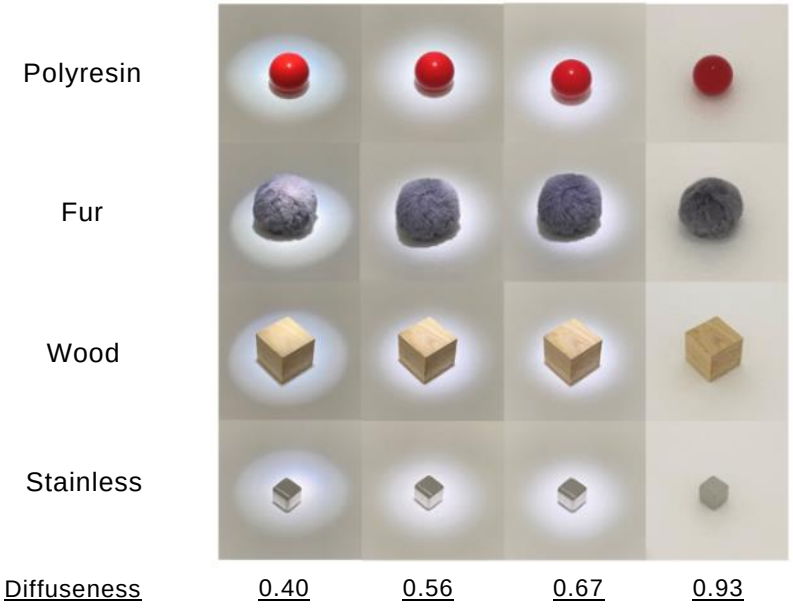

Figure 4 – Experimental stimulus of Experiment I. Polyresin, fur, wood, and stainless steel in order from the top. Diffuseness level 0.40 (Low), 0.56 (Middle), 0.67 (High), and 0.93 (Very High) in order from the left.

2.3 Evaluation methods

The semantic differential scale (SD) method (3-0-3) with ten items was used to evaluate the impression of the object: “Weight”, “Hardness”, “Naturalness”, “Roughness”, “Value”, “Glossiness”, “Preference”, “Visibility”, “Brightness”, and “Transparency”. In addition to the impression evaluation of the SD method, observers selected the best illumination condition to faithfully produce the object’s appearance in their memory (fidelity illumination) and the best illumination condition to ideally produce the feature of the object’s surface (ideal illumination).

2.4 Procedure

As a pre-observation condition, observers memorized the appearance of the stimuli by touching and viewing them at a window and in an office room for 5 minutes each for a total of 10 minutes in two separate days. The illuminance at the window ranged from 432 lx to 5340 lx. The room lighting was white fluorescent lamps (National FHF32EX-NH; CCT 5000K; Ra 84), and the

illuminance ranged from 112 lx to 497 lx. As a pre-evaluation, the observers evaluated the impression of the stimuli after viewing them in the office room.

In the main evaluation, the observers viewed the stimulus in four different lighting conditions in the viewing booth, and the impression evaluation was performed. The observation time of the stimulus was unlimited, and the lighting conditions' order was randomized. After viewing the stimuli, the observer selected the fidelity illumination and the ideal illumination. The pre-evaluation and the main evaluation were combined into one session, and five sessions were conducted.

2.5 Observer

Three male and two female observers in their twenties participated.

2.6 Result and Discussion

The profile of the impression evaluation of observer A is shown in Fig. 5 (a). The averages of the selection rate of the fidelity illumination and ideal illumination of all observers are shown in Fig. 5 (b) and (c). Condition of very high diffuseness tends to change the impression of polyresin and stainless objects. In the faithful selection, polyresin has a high rating for low diffuseness, whereas other stimuli have a high rating for middle diffuseness. The ideal choice showed no consistent tendency overall.

For fidelity illumination, the selection ratio of "Middle (0.55)" was the highest. This diffuseness condition is the closest to the average diffuseness (0.51) of the pre-observation condition. For ideal illumination, polyresin and stainless stimuli had a high selection rate for low diffuseness. Fur and wood had a high selection rate for high diffuseness.

The evaluation results of the SD method at the pre-evaluation show the characteristics of the stimuli memorized in the daily environment. Polyresin and stainless stimuli have a high score in the "glossiness" item.

The range of diffuseness during observation did not cover low diffuseness. We needed a more extensive diffuseness range of illumination to investigate a comprehensive relationship between the appearance of objects and the illumination. Therefore, we conducted Experiment II.

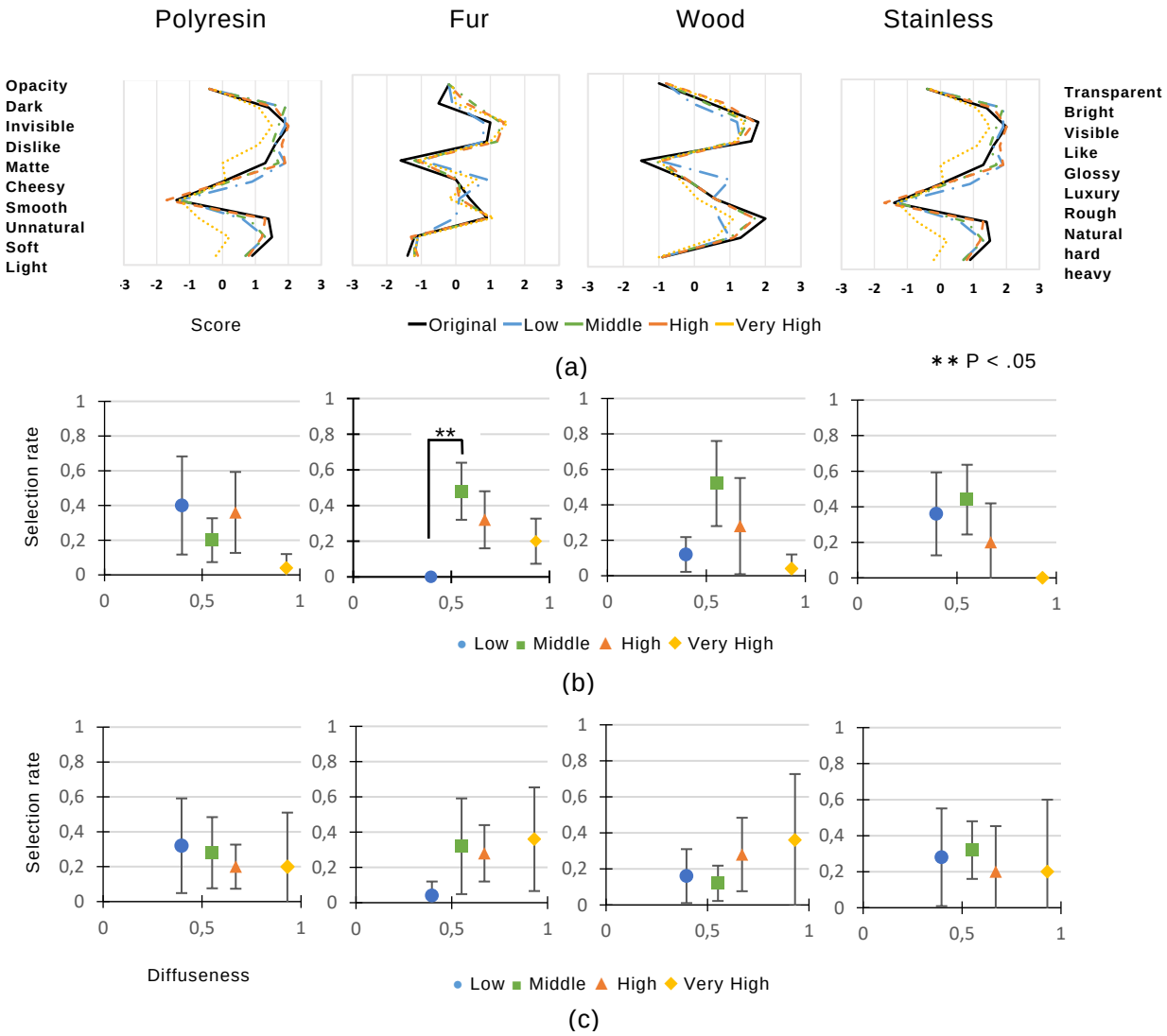

Figure 5 – Results of Experiment I. (a) The profile of the impression evaluation result of observer A. (b) the average selection rate of all observers for the fidelity illumination. (c) the average selection rate of all observers for the ideal illumination.

3 Experiment II

3.1 Environment

The viewing booth was the same as in Experiment I, except that we added a low diffuseness condition by covering the inside of the upper half of the styrofoam sphere with a black cloth to extend the diffuseness range. Therefore, we tested five diffuseness conditions (0.26, 0.40, 0.55, 0.67, and 0.93) in Experiment II as shown in Fig. 6.

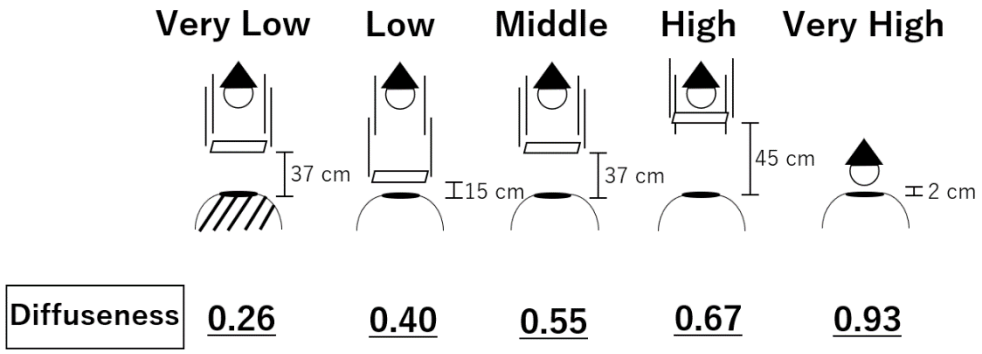

Figure 6 – Five-level diffuseness conditions

3.2 Stimulus

The same objects as in Experiment I was used. Figure 7 shows the state of the stimulus under each illumination.

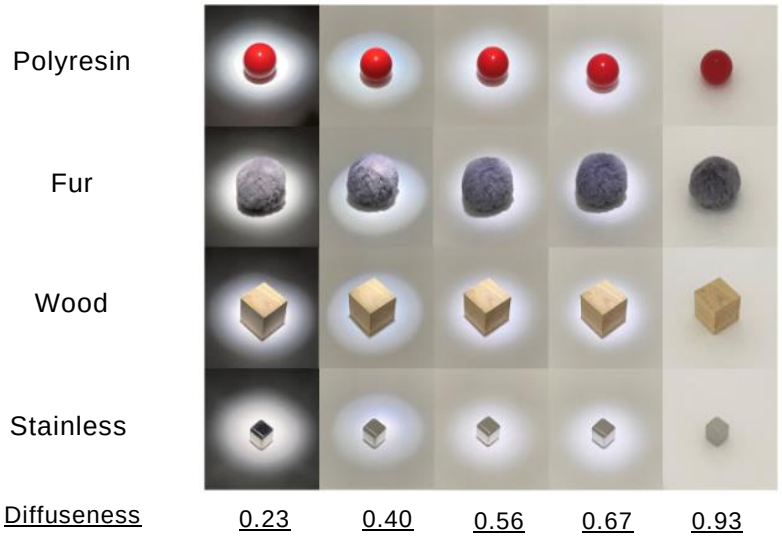

Figure 7 – Experimental stimulus of Experiment II. From top to bottom: Polyresin, fur, wood, and stainless steel. From left to right: Diffuseness level 0.23 (Very Low), 0.40 (Low), 0.56 (Middle), 0.67 (High), and 0.93 (Very High).

3.3 Evaluation methods

Under each diffuseness condition, observers evaluated using ten steps from 1 to 10 for the two items regarding the fidelity to the stimulus appearance memorized in the daily environment and how much the stimulus appearance was ideally represented (appearance evaluation).

3.4 Procedure

The pre-observation was performed in the same process as Experiment I. The illuminance at the window ranged from 51 lx to 4 650 lx. The illuminance inside the room ranged from 150 lx to 454 lx. After viewing the stimulus for 10 minutes in the same environment as in the pre-observation, the observer viewed the stimulus in the viewing booth under five lighting conditions. Then, the observer performed appearance evaluation. The observation time was unlimited, and the order of the illumination conditions was randomized. The order of presenting stimuli was also randomized, and all four types of stimuli were evaluated in one session. Five sessions were conducted.

3.5 Observer

Observers were two males who participated in Experiment I and two females who did not participate in Experiment I.

3.6 Result and Discussion

Figure 8 (a) and (b) show the average score of the fidelity and ideal lighting conditions for all observers and all stimuli. Low lighting conditions obtained a high score in the ideal evaluation for stainless, and medium score for other evaluations. Besides, Middle and High diffuseness lighting conditions had a high score in the fidelity evaluation and the ideal evaluation.

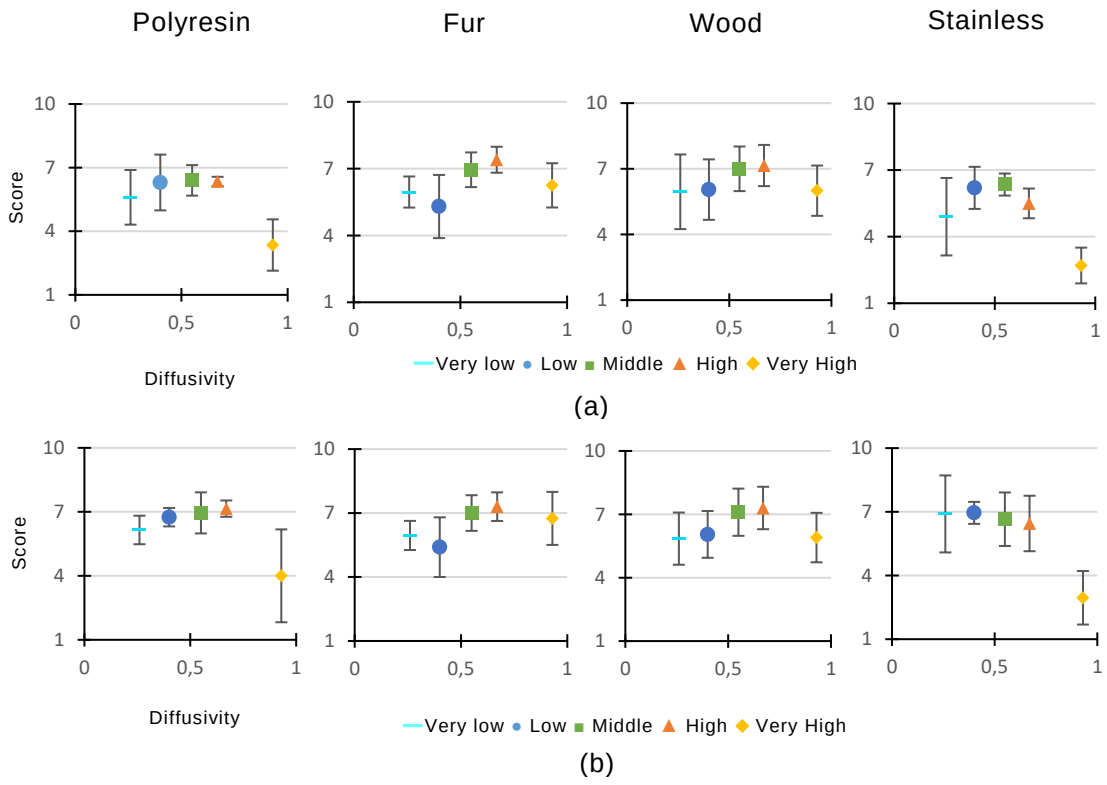

Figure 8 – Results of Experiment II. (a) the average score of the fidelity illumination for all observers. (b) the average score of the ideal illumination for all observers.

4 Discussion

The results of appearance evaluations are different in Experiment I and II, probably because the evaluation method was different. In Experiment I, selecting the most faithful and ideal lighting one by one caused a large variation in evaluation. On the other hand, it was able to obtain quantitative evaluations for all stimuli in Experiment II. It was found that the scores of middle diffusenesses that were not selected in Experiment I were also high in all stimuli. There is variability in evaluation at very low and high diffuseness. It is considered that the results of Experiment II, including a large amount of data, are highly reliable.

In the experiment by Yamazoe et al. (2019), the diffuseness range was from 0.18 to 0.43, and the fidelity increased as the diffuseness increased. In the present experiments, Very Low (0.23) and Low (0.40) were within that range, and similar results to Yamazoe et al. were obtained for all objects except for fur.

The differences in evaluation between stimuli in Experiment II are similar for polyresin and stainless (P-S), and for fur and wood (F-W) in general, as shown in the average data in Table 1 and 2. In the impression evaluation in Experiment I, polyresin and stainless (P-S), and fur and wood (F-W) also had similar evaluations in average data in terms of glossiness and roughness item, as shown in Tables 3 and 4. These results suggest that objects with similar property (e.g.

both glossy polyresin and stainless) give shimilar impression. It can be considered that the surface appearance was influenced by the surface properties of the object.

Table 1 – Difference in appearance evaluation between stimuli (Fidelity) in Experiment II
P: Polyresin, F: Fur, W: Wood, S: Stainless

	Very Low	Low	Middle	High	Very High	Average
P-F	0.35	1.00	0.55	1.05	2.90	1.17
P-W	0.35	0.25	0.60	0.80	2.65	0.93
P-S	0.70	0.10	0.05	0.85	0.65	0.47
F-W	0.00	0.75	0.05	0.25	0.25	0.26
F-S	1.05	0.90	0.60	1.90	3.55	1.60
W-S	1.05	0.15	0.65	1.65	3.30	1.36

Table 2 – Difference in appearance evaluation between stimuli (Ideal) in Experiment II

	Very Low	Low	Middle	High	Very High	Average
P-F	0.20	1.35	0.05	0.15	2.75	0.90
P-W	0.30	0.70	0.15	0.15	1.90	0.64
P-S	0.75	0.20	0.30	0.70	1.05	0.60
F-W	0.10	0.65	0.10	0.00	0.85	0.34
F-S	0.95	1.55	0.35	0.85	3.80	1.50
W-S	1.05	0.90	0.45	0.85	2.95	1.24

Table 3 – Difference in impression evaluation between stimuli (Glossiness) in Experiment I

	Original	Low	Middle	High	Very High	Average
P-F	2.84	2.68	2.32	2.30	1.90	2.41
P-W	2.40	2.66	2.74	2.28	1.44	2.30
P-S	0.80	0.28	0.22	0.10	0.46	0.37
F-W	0.44	0.02	0.42	0.02	0.46	0.27
F-S	3.64	2.96	2.54	2.40	1.44	2.60
W-S	3.20	2.94	2.96	2.38	0.98	2.49

Table 4 – Difference in impression evaluation between stimuli (Roughness) in Experiment I

	Original	Low	Middle	High	Very High	Average
P-F	2.60	2.40	2.40	2.42	2.36	2.44
P-W	1.54	1.86	1.42	1.66	0.90	1.48
P-S	0.44	0.14	0.08	0.00	0.06	0.14
F-W	1.06	0.54	0.98	0.76	1.46	0.96
F-S	3.04	2.26	2.48	2.42	2.30	2.50
W-S	1.98	1.72	1.50	1.66	0.84	1.54

The reason why the middle diffuseness was highly evaluated would be because it was within the diffuseness range at pre-observation, where observers memorized the appearance of objects. The other possibility would be related to the naturalness of lighting conditions. Fleming et al. (2003) revealed that the reflection properties of objects in familiar environments are easier to distinguish than in unfamiliar environments. It can be considered that the moderate diffuseness was preferred because it is commonly seen in our ordinary life. Our results suggest that unfamiliar lighting conditions (very low and very high diffuseness) did not correctly represent the appearance of objects.

5 Conclusion

In this study, the observers viewed objects with different materials, shapes, and textures. They evaluated the impression of those objects, as well as the fidelity and the ideality of objects' appearance under different diffuseness levels of illumination. The results showed that illumination with middle diffuseness reproduced the appearance of objects faithful and ideally, and extremely low and high diffuseness were not. It was also suggested that the diffuseness, which ideally reproduces the surface appearance, would be different in object's properties.

To summarize, we showed that the impression of surface appearance was influenced by the surface properties of the object and lighting distribution. Our results suggest that it is possible to define a diffuseness level for accurate appearance common to objects with different materials. However, the difference in the material should be considered for the diffuseness condition for an ideal appearance to realize the ideal appearance.

Acknowledgments

Supported by JSPS KAKENHI JP16K00368 and JP19H04196.

References

CUTTLE, C. 2014. Research note: A practical approach to cubic illuminance measurement. *Lighting Research & Technology*, 46(1), 31-34.

FLEMING, W. R., DROR, O. R., ADELSON, H. E. 2003. Real-world illumination and the perception of surface reflectance properties. *Journal of Vision*, 3(5), 347-368.

FLEMING, R. W., DROR, R. O., ADELSON, E. H. 2003. Surface reflectance estimation under unknown natural illumination. *Journal of Vision*, 1(3), 43.

FUJISAKI, W., TOKITA, M., KARIYA, K. 2015. Perception of the material properties of wood based on vision, audition, and touch. *Vision Research,* 109, 185–200.

HARTUNG, B., KERSTEN, D. 2002. Distinguishing shiny from matte. *Journal of Vision*, 2(7), 551.

HO, Y. X., LANDY, M. S., MALONEY, L. T. 2008. Conjoint measurement of gloss and surface texture. *Psychological science*, 19(2), 196-204.

LANGER, M. S., BULTHOFF, H. H., 2001. A prior for global convexity in local shape-from-shading. *Perception*, 30(4), 403-410.

MALONEY, L. T., GERHARD, H. E., BOYACI, H. DOERSCHNER, K. 2011. Surface color perception and light field estimation in 3D scenes. Natural-scene perception. *Journal of Vision*, 1(3), 280-307.

MAMASSIAN, P., LANDY, M. S., MALONEY, L. T. 2002. Bayesian Modelling of Visual Perception. Probabilistic Models of brain: *Perception and Neural Function* (13-36). Cambridge, MA: MIT Press.

MIZOKAMI, Y., KIYASU, Y., YAGUCHI, H. 2019. Change in the appearance of objects according to the ratio of direct and diffusive light. *CIE x046: 2019 Proceedings of the 29th CIE SESSION Washington DC, USA*, DOI 10.25039/x46.2019.PP05.

OBEIN, G., KNOBLAUCH, K., VIE ´NOT, F. 2004. Difference scaling of gloss: Nonlinearity, binocularity, and constancy. *Journal of Vision*, 4(9), 711-720.

OLKKONEN, M., BRAINARD, D. H. 2010. Perceived glossiness and lightness under real-world illumination. *Journal of Vision*, 10(9), 1–19.

PONT, S. C., TE PAS, S. F. 2006. Material—Illumination ambiguities and the perception of solid objects. *Perception*, 35(10), 1331-1350.

XIAO, B., BI, W., JIA, X., WEI, H., ADELSON, E. H. 2016. Can you see what you feel? Color and folding properties affect visual–tactile material discrimination of fabrics. *Journal of Vision*, 16(3), 34.

XIA, L., PONT, S. C., HEYNDERICKX, I. 2016. Diffuseness metric Part 1: Theory. *Lighting Research & Technology*, 49(4), 411-427.

YAMAZOE, T., FUNAKI, T., KIYASU, Y., MIZOKAMI, Y. 2019. Evaluation of material appearance under different spotlight distributions compared to natural illumination. *Journal of Imaging*, 5(2), 31.

International Commission on Illumination
Commission Internationale de l'Eclairage
Internationale Beleuchtungskommission

PO43

COLOUR CONTRIBUTION IN SPONTANEOUS IDENTIFICATION OF COPPER MATERIALS

Hiroki Ishiyama et al.

DOI 10.25039/x47.2020.PO43

Paper accepted for the 5th CIE Symposium on Colour and Visual Appearance

The paper was selected by the International Scientific Committee (ISC) for presentation at the 5th CIE Symposium on Colour and Visual Appearance, Hong Kong, CN, April 21–22, 2020, which, due to the corona pandemic, could not take place. The paper has not been peer-reviewed by CIE.

CIE Central Bureau
Babenbergerstrasse 9
A-1010 Vienna
Austria
Tel.: +43 1 714 3187
e-mail: ciecb@cie.co.at
www.cie.co.at

PO43

COLOUR CONTRIBUTION IN SPONTANEOUS IDENTIFICATION OF COPPER MATERIALS

Ishiyama, H.[1], Tanaka, M.[2], Horiuchi, T.[1]
[1] Graduate School of Science and Engineering, Chiba University, JAPAN,
[2] College of Liberal Arts and Sciences, Chiba University, JAPAN
horiuchi@faculty.chiba-u.jp

Abstract

In this study, we conduct a psychophysical experiment based on the hypothesis that colour information affects the spontaneous identification of copper. We created six types of copper metal balls as test images using computer graphics. The surrounding colour scene was reflected on the balls of the test images. In each test image, we generated test stimuli in which the colour gamut was expanded in ten steps, such that a part of the reflected colour was deviated from the colour gamut of the copper material. In our experiment, we checked the accuracy and speed of copper material identification using rapid presentations. Experiments have shown that colour distribution in an object contributes to the spontaneous perception of metals by humans. Participants identified copper materials in only a few hundred milliseconds, and the colour gamut and speed of recognition were scene-dependent. In addition, it was found that the location where the colour gamut was expanded affected spontaneous perception.

Keywords: Material perception, Spontaneous identification, Metallic object, Visual experiment

1 Introduction

Metallic materials are common in our daily life. Copper has the same chromaticity as orange and reddish brown, but it can be identified as a metallic colour using higher-order physical information associated with the gloss phenomena, such as spatial light reflection. However, as we can instantly perceive that a material made of copper is metallic, it is natural to consider that complex physical information is not processed in early vision.

Conventional studies reported that humans could quickly identify materials. Motoyoshi et al. focused on the perception of surface gloss [1]. They hypothesized that simple image statistics contributed to the identification of surface gloss and showed that the skewness of the luminance histogram and sub-band filter outputs correlated to surface gloss and inversely correlated to surface albedo. They also found evidence that human observers use skewness, or a similar measure of histogram asymmetry, to judge the characteristics of surfaces. Sharan et al. investigated the speed of material categorization [2]. They displayed images classified into nine categorizes based on the material with short presentation times of 40, 80, and 120 ms, and found that the categories could be identified quickly, requiring only 100 ms more than simple baseline tasks. However, they did not investigate metal objects or discuss metal perception. Based on both the results, it is expected that metallic objects can be identified using simple image features.

In this study, we conducted a psychophysical experiment based on the hypothesis that colour information affects the spontaneous identification of copper materials. Reference [1] discussed only luminance information for the perception of surface gloss. This is the first study to investigate colour information. In Ref. [3], a preliminary study was conducted. In this paper, we conduct analysis by increasing the number of test images.

2 Analysis of copper material

In Ref. [3], we measured the reflected colour of a copper object to analyze the properties of the colour generated by metal objects. The X-Rite ColorChecker under the illuminant at a temperature of 6000 K was reflected on a real copper board, and spectral power distributions

of the original colour patch and reflected components were measured using a spectroradiometer (Konica Minolta CS-2000). Subsequently, we derived a spectral reflectance of the copper board from the data. To simulate changes in the colour gamut from the original object to the reflected colour, we used the spectral reflectance database [4], which included 24 colours of the Macbeth colour checker and 1269 colours of the Munsell colour chart. A partial dataset of the database was used as the surface spectral reflectance of the original object. Using the derived spectral reflectance of the copper board, we calculated the spectral power distribution of the reflected colour component.

Figure 1 shows the changes in the colour gamut from the original colour to the reflected colour. The green points represent the chromaticity of the original object, and the orange points represent the chromaticity of the reflected component on the copper board. The coloured area represents the colour gamut. The arrows extending from the chromaticity points show the changes in chromaticity. The colour gamut of the reflected colour generally shrank compared to that of the original object, and each metal type had a unique colour gamut.

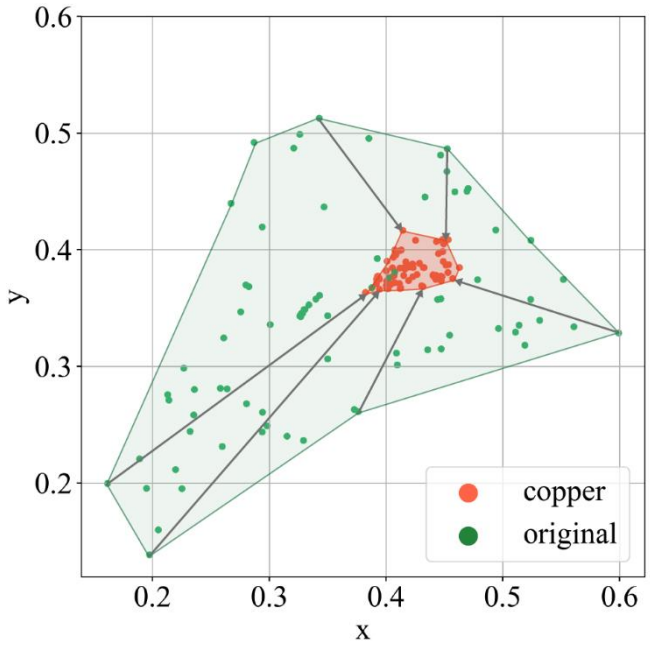

Figure 1 – Changes in the colour gamut

3 Experiment

3.1 Test stimuli

To verify whether colour information has an effect on the identification of metals, we focused on the colour gamut of the reflected colour component from a copper object. As the test stimulus, we considered using either a real metal or computer graphics (CGs). Subsequently, in this study, we decided to create a copper material image using CGs, which could freely set the colour.

The image was created using a 3D software (MAXON Computer, Cinema4D). The reflection property of a spherical surface was provided by the Trowbridge-Reitz model (GGX). Only the specular reflection was set with parameters of a metal sphere. The copper material in the layer Fresnel preset was applied. Six types of high dynamic range images in Ref. [5] were used as images of environment scenes. Therefore, six types of original scenes were generated. As these original scenes exceeded the colour gamut of the copper board from the previous section, the colour gamut was normalized such that 98% of all pixels would exist within the colour gamut. Figure 2 shows the normalized images. Further, in each spherical image, we generated 10 samples that extended the colour gamut of a specific object reflected in the image by extending the distance from the white point to the chromaticity point of each pixel at equal intervals. Scenes 1-4 have changed the colour of some of the objects, while scenes 5 and 6 have changed the colour of the entire scene. The intervals were the ratio to the distance measured subjectively

for each normalized image, as follows Table 1. In other words, when the colour gamut of the normalized spherical image was 1, the ratio of the maximum colour gamut for each scene was determined as follows: 6.4, 37.0, 5.5, 6.4, 4.6 and 4.6 for scenes 1, 2, 3, 4, 5 and 6, respectively. The ratio of scene 2 was high because the allowable range of the colour gamut of the sky region was large in the preparation experiment. Figure 4 shows a partial sample for scene 2.

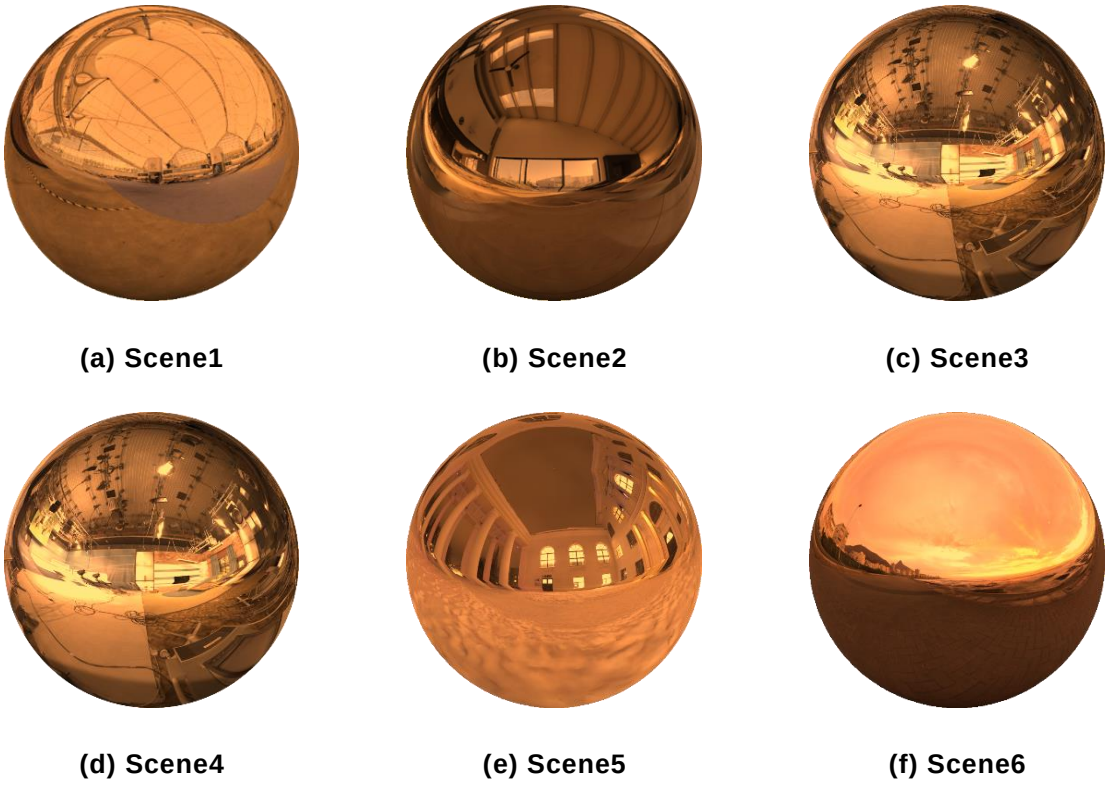

(a) Scene1 **(b) Scene2** **(c) Scene3**

(d) Scene4 **(e) Scene5** **(f) Scene6**

Figure 2 – Six types of normalized spherical images

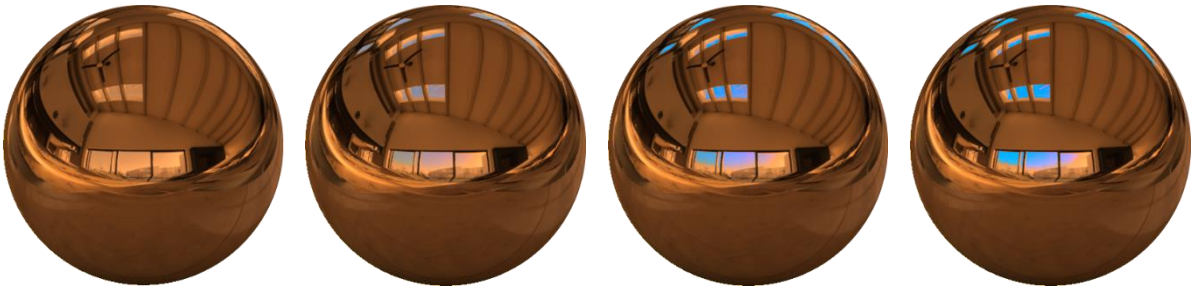

(a) Ratio = 1 **(b) Ratio = 13** **(c) Ratio = 25** **(d) Ratio = 37**

Figure 3 – A partial sample for Scene2

Table 1 – Colour gamut expansion ratio

	Scene1	Scene2	Scene3	Scene4	Scene5	Scene6
Min-Max	1.0-6.4	1.0-37.0	1.0-5.5	1.0-6.4	1.0-4.6	1.0-4.6

Step	0.6	4.0	0.5	0.6	0.4	0.4

3.2 Procedure

The experiment followed the procedure by Sharan et al. [1], but the presentation times were 40, 80, and 120 ms. Their experiments aimed at categorizing materials into a single stimulus image. This study aimed at the perception of metals using chromaticity change, and the presentation time was too short to perceive differences among the stimuli. In our experiment, an initial stimulus was presented for 100, 200, 300, 400, or 500 ms. The initial stimulus was followed by six perceptual masks appearing for 33 ms (Fig. 4). We created the masks using the Portilla-Simoncelli texture synthesis method [6], which matches the statistics of the mask images to the statistics of the stimulus images at multiple scales and orientations, thereby allowing for more effective masking compared to the commonly used pink noise masks. Finally, a second stimulus was presented for the same duration as the initial stimulus. In each trial, the task was to report which stimuli were perceived as a copper material. All 45 combinations of 10 samples were evaluated for each scene using two Alternative Forced Choice Task.

For all experiments, stimuli were displayed centrally on a calibrated liquid crystal display monitor (ColorEdge CG-277, EIZO) against a gray background. The vertical scanning frequency of the display was 61 Hz, and it included the AdobeRGB colour gamut. The viewing distance was 95 cm, and the viewing angle of the stimulus image was 12°, based on the experiment by Sharan et al. [1]. The experiment was performed under fluorescent lamps. Seven university students with normal colour vision participated. Figure 5 shows the experimental setup.

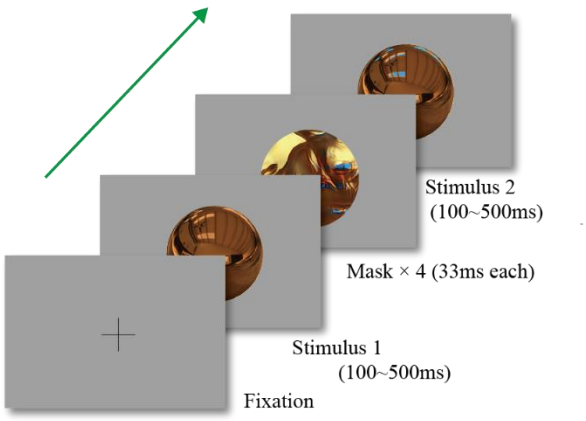

Figure 4 – Procedure of the experiment

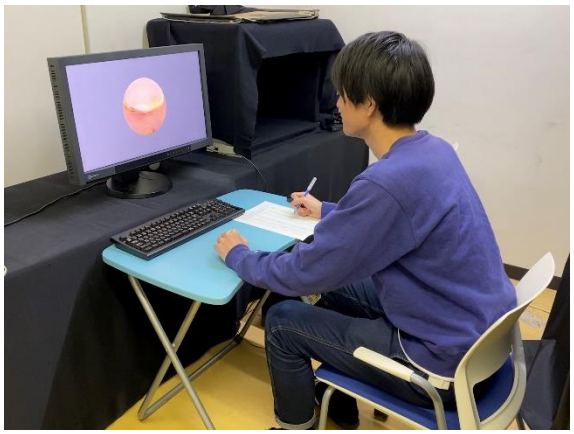

Figure 5 – Experimental environment

4 Results

Figures 6 and 7 shows examples of the experimental results by representing the Z-score for scene 2 and 5, respectively. The horizontal axis indicates the magnification rate of the colour gamut of 10 samples from the normalized image, and the vertical axis indicates the Z-value. Smaller Z-value indicates that the stimulus is more likely to be perceived as copper. The experimental results revealed the following:

(1) Compared to the colour gamut of the reflected colours of real copper objects, stimuli could not be easily identified as copper material when they were too narrow or wide.

(2) A reproduced colour image with a colour gamut slightly wider than that of the reflection of a real copper object was easily identified as a copper material.

(3) When the presentation time was shortened, identifying the copper material was difficult. In the case of complex reflection scenes, identifying the copper material was unstable for longer presentation time as shown in Fig. 7. However, the colour gamut boundary identifiable as the copper material was stable.

(4) The presentation time required to identify the copper material varied depending on the reflected surrounding scene.

The identification task was successfully performed when the presentation time was 300 ms for complex reflection scenes However, in simple reflection scenes, participants identified the copper material in less than 100 ms, but it was unstable for the identification over 300 ms due to the use of features higher than colour.

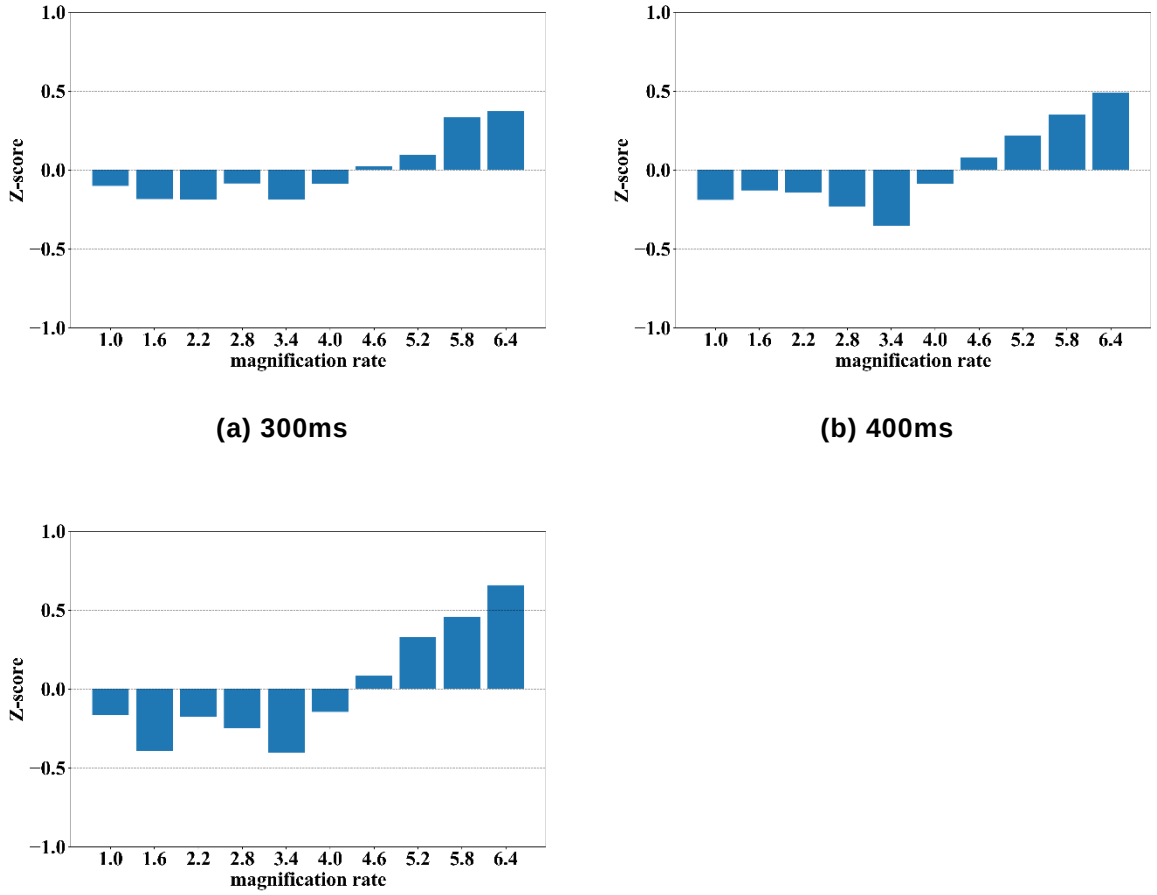

(a) 300ms

(b) 400ms

(c) 500ms

Figure 6 – Z-score for Scene 2

5 Conclusions

This study investigated the effect of colour information in the spontaneous perception of copper. In our experiment, we checked the accuracy and speed of copper material identification using rapid presentations. We confirmed that colour distribution in an object contributed to spontaneous perception of metals by humans. Participants identified copper materials in only a few hundred milliseconds, and the colour gamut and speed of recognition were scene-dependent. In addition, it was found that the location where the colour gamut was expanded affected spontaneous perception. In the future, studies should be conducted on verification of different metals in various scenes.

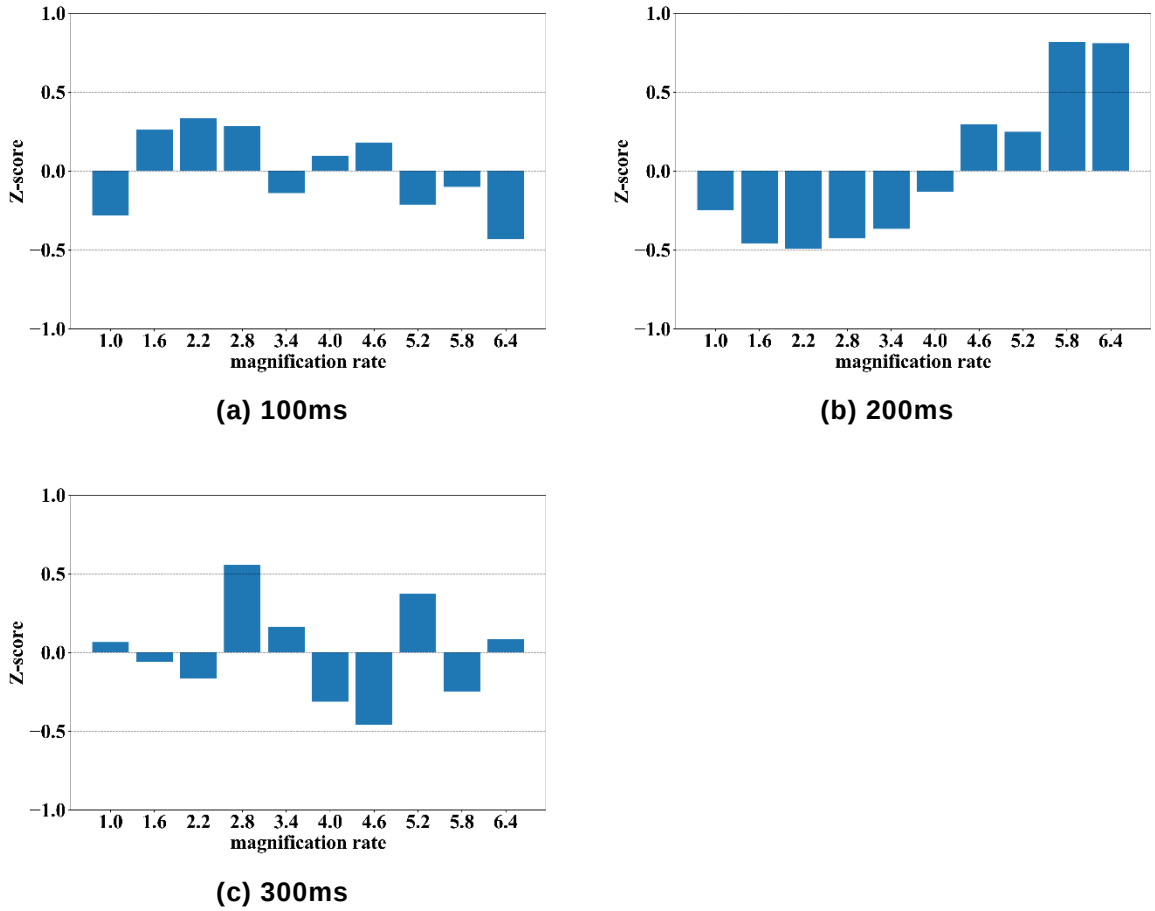

(a) 100ms **(b) 200ms**

(c) 300ms

Figure 7 – Z-score for Scene 5

Acknowledgment

This work was supported by Grant-in-Aid for Scientific Research on Innovative Areas (No. 15H05926) from MEXT, Japan.

References

1. Sharan, L., Rosenholtz, R., & Adelson, E. H. 2014. Accuracy and speed of material categorization in real-world images. *Journal of Vision*, 14(9), 1-24.
2. Motoyoshi, I., Nishida, S., Sharan, L., & Adelson, E. H. 2007. Image statistics and the perception of surface qualities. *Nature*, 447, 206-209.
3. Ishiyama T., Tanaka M., & Horiuchi, T. 2019. Contribution of color information in instantaneous identification of copper materials. Proc. 5th conference of the Asia Color Association ACA, 266-271.
4. Barnard, K., Martin, L., Funt, B., & Coath, A. 2002. A Data Set for Colour Research, *Color Research and Application*, 27(3), 147-151.
5. sIBL Archive, http://www.hdrlabs.com/sibl/archive.html.
6. Portilla, J., & Simoncelli, E. P. 2000. A Parametric Texture Model based on Joint Statistics of Complex Wavelet Coefficients. *International Journal of Computer Vision*, 40, 49-70.